

**STATIC AND DYNAMIC ANALYSIS  
OF NEAR INFRA-RED DORSAL  
HAND VEIN IMAGES FOR  
BIOMETRIC APPLICATIONS**

**by**

**Huaigeng Zheng**

*A thesis submitted in partial fulfilment for the requirements for the degree of*

*Doctor of Philosophy*

*at*

*the University of Central Lancashire*

September 2017

# STUDENT DECLARATION FORM

## Concurrent registration for two or more academic awards

Either \*I declare that while registered as a candidate for the research degree, I have not been a registered candidate or enrolled student for another award of the University or other academic or professional institution

or ~~\*I declare that while registered for the research degree, I was with the University's specific permission, a \*registered candidate/\*enrolled student for the following award:~~

---

## Material submitted for another award

Either \*I declare that no material contained in the thesis has been used in any other submission for an academic award and is solely my own work

or ~~\*I declare that the following material contained in the thesis formed part of a submission for the award of~~

---

(state award and awarding body and list the material below):

## Collaboration

This work presented in this thesis was carried out partly in the North China University of Technology, Beijing, China. And most of the work was carried out in the University of Central Lancashire. The work described in the thesis is entirely the candidate's own work.

Signature of Candidate Huaigeng Zheng

Type of Award Doctor of Philosophy

School School of Engineering, University of Central Lancashire

## **Acknowledgements**

I hereby give great thanks to my director of study, Dr. Martin Varley, for his patience, kindness and support. Special thanks to my supervisor, Prof. Lik-Kwan Shark, for his hard work and kind heart, valuable guidance and consistent support.

I am particularly thankful to my good friend Dr. Guan Xiao Yin for her encouragement and helpful advices whenever I asked. Thanks must also go to other friends at UCLan for all the great times that we have shared.

Most of all, I will forever be thankful to my family, especially my wife Qian. Her love and support provided me strength and motivation. A hearty thanks to my parents for their company all the while.

## **Abstract**

This thesis presents the work carried out on static and dynamic analysis of near infra-red dorsal hand vein images for biometric applications. It focuses on the investigation of the classification of old and young groups of people, and analyses vital signs underlying dorsal hand vein images.

All research is based on the database used in this work. Focusing on the aged group of dorsal hand vein images, a database including static images and video images was first created. The static database contained 1000 images from 50 individuals and the dynamic database included 40 videos from 20 old participants.

For static analysis, dorsal hand vein images were pre-processed by geometry correction, regions of interest extraction (ROI), grey level normalisation, noise reduction and image enhancement. Then, skin and vein areas from the dorsal hand were segmented using maximum curvature based algorithms. Due to varying haemoglobin and water levels in the vein and skin, intensity based parameters were investigated and extracted as features for the classification of old and young groups. Two classifiers, linear discriminant analysis (LDA) and k-nearest neighbours (KNN) were adopted for comparative discussions. The experimental results turned out to be satisfactory and the two groups were well classified, using statistical intensity based features.

For dynamic analysis, mean grey levels were extracted from the ROI of each frame of the dorsal hand vein image videos. Then, all parameters were connected to form a biometric signal. The signal was analysed in a spectrum to detect a major peak for liveness. A fake dorsal hand video was introduced for comparative studies.

Experimental results showed that a respiratory like signal was detected as the main peak in the spectrum, verifying the vital signs of dynamic dorsal hand vein images and proposing a new method of liveness detection in biometric applications

# Table of contents

<b>List of figures</b>	<b>vii</b>
<b>List of tables</b>	<b>xiii</b>
<b>1 INTRODUCTION</b>	<b>1</b>
1.1 Background . . . . .	1
1.1.1 Current research on biometric application . . . . .	2
1.1.2 Dorsal hand vein biometrics . . . . .	4
1.2 Aim of the Research . . . . .	7
1.3 This Structure . . . . .	8
<b>2 IMAGE ACQUISITION AND DATABASE</b>	<b>9</b>
2.1 Introduction . . . . .	9
2.2 Image Acquisition Principle and Set-up . . . . .	10
2.2.1 Near infra-red illumination . . . . .	10
2.2.2 NIR imaging mode . . . . .	11
2.2.3 NIR imaging module . . . . .	12
2.2.4 Hardware . . . . .	15
2.3 Database . . . . .	16
2.3.1 Static dorsal hand vein images . . . . .	17
2.3.2 Dynamic dorsal hand vein images . . . . .	18
2.4 Concluding Remarks . . . . .	19

---

<b>3</b>	<b>DORSAL HAND VEIN IMAGE PRE-PROCESSING</b>	<b>20</b>
3.1	Introduction . . . . .	20
3.2	Geometry Correction . . . . .	21
3.3	Region of Interest Extraction . . . . .	23
3.4	Grey-level Normalisation . . . . .	24
3.5	Noise Reduction . . . . .	25
3.5.1	Noise measurement . . . . .	25
3.5.2	Noise reduction . . . . .	27
3.5.3	Filtering results . . . . .	29
3.6	Image Enhancement . . . . .	31
3.7	Concluding Remarks . . . . .	33
<b>4</b>	<b>DORSAL HAND VEIN SEGMENTATION</b>	<b>34</b>
4.1	Introduction . . . . .	34
4.2	Segmentation Algorithms . . . . .	35
4.2.1	Threshold methods . . . . .	35
4.2.2	Maximum curvature based segmentation . . . . .	39
4.3	Post-processing . . . . .	42
4.4	Concluding Remarks . . . . .	44
<b>5</b>	<b>STATIC ANALYSIS OF DORSAL HAND VEIN IMAGES FOR BIOMET- RIC APPLICATION</b>	<b>45</b>
5.1	Introduction . . . . .	45
5.2	Statistical Parameters Analysis . . . . .	46
5.2.1	Histogram analysis . . . . .	46
5.2.2	Statistical parameters . . . . .	50
5.2.3	Selection of parameters for classification . . . . .	57
5.3	Classification Analysis and Experiments . . . . .	58
5.3.1	Classifiers . . . . .	58
5.3.2	Classification Parameters . . . . .	60

---

5.3.3	Training experiments . . . . .	62
5.3.4	Testing experiments . . . . .	65
5.4	Concluding Remarks . . . . .	67
<b>6</b>	<b>DYNAMIC ANALYSIS OF DORSAL HAND VEIN IMAGES FOR BIOMET-</b>	
	<b>RIC APPLICATION</b>	<b>68</b>
6.1	Introduction . . . . .	68
6.2	Signal Extraction and Filtering . . . . .	69
6.2.1	Signals extracted from regions of interest . . . . .	69
6.2.2	Signal Filtering . . . . .	71
6.3	Spectrum Analysis of the Extracted Signals . . . . .	74
6.3.1	Discrete Fourier Transform . . . . .	74
6.3.2	Peak detection . . . . .	75
6.4	Dynamic Analysis of live dorsal hands . . . . .	76
6.4.1	Live and fake dorsal hand vein images contrast . . . . .	77
6.4.2	Possible vital signs analysis . . . . .	79
6.5	Concluding Remarks . . . . .	80
<b>7</b>	<b>CONCLUSIONS AND FUTURE WORK</b>	<b>81</b>
7.1	Conclusions . . . . .	81
7.2	Original Contributions . . . . .	83
7.3	Future Work . . . . .	83
	<b>References</b>	<b>85</b>
	<b>Appendix A The AGE DISTRIBUTION OF THE DATABASE</b>	<b>90</b>
	<b>Appendix B SEGMENTATION RESULTS OF OLD HANDS</b>	<b>91</b>
	<b>Appendix C SEGMENTATION RESULTS OF YOUNG HANDS</b>	<b>100</b>

# List of figures

1.1	Anatomy of the dorsal hand veins, modified from [Gray and Standing, 2008]. There are two types of dorsal hand veins, the cephalic and basilica veins. The latter are the main focus of this project. . . . .	5
1.2	Anatomy of skin tissue . . . . .	6
2.1	Infrared absorption spectrum of water and haemoglobin [Chen and Lu, 2000] . . . . .	10
2.2	The three main modes of NIR imaging . . . . .	11
2.3	Different imaging modes . . . . .	11
2.4	Structure of an imaging module . . . . .	12
2.5	Spectral response of the BPF-850 filter, modified from [Accute Optical Technology Co., 2012] . . . . .	13
2.6	WATEC 902B CCD camera . . . . .	13
2.7	A PENTAX H1214-M (1/2') . . . . .	13
2.8	The Mine 2860 USB capture card . . . . .	14
2.9	<b>(a)</b> The capturing hardware: the hand reflects NIR light coming from infra-red LED arrays. <b>(b)</b> Schematic of the DHV image acquisition system: the green (camera, lens and infra-red filter) represents the imaging module and the blue indicates the illumination module and the black line surrounding the diagram indicates a box, covering the illumination and imaging components to reduce visible light. . . . .	15
2.10	Age distribution of young and old groups . . . . .	17
2.11	DHV images from old participants . . . . .	18

---

2.12	DHV images from young participants . . . . .	18
3.1	Pre-processing of DHV images . . . . .	20
3.2	Affine transformations . . . . .	21
3.3	DHV images with shearing distortion . . . . .	21
3.4	Calculating the centroid point (red) of DHV images . . . . .	22
3.5	Shearing correction . . . . .	23
3.6	Shearing correction examples . . . . .	23
3.7	ROI extraction data . . . . .	24
3.8	Normalisation images . . . . .	25
3.9	Profile of grey levels along the middle of an ROI image . . . . .	26
3.10	TV value pixels . . . . .	26
3.11	Results of filtering . . . . .	29
3.12	Grey level profiles of middle row forms before and after filtering images. The X-axis represents the pixel position, and Y-axis represents the grey level.	30
3.13	Image enhancements . . . . .	33
4.1	Otsu's segmentation . . . . .	37
4.2	Niblack segmentation . . . . .	38
4.3	Comparative segmentation data using different $k$ selections . . . . .	39
4.4	Cross-sectional profile of veins . . . . .	40
4.5	Dorsal hand vein segmentation using the maximum curvature method . . . . .	42
4.6	Wrongly segmented veins . . . . .	42
4.7	Morphological processing . . . . .	43
4.8	Segmented veins and skin areas from a DHV image . . . . .	43
5.1	ROI images of old and young veins . . . . .	46
5.2	Histograms of ROI images from old and young veins . . . . .	47
5.3	Vein image of old and young veins . . . . .	48
5.4	Histograms of vein areas from old and young hands . . . . .	48
5.5	Vein image of old and young veins . . . . .	49

---

5.6	Histograms of skin areas from old and young participants . . . . .	49
5.7	Sketch map of statistical parameters . . . . .	50
5.8	Comparison of hands from young and old groups based on minimum grey levels of skin areas . . . . .	51
5.9	Comparison of hands from young and old groups based on minimum grey levels of vein areas . . . . .	51
5.10	Comparison of hands from young and old groups based on maximum grey levels of skin areas . . . . .	52
5.11	Comparison of hands from young and old groups based on maximum grey levels of vein areas . . . . .	52
5.12	Comparison of hands from young and old groups based on median grey levels of skin areas . . . . .	53
5.13	Comparison of hands from young and old groups based on median grey levels of vein areas . . . . .	53
5.14	Comparison of hands from young and old groups based on mode grey levels of skin areas . . . . .	54
5.15	Comparison of hands from young and old groups based on mode grey levels of vein areas . . . . .	54
5.16	Comparison of hands from young and old groups based on mean grey levels of skin areas . . . . .	55
5.17	Comparison of hands from young and old groups based on mean grey levels of vein areas . . . . .	55
5.18	Comparison of hands from young and old groups based on SD grey levels of skin areas . . . . .	56
5.19	Comparison of hands from young and old groups based on SD grey levels of vein areas . . . . .	56
5.20	Plot profiles of sample averages from 500 DHV images of the right hand .	57
5.21	Parameter K plots for training skin features . . . . .	63
5.22	Parameter K plots for training vein features . . . . .	63

---

5.23	Parameter plots of $K$ for training feature $F$ . . . . .	65
5.24	Plotting the testing set using $F$ features by KNN . . . . .	67
6.1	Dynamic DHV analysis . . . . .	69
6.2	DHV video sequences and ROI extraction for each frame . . . . .	69
6.3	An example of a ROI based signal $y'(t)$ . . . . .	70
6.4	Signals from different ROI selections . . . . .	71
6.5	Frequency response to the Butterworth filter . . . . .	72
6.6	ROI signals after band pass filtering . . . . .	72
6.7	The Hanning window for the 250 frame signal . . . . .	73
6.8	ROI signals after Hanning window . . . . .	73
6.9	ROI main peak detection . . . . .	75
6.10	Peak frequency detection of all ROI signals in the video database . . . . .	76
6.11	A fake dorsal hand ROI image sequences . . . . .	77
6.12	Comparison of a fake signal (red) with a real signal (blue) . . . . .	78
6.13	Spectrum comparison of a fake signal (red) with a real signal (blue) . . . . .	78
6.14	Peak detection in hands from the same person . . . . .	79
6.15	Right hand peak values versus left hand peak values from 20 samples . . . . .	80
7.1	Age distribution using combined mean values . . . . .	84
B.1	Segmentation result of Old No.1 . . . . .	91
B.2	Segmentation result of Old No.2 . . . . .	91
B.3	Segmentation result of Old No.3 . . . . .	92
B.4	Segmentation result of Old No.4 . . . . .	92
B.5	Segmentation result of Old No.5 . . . . .	92
B.6	Segmentation result of Old No.6 . . . . .	92
B.7	Segmentation result of Old No.7 . . . . .	92
B.8	Segmentation result of Old No.8 . . . . .	93
B.9	Segmentation result of Old No.9 . . . . .	93
B.10	Segmentation result of Old No.10 . . . . .	93

---

B.11 Segmentation result of Old No.11 . . . . .	93
B.12 Segmentation result of Old No.12 . . . . .	93
B.13 Segmentation result of Old No.13 . . . . .	94
B.14 Segmentation result of Old No.14 . . . . .	94
B.15 Segmentation result of Old No.15 . . . . .	94
B.16 Segmentation result of Old No.16 . . . . .	94
B.17 Segmentation result of Old No.17 . . . . .	94
B.18 Segmentation result of Old No.18 . . . . .	95
B.19 Segmentation result of Old No.19 . . . . .	95
B.20 Segmentation result of Old No.20 . . . . .	95
B.21 Segmentation result of Old No.21 . . . . .	95
B.22 Segmentation result of Old No.22 . . . . .	95
B.23 Segmentation result of Old No.23 . . . . .	96
B.24 Segmentation result of Old No.24 . . . . .	96
B.25 Segmentation result of Old No.25 . . . . .	96
B.26 Segmentation result of Old No.26 . . . . .	96
B.27 Segmentation result of Old No.27 . . . . .	96
B.28 Segmentation result of Old No.28 . . . . .	97
B.29 Segmentation result of Old No.29 . . . . .	97
B.30 Segmentation result of Old No.30 . . . . .	97
B.31 Segmentation result of Old No.31 . . . . .	97
B.32 Segmentation result of Old No.32 . . . . .	97
B.33 Segmentation result of Old No.33 . . . . .	98
B.34 Segmentation result of Old No.34 . . . . .	98
B.35 Segmentation result of Old No.35 . . . . .	98
B.36 Segmentation result of Old No.36 . . . . .	98
B.37 Segmentation result of Old No.37 . . . . .	98
B.38 Segmentation result of Old No.38 . . . . .	99
B.39 Segmentation result of Old No.39 . . . . .	99

---

B.40	Segmentation result of Old No.40 . . . . .	99
C.1	Segmentation result of Young No.1 . . . . .	100
C.2	Segmentation result of Young No.2 . . . . .	100
C.3	Segmentation result of Young No.3 . . . . .	101
C.4	Segmentation result of Young No.4 . . . . .	101
C.5	Segmentation result of Young No.5 . . . . .	101
C.6	Segmentation result of Young No.6 . . . . .	101
C.7	Segmentation result of Young No.7 . . . . .	101
C.8	Segmentation result of Young No.8 . . . . .	102
C.9	Segmentation result of Young No.9 . . . . .	102
C.10	Segmentation result of Young No.10 . . . . .	102

# List of tables

2.1	Comparison of the three different modes of imaging . . . . .	12
2.2	Lens parameters and optical performance . . . . .	14
2.3	Components and main parameters of acquisition devices [Li, 2013] . . .	16
2.4	Video parameters . . . . .	18
3.1	TV values comparison . . . . .	31
5.1	Confusion matrix . . . . .	61
5.2	Classification performances with KNN . . . . .	64
5.3	Classification performances with LDA . . . . .	64
5.4	Classification performances using feature F with KNN . . . . .	65
5.5	Classification performances using feature F with LDA . . . . .	65
5.6	Results of correct prediction rates . . . . .	66
A.1	Age distribution of the static DHV database . . . . .	90

# Chapter 1

## INTRODUCTION

### 1.1 Background

Over the last few decades, biometric applications have become increasingly explored due to significant advances in the field of computer technology and image processing. More and more human characteristics have been used for biometric technologies, mainly for human identification in security access control and surveillance systems. These characteristics are known as biometric identifiers, they are used to label and describe individuals, and they can be categorised as physiological or behavioural [Jain et al., 2000, 2011]. The former characteristics are related to the shape of the body such as face, iris, fingerprint, palm and dorsal hand vein, while the latter reflects the behaviour of a person, including but not limited to gait, voice and typing rhythm.

Significant characteristics are often selected for, based on several factors: uniqueness, stability, universality, collectability, acceptability and security [Bolle and Pankanti, 1998; Clarke, 1994]. However, none of these characteristics are absolutely reliable or secure when threats like spoofing, artificially created biometrics and database attacks exist [Schuckers and Abhyankar, 2004]. Hence, the increasing demand for more reliable and convenient security systems, thereby generating renewed interest in biometrics. Emerging into this field is an area of novel research exploring biometric applications such as multi-modal biometrics [Akhtar, 2012; Ross and Jain, 2004], soft biometrics [Dantcheva et al., 2011] and liveness detection [Kang et al., 2003; Pan et al., 2008], Therefore, biometrics

technology is developing extensively in addition to personal identification when biometric applications are increasingly enlarged.

### **1.1.1 Current research on biometric application**

In general, biometric applications refer to biometric authentication which simply enables the identification of humans. There are numerous applications for the use of biometric recognition systems, e.g. PC Logon, National Border Crossing, Prison System and Physical Access [Day, 2009]. While there is a large body of research exploring biometrics as a means of verifying identity, very little work has been done to see if biometric measures can determine specific human attributes. Due to their properties, various biometric characteristics are adopted for exploring biometric applications. Some widely studied and popular biometric characteristics are:

- *The face*

The face is the most intuitive biometric for identity documents. Major advances and initiatives in the past ten years have propelled face recognition into the spotlight [Jain and Li, 2005]. One key advantage of face biometrics is that it does not require cooperation of the test subject to function, face recognition is not perfect and struggles to perform under certain conditions like poor lighting, sunglasses or long hair. In fact, there is abundant information in the face that could be further investigated for biometric applications.

Other face biometric applications include: facial expression analysis [Kanade et al., 2000]; the perception of face for gender classification [O'Toole et al., 1998]; face age estimation and classification [Gao and Ai, 2009] and face liveness detection [Tan et al., 2010]. In addition, researchers have detected human vital signs on the face, using dynamic analysis of video based face images, and successfully extracted human heart rates and monitoring patient's physiological signals [Ming-Zher et al., 2011].

- *The iris*

Using the iris for authentication is more accurate than other biometric features as there are more characteristics within this organ. However, authentication methods makes users feel uncomfortable when placing items close to the eye. There are also difficulties when registering blind people [Negin et al., 2000]. Although it is highly secure to use irises, spoofing still occurs. In their work, Bowyer et al., Ruiz-Albacete et al. and Tome-Gonzalez et al. explored ‘direct attack’ on an iris biometric system by printing images of an iris [Bowyer et al., 2013; Ruiz-Albacete et al., 2008], Bodade and Talbar proposed a novel approach using multiple images of the same eye to look at variations in pupil dilation to detect iris spoofing [Bodade and Talbar, 2009] In addition, Thomas et al. employed machine learning techniques to develop models that predicted gender, based on iris texture features [Thomas et al., 2007].

- *The fingerprint*

Of all the biometric techniques, fingerprint-based identification is the oldest method successfully used in many applications as it is convenient with an inherent ease in acquisition [Maltoni et al., 2009]. However, the fingerprint is easy to forge which makes it susceptible to anti-spoofing biometric applications. Some researchers have introduced liveness detection for anti-spoofing [Abhyankar and Schuckers, 2006; Galbally et al., 2012; Moon et al., 2005]. In addition, gender classification has been investigated for fingerprint biometric applications [Badawi et al., 2006; Kaur and Mazumdar, 2012; Tom et al., 2013].

- *The gait*

Biometric gait recognition, which is recognising people by the way they walk, is a behavioural biometric technique. It is also a remote biometric technique which enables the filtering of people of interest in public areas such as stations, airports and shops [Gafurov, 2007]. However, there are several confounding factors to this approach, such as footwear variation, terrain, fatigue, injury and passage of time, which makes gait biometrics complicated [Boulgouris et al., 2005; Boyd and Little, 2005]. However, gait biometrics have been increasingly explored for gender

classification [Yoo et al., 2005; Yu et al., 2009] and investigated for age estimation in combination with medical diagnoses [Barth et al., 2011; Makihara et al., 2011].

- Vein patterns

Vein pattern recognition technology, has its own unique features and advantages, and thus far has maintained a dominant position in biometrics. The commonly used vein recognition patterns come from the hand, wrist or finger and is carried out by using near infra-red imaging. When a user's hand is placed on a scanner, a near infra-red light maps vein locations. Thanks to the optical attributes of venous blood, vein patterns are displayed as black lines, while the remaining parts shows up as white [Kumar and Prathyusha, 2009; Wang and Leedham, 2006; Wilson, 2010]. Vein pattern recognition is emerging as one of the fastest-growing technologies for commercial development, and is proving successful in this arena. Fujitsu, Japan have built an authentication system based on palm vein patterns with a reliability of 100% [Fujitsu, 2003]. However, in terms of exploring biometric applications, little research has been done to determine if vein measures can determine specific human attributes such as gender, age or liveness indices.

Other biometric characteristics exist; the voice, the signature and the ear etc. Indeed, since each human is unique, potential human biometric traits are simply limited by our own imagination. In developing such biometrics, applications beyond human identification will be explored and exploited for commercial use.

### **1.1.2 Dorsal hand vein biometrics**

This research is focused on the analysis of dorsal hand vein (DHV) biometrics. The dorsal hand vein pattern is a vein pattern which has been favoured for representing personal identity. To investigate dorsal hand vein images, it is important to understand the veins and the skin of the hand (Figure 1.1).

A vein pattern is a vast network of blood vessels beneath the skin. Anatomically, aside from surgical intervention, vascular patterns in the body are distinct from each other,

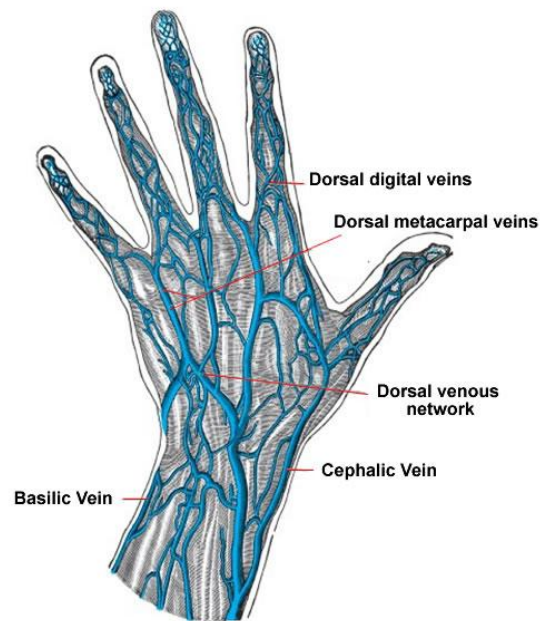


**Figure 1.1:** Anatomy of the dorsal hand veins, modified from [Gray and Standring, 2008]. There are two types of dorsal hand veins, the cephalic and basilica veins. The latter are the main focus of this project.

and are stable over long periods of time [Lingyu and Leedham, 2006]. In addition, as blood vessels are hidden beneath the skin and are practically invisible to the eye, vein patterns are extremely difficult for intruders to copy, when compared to other biometric features. The uniqueness, stability and high immunity to vein pattern forgeries, makes these veins excellent biometric features, offering secure and reliable qualities for person identity verification [Choi, 2001].

However, three key processes may alter vascular patterns in the hand: 1) natural changes in the vascular system throughout the life span, 2) natural changes in the vascular system, associated with disease and 3) changes in the vascular system induced by other factors [Nadort, 2007].

Firstly, during life, vein length extends while the body is growing, since the function of the vascular network is to provide oxygen to the entire body. Therefore, the vascular system must adapt to the size of the body. It will extend and shrink throughout life, with major changes before the age of 20 and minor changes during the aging process, from 20 onwards. Similarly, there is an inevitable decline in bone and muscle strength in the body,

due to a time-dependent weakening of blood supply to muscles [Cross and Smith, 1995; Riggs et al., 1999; Rubin, 2003].

Secondly, due to the dynamic character of the vascular system, it is sensitive to body conditions that deviate from normal or healthy forms. Diabetes, hypertension, atherosclerosis, metabolic diseases or tumours can significantly remodel vascular systems. They induce effects on the mechanical properties of vessel walls, generating hemodynamic changes. The remodelling process results in thickening or thinning of vessel walls in the lumen and in the external diameter. Another process influencing the vascular system during disease is angiogenesis, a hallmark of cancer and various ischaemic and inflammatory diseases [Carmeliet and Jain, 2000; Carretero, 2005; Risler et al., 2005].

Thirdly, other factors that influence the vascular system are environmental temperatures, physical activities and alcohol. This last factor should be considered not as unhealthy use of alcohol causing permanent pathological changes in the vessels, but rather the temporary influence of alcohol while in the body. In this way, alcohol is a vessel dilator. Vessels also dilate if body temperatures are too high; blood flow can increase by up to 150 times to expel excess heat. In cold weather, skin constricts blood vessels and causes heat loss. During physical activity, blood vessels will also dilate to provide enough oxygen to muscles [Conrad and Green, 1964; Nadort, 2007].

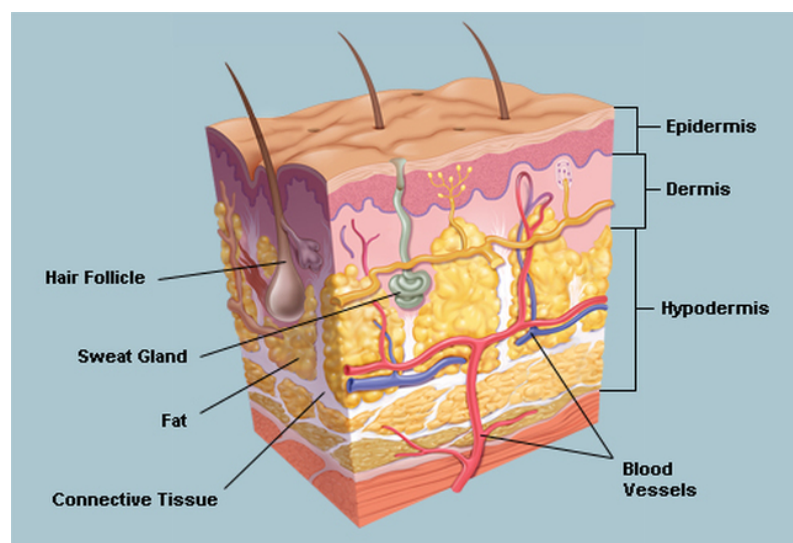


**Figure 1.2:** Anatomy of skin tissue

As shown in Figure 1.2, the skin is made up of three layers: the epidermis, the dermis and the hypodermis (also known as subcutaneous tissue). The top layer of skin is called the epidermis. It protects underlying skin layers from the outside environment and contains cells that make keratin, a protein that waterproofs and strengthens the skin. The epidermis contains cells that express melanin, the dark pigment that gives skin its colour. Other cells in the epidermis allow the sensation of touch and provide the body with immunity against foreign invaders like germs and bacteria. The bottom layer of the skin is the hypodermis [Carlson, 2013]. It contains fat cells, or adipose tissue, which insulates the body to conserve heat. The layer between the epidermis and the hypodermis is the dermis, which contains cells that give the skin strength, support, and flexibility [Kusuma et al., 2010].

As a person ages, the cells in the dermis lose strength and flexibility, causing the skin to lose its youthful appearance [Papakonstantinou et al., 2012]. Changes in aging skin dynamics occur: skin becomes more transparent, which is caused by epidermal thinning; skin becomes slack due to the loss of elastic tissue and loss of fat below the skin may result in a loosening ‘skeletal’ appearance [Gniadecka et al., 1998; Waller and Maibach, 2005; Wilhelm et al., 1991].

## **1.2 Aim of the Research**

According to literature reviews on current biometric applications and physiological and anatomic characteristics of dorsal hand veins, potentially, there are significant applications of dorsal hand veins to the biometrics arena. Due to varying optical traits between veins and skin of the dorsal hand, and considering aging issues, an investigation was carried out on the classification of hands from old and young groups. Furthermore, inspired by liveness detection studies for various biometrics, dorsal hand vein images were analysed to detect human vital signs for liveness detection.

The aim of this research was to investigate the classification of hands from old and young participants based on NIR dorsal hand vein images. The aim was to find possible de-

scriptors from NIR dorsal hand vein images for liveness detection. The specific objectives are:

- Set up a dorsal hand vein (DHV) image database.
- Static analysis on DHV images for classification of old and young groups.
- Dynamic analysis on DHV videos for liveness detection.

## 1.3 Thesis Structure

The thesis is structured into six chapters:

Chapter 2 introduces data acquisition systems, including near infra-red imaging methods and hardware. DHV databases are then created for static and dynamic analyses.

Chapter 3 introduces pre-processing methods including ROI extraction, image normalisation and noise reduction.

Chapter 4 compares segmentation methods. A maximum curvature based segmentation algorithm is adopted for the extraction of vein pattern and skin areas for further analysis.

Chapter 5 investigates static DHV images for intensity based feature extraction before classification analysis between old and young groups. Two classifiers KNN and LDA are adopted for discussion.

Chapter 6 investigates dynamic DHV images to find descriptors representing vital signs for liveness detection.

Chapter 7 draws conclusions and assesses the thesis contributions to knowledge. The chapter describes future work in developing dorsal hand vein biometric applications.

## **Chapter 2**

# **IMAGE ACQUISITION AND DATABASE**

### **2.1 Introduction**

In this chapter, a database of near infra-red dorsal hand vein images will be introduced. These were captured at North China University of Technology (NCUT) under a project funded by the National Natural Science Foundation of China (grant number: 61271368). The database comprises two parts: static dorsal hand vein images and dynamic video based dorsal hand vein images.

Since hand dorsal veins are unique, they are of convenient access, and they have a higher security when compared to other biometrics like fingerprints, face and irises, researchers have set up hand dorsal vein image databases for biometric applications. However, for these biometric practices, personal identification is the primary focus. All databases are built up for individual identification when age information is not taken into account.

Thus, to further explore dorsal hand vein biometric applications, a new database, including static and dynamic images, was established, and importantly took into consideration, participant ages. Based on the near infra-red dorsal hand vein image capturing system from NCUT, image acquisition principles and hardware set-ups are presented in the following

sections. Similarly, the new database, including static and dynamic components, is also introduced.

## 2.2 Image Acquisition Principle and Set-up

### 2.2.1 Near infra-red illumination

Due to the absorption and reflection properties of human tissue and blood, the NIR imaging method is based on irradiation of the dorsal hand with near infra-red light. Being composed of water, proteins and lipids, the chemical make-up of the skin influences optical absorption properties.

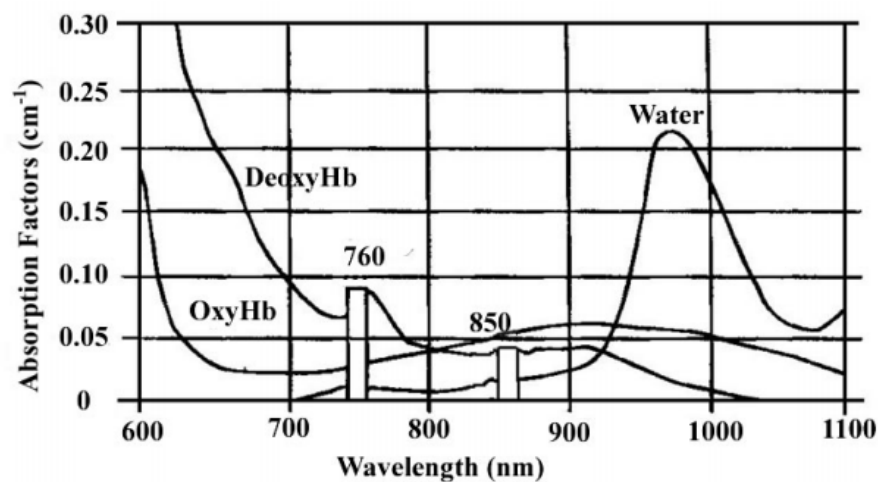


**Figure 2.1:** Infrared absorption spectrum of water and haemoglobin [Chen and Lu, 2000]

As depicted (Figure 2.1), for wavelengths  $> 900$  nm, water strongly absorbs photons, whereas haemoglobin (Hb), including OxyHb and DeoxyHb (with or without oxygen), reaches its absorption peak between 700-900 nm (DeoxyHb: 760 nm; OxyHb: 900 nm), which is higher than that of water. The region between 700-900 nm is known as the ‘tissue optical window’ (the NIR region) [Ntziachristos et al., 2003]. Importantly, as DeoxyHb and OxyHb are the main blood components in dorsal hand veins, and these veins absorb more irradiating light than surrounding tissues, NIR wavelengths could be used for illumination. Considering costs, the authors adopted an 850 nm NIR source for DHV image capture [Wang et al., 2010].

### 2.2.2 NIR imaging mode

Normally, there are three modes of NIR imaging: transmission, reflection and hybrid modes (Figure 2.2).

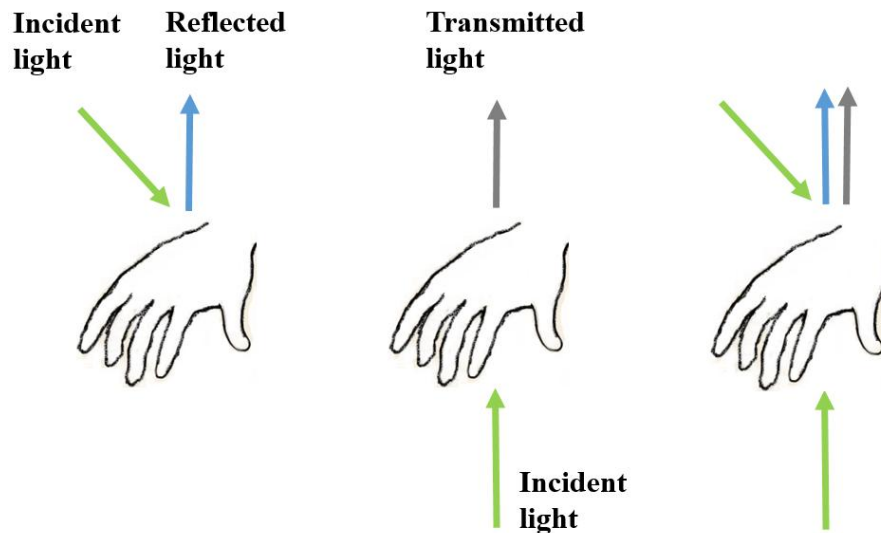


**Figure 2.2:** The three main modes of NIR imaging

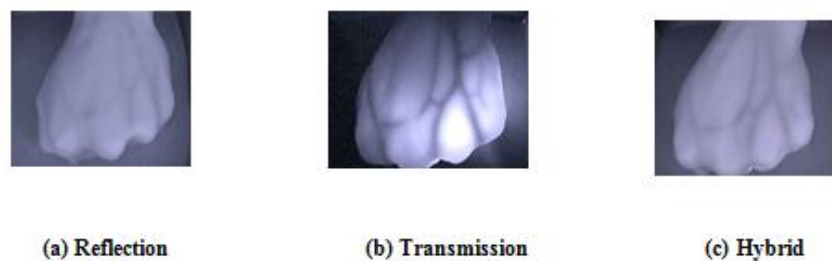


**Figure 2.3:** Different imaging modes

Images from different imaging modes can be observed in Figure 2.3 and a comparison of the three modes is shown in Table 2.1.

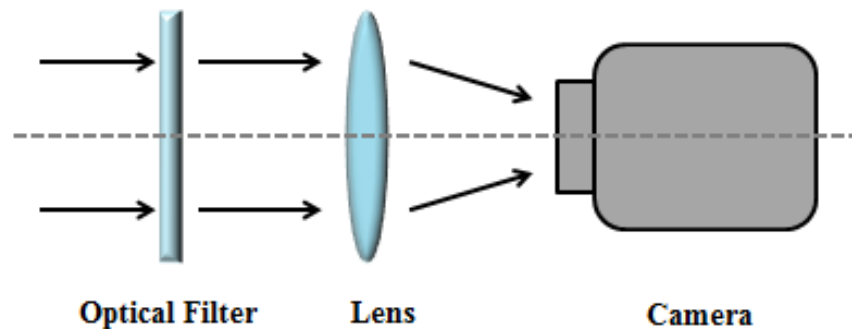
As part of their research, Li et al, selected reflection modes as they were unsusceptible to the environment, had low running costs and emitted low power [Li, 2013]. Moreover, generated dorsal hand vein images were good enough. Hand veins were visible and could be improved by increasing illumination intensity and coverage and image processing.

**Table 2.1:** Comparison of the three different modes of imaging

<b>Imaging Mode</b>	<b>Advantages</b>	<b>Disadvantages</b>
Reflection	High contrast after optimising low cost low power	High Quality requirement for NIR sources and components
Transmission	Relatively high contrast	Inhomogeneity in images Requires higher power
Hybrid	High contrast and definition	Complicated and high cost

### 2.2.3 NIR imaging module

An NIR imaging module functions as follows: incident light is controlled by the optical filter and lens for image quality improvement. A camera captures light from the lens and optical filter to form an image (Figure 2.4).

**Figure 2.4:** Structure of an imaging module

#### 1. *The optical filter*

Infra-red filters can be applied to pass or block infra-red light. There are three types of infra-red filters: 1) infra-red pass filters, 2) infra-red cut-off filters, and 3) infra-red band-pass filters. Considering NIR imaging principles, the infra-red band-pass filter, the BPF-850 was selected. The selected filter had a centre wavelength of 850 nm, a half-main-lobe width of  $60 \pm 10$  nm and the transmittance at 850 nm was 91.99% (Figure 2.5).

#### 2. *The camera*

Charge-Coupled Device (CCD) camera is a good choice for capturing vein images because of its high precision [Chih-Lung and Kuo-Chin, 2004]. In the dorsal hand

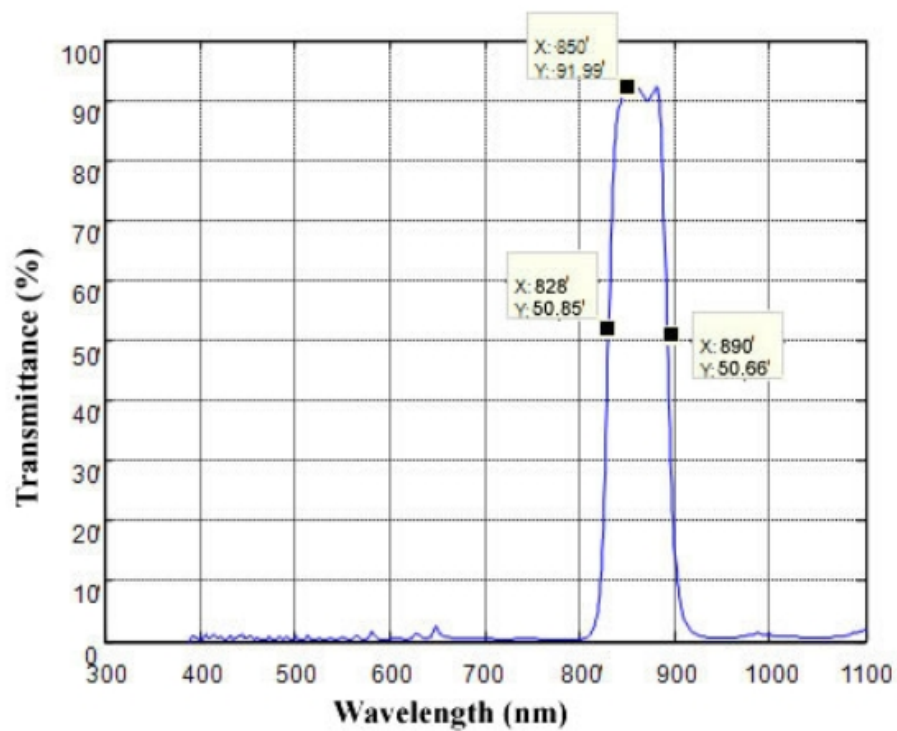


**Figure 2.5:** Spectral response of the BPF-850 filter, modified from [Accute Optical Technology Co., 2012]

vein image acquisition system, some main parameters of a CCD camera should be taken into account: the effective pixels, the resolution, the capturing frame rate, scanning system, S/N, minimum illumination. According to the parameters assessment and integrating the various requirements in [Li, 2013], a WATEC 902B CCD camera is selected, of which main parameters are listed in Table 2.3. Figure 2.6 shows the picture of a WATEC 902B CCD camera.



**Figure 2.6:** WATEC 902B CCD camera



**Figure 2.7:** A PENTAX H1214-M (1/2')

### 3. The lens

The lens is an important factor for imaging quality. There are two basic parameters

for an optical lens: the focal length  $f$  and the maximum aperture  $D$ . The maximum available aperture of a lens is specified as the focal ratio or  $f$ -number  $F$  [Smith, 2005], which can be calculated by:

$$F = \frac{f}{D} \quad (2.1)$$

These parameters exert great effects on the optical performance (Table 2.2).

**Table 2.2:** Lens parameters and optical performance

Parameters	Optical Performance
Focal length (short)	Depth of focus: deep Distortion: high Vignetting: high
Aperture (small)	Illumination: weak Depth of field: deep Resolution: low
Image field (small)	Resolution in centre: high Illumination: Strong
Incident wavelength (short)	Resolution: high

As shown (2.2), some parameters are evaluated for optical performance. In the capturing system, a PENTAX H1214-M (1/2') lens was used (Figure 2.7). Its main parameters are listed (Table 2.3) in the following section.



**Figure 2.8:** The Mine 2860 USB capture card

#### 4. The Capture Card

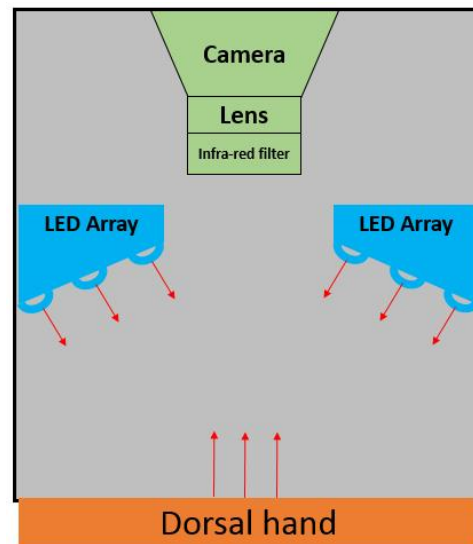
The capture card transforms data and converts Analogue/Digital (A/D) to digital image processing in the PC. Depending on CCD camera choice, several parameters have to be considered: colour depth, decoder mode, output resolution, interface mode and Software Development Kit (SDK). Based on the acquisition system, a Mine 2860 USB capture card was employed (Figure 2.8). And the Mine 2860 USB capture card parameters are shown (Table 2.3) in the following section.

### 2.2.4 Hardware

Figure 2.9a shows the capturing hardware. The hand reflects NIR light coming from infrared LED arrays to CCD sensors through an infrared filter and lens, forming an image of the dorsal hand. As illustrated in Figure 2.9b, the acquisition system was composed of an illumination and an imaging module: the green constitutes the imaging module and the blue shows the illumination module.



(a) The capturing hardware



(b) Schematic of the DHV image acquisition system

**Figure 2.9:** (a) The capturing hardware: the hand reflects NIR light coming from infra-red LED arrays. (b) Schematic of the DHV image acquisition system: the green (camera, lens and infra-red filter) represents the imaging module and the blue indicates the illumination module and the black line surrounding the diagram indicates a box, covering the illumination and imaging components to reduce visible light.

As discussed, the main parameters of the hardware implemented in the dorsal hand vein system are concluded and listed in Table 2.3.

**Table 2.3:** Components and main parameters of acquisition devices [Li, 2013]

Modules	Components	Parameters
<b>Illumination</b>	2 Near infra-red LED series (reflection)	Size: $\varnothing$ 8mm LED Type: Round LED Power: $1.5V \times 200mA$ Wavelength: 850nm Array Series: $3 \times 3$ Lighting distance: 100mm Distance between 2 LED series: 56mm
	Camera: WATEC 902B CCD (1/2')	Size: $35.5 \times 36 \times 58mm$ Scanning system: 1/2 inch Resolution: 570 TVL Frame rate: 25 fps Effective pixels: $752 \times 582$ S/N: 50dB Power: $DC12V \times 160mA$ Minimum illumination: 0.003 Lux F1.2
<b>Imaging</b>	Lens: Pentax H1214-M(KP) (1/2')	Size: $\varnothing 34.0 \times 43.5mm$ Focal length: 12mm Relative aperture: F1.4 FOV(D/H/V,mm): (102.3 47.6/81.3 38.2/60.4 28.7)
	Optical filter: 850nm	Size: $\varnothing 30.0 \times 3mm$ Half-main-lobe width: 6010nm Transmittance: 91.99%
	Capture card: Mine V2860 USB	Size: $103 \times 60 \times 19mm$ Interface port: USB 2.0 Standard: PAL, NTSC Resolution: $640 \times 480$ Dynamic adjusting

## 2.3 Database

A database of dorsal hand vein images was created based on NIR imaging. The database was divided into two categories: a static and a dynamic database. Both databases were captured using the devices as previously mentioned. Also, participants were told to hold their hands steady during image capture.

The target aged participants were from an elderly activity centre in NCUT, where most people were over 60 years old. The capturing process was carried out according to capturing agreements and protocols with the participants. Acquisition time took approximately one week, three hours per day, including waiting times.

### 2.3.1 Static dorsal hand vein images

With regard to the age between old and young groups, individuals older than 60 years were defined as “old” and those younger than 30 were defined as “young” in this research. The static DHV database contained approximately 1000 images from 50 individuals, of which 40 were termed as “old” and the rest (10) were termed as “young”. Ten images of each hand were captured from each participant. The left and the right hand were placed alternately under the imaging device and images captured.

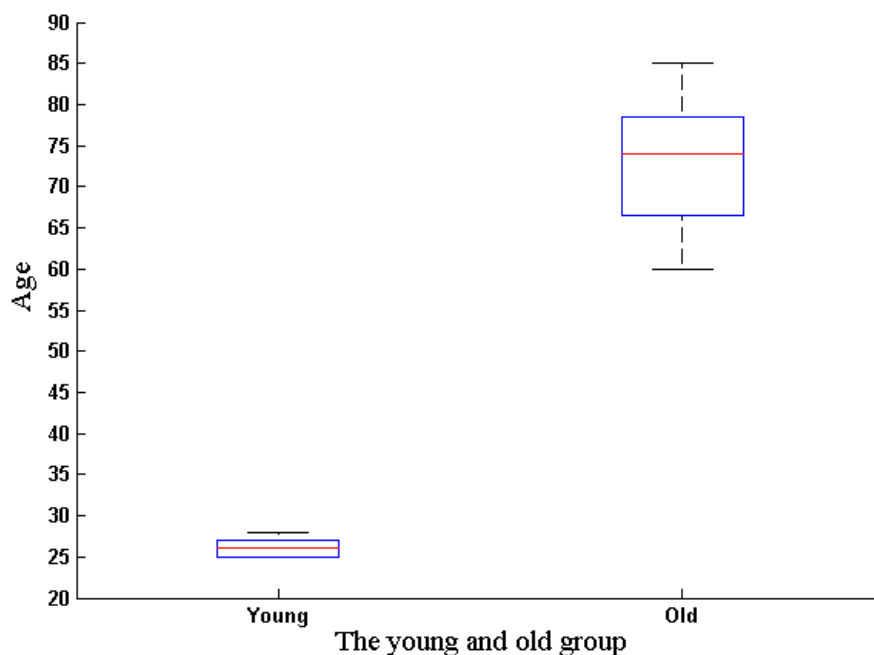


**Figure 2.10:** Age distribution of young and old groups

As shown (Figure 2.10), the 10 young participants had an average age of 26, with smaller deviations than those of the old group. The median age of the old group was 75 years old. For more details see **Appendix A**. Since no databases of dorsal hand vein images existed for this aged group, this work was instrumental in setting up a new DHV

image database for the classification of young and old people, based on near infra-red dorsal hand vein biometrics. Figure 2.11 and 2.12 show some DHV images from old and young participants.



**Figure 2.11:** DHV images from old participants



**Figure 2.12:** DHV images from young participants

### 2.3.2 Dynamic dorsal hand vein images

Dynamic DHV images are the video records of specific participants acquired during static DHV image capturing. Since the capturing process was designed mainly for old group, and considering the capturing time suitable for old people, a short period (10 seconds) of video recordings were conducted on those participants who agreed.

**Table 2.4:** Video parameters

Video Type	AVI
Length	10 seconds
Frame Rate	25 frames/second
Resolution	640 × 480

All videos were recorded as grey images at 25 frames per second (fps) with a pixel resolution of 640 × 480. Images were saved in AVI format (Table 2.4).

Not all old participants agreed to endure the 10s video capturing; in total there were 40 video recordings from 20 old participants, each having their left and right hand recorded.

Some videos of young participants were captured as possible supplements for comparative studies.

## **2.4 Concluding Remarks**

In this chapter, NIR imaging methods and the databases used for storage were described. The capturing system was based on low-cost and non-invasive principles, factors easily adopted when exploring biometric applications. Since nearly all dorsal hand vein databases are static and used for personal identification, it would be innovative to investigate old dorsal hands by establishing a database of old DHV images. In addition, establishing the video based DHV database was also important for dynamic analysis. Based on the principle of NIR imaging and age distributions within the database, further biometric applications beyond personal identification will be discussed later.

# Chapter 3

## DORSAL HAND VEIN IMAGE PRE-PROCESSING

### 3.1 Introduction

In general, most of the dorsal hand vein images collected contained not only vein structures but other information such as knuckles and fingers, which was redundant for this research. The original vein images could not be used for direct features extraction for the following reasons: geometrical variations such as shift, rotation and scale caused by different hand poses, non-uniform and non-constant illumination resulting in different image qualities and inherent noise in the vein images.

Therefore for this research, pre-processing methods were applied prior to segmentation of the vein images. To ensure that key features relevant to hand orientation were maintained, geometry correction was done prior to the extraction of regions of interest (ROI) from dorsal hand vein images. Grey-level processing methods, including image normalisation and filtering, were employed followed by image enhancement to enlarge image contrast for segmentation of vein patterns and skin areas.

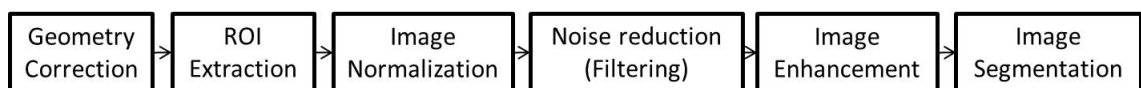


**Figure 3.1:** Pre-processing of DHV images

## 3.2 Geometry Correction

Geometry correction was divided as plane (2D) or space (3D) corrections. In this research, the former correction method was adopted. It is based on affine transformation including shift, scaling, shearing and rotation (Figure 3.2).

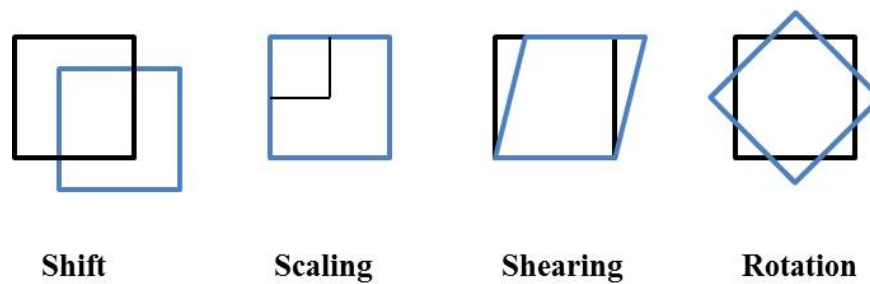


**Figure 3.2:** Affine transformations

Based on the databases established by this research, there were no shifts, scaling or rotation effects thanks to the fixed cushion on which participants laid their hands. Shearing effects occurred over different DHV images, which may have led to different orientations (Figure 3.3). Thus, it was necessary to correct shearing effects by angle adjusting to generate good data from ROI extractions.

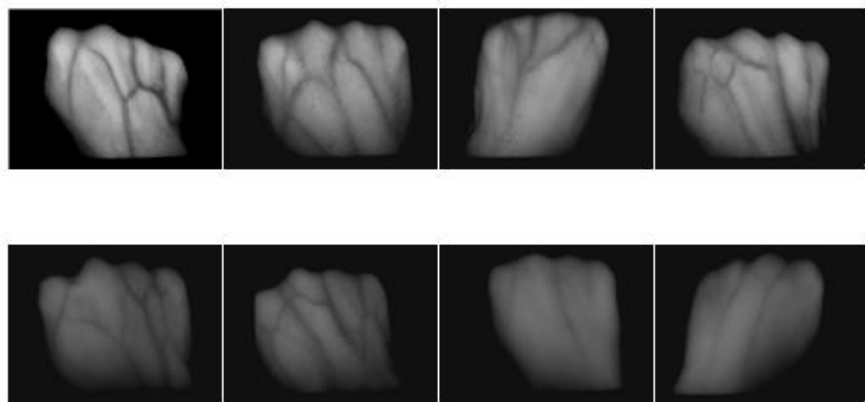


**Figure 3.3:** DHV images with shearing distortion

Geometry corrections comprised of:

1. *Calculating the centroid point of DHV images*

The binary image is first obtained using a global threshold, which can be regarded

as an irregular object (Figure 3.4). For a digital binary image denoted by  $F(x,y)$ , its centroid  $(x_0,y_0)$  can be calculated as:

$$x_0 = \frac{\sum_{i,j} i \times f(i,j)}{\sum_{i,j} f(i,j)}; \quad y_0 = \frac{\sum_{i,j} j \times f(i,j)}{\sum_{i,j} f(i,j)} \quad (3.1)$$

Where  $i, j$  represent the image coordinates and  $f(i,j)$  denote the grey value of the pixel  $(i,j)$ .



**Figure 3.4:** Calculating the centroid point (red) of DHV images

## 2. Finding the reference line and calculating the slope

After calculating the centroid point, four boundary points ( $P1, P2, P3, P4$ ) of the dorsal hand were obtained by setting two horizontal lines: one positioned at 50 pixels from the bottom and the other across the centroid point. Then, two middle points of the two lines are calculated as A and B, and the shearing factor determined, based on the slope of the connected line AB (Figure 3.5).

For this research, the slope is:

$$\theta = \tan^{-1} \frac{|AC|}{|BC|} \quad (3.2)$$

Where  $C$  is the vertical projection of  $B$ .

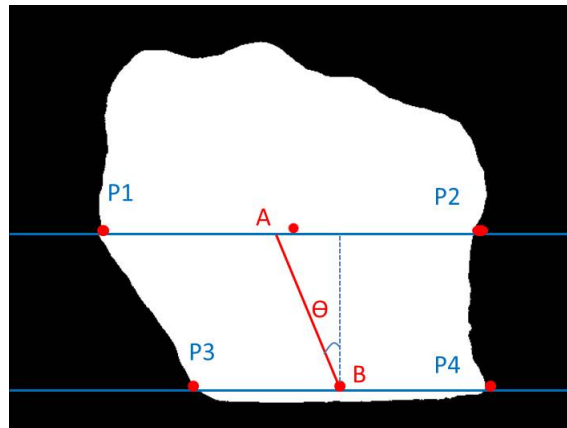


**Figure 3.5:** Shearing correction

With the use of the shearing factor, the DHV images were corrected (Figure 3.6).

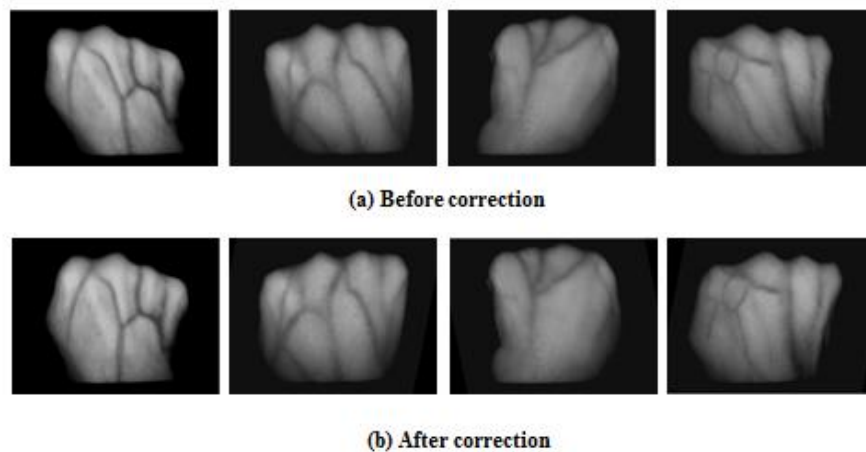


**Figure 3.6:** Shearing correction examples

### 3.3 Region of Interest Extraction

For dorsal hand vein features, ROI extractions have been widely discussed [Kumar and Prathyusha, 2009; Li, 2013]. From the DHV static database, once the centroid point of a DHV image was calculated (as discussed previously), the ROI can be extracted by selecting a rectangular area, based on the centroid point.

The size of the square ROI was decided by comparing different  $R$  values (Figure 3.7).

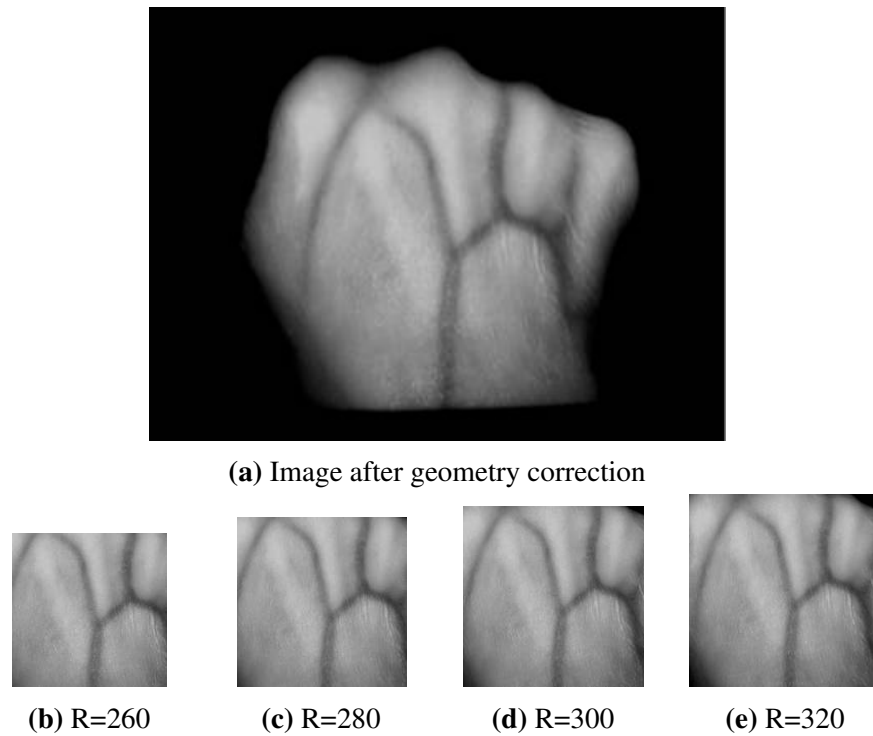


**Figure 3.7:** ROI extraction data

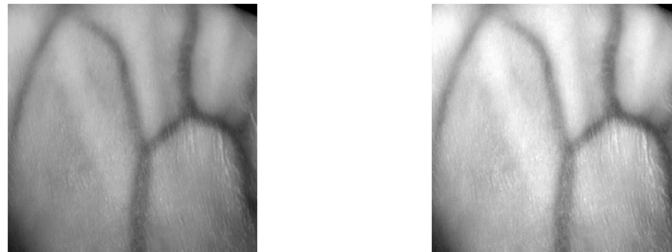
As seen from Figure 3.7, with different  $R$  value selections, dorsal hand vein information was different. When choosing  $R$  values above 300 pixels, redundant background information appears. DHV images with  $R = 260$  pixels contain less vein information than those of  $R = 280$  pixels and  $R = 300$  pixels. From the examination of all dorsal hands, the choice of  $R = 300$  pixels would include useful information with some redundant background information.

### 3.4 Grey-level Normalisation

To simplify segmentation and reduce illumination variations of DHV images, normalisation was carried out. In image processing, normalisation changes the range of pixel intensity values. The process transforms a grey-scale image  $f$  with intensity values in the range  $(f_{min}, f_{max})$ , into a normalised image  $N$ . The normalisation of a grey-scale digital image is performed according to the formula:

$$N = 255 \times \frac{f - f_{min}}{f_{max} - f_{min}} \quad (3.3)$$

Through normalisation, image contrast is stretched (Figure 3.8).



(a) Before normalisation

(b) After normalisation

**Figure 3.8:** Normalisation images

## 3.5 Noise Reduction

From NIR capture of dorsal hand veins, noise appeared almost everywhere. During imaging, randomness occurs in light entering a CCD camera, leading to noise. Inside the camera, dust also may affect imaging quality. Noise also appears during object capturing when the hand is not absolutely fixed. As noise is always unwanted in vein images, it was important to measure and remove noise during vein image pre-processing.

### 3.5.1 Noise measurement

Since veins mainly appeared in vertical directions along the dorsal hand, the grey value variations in images were often subjected to noise. Therefore, the grey level profiles along the middle row of a dorsal hand vein image was adopted as an example to illustrate the noise effect (Figure 3.9).

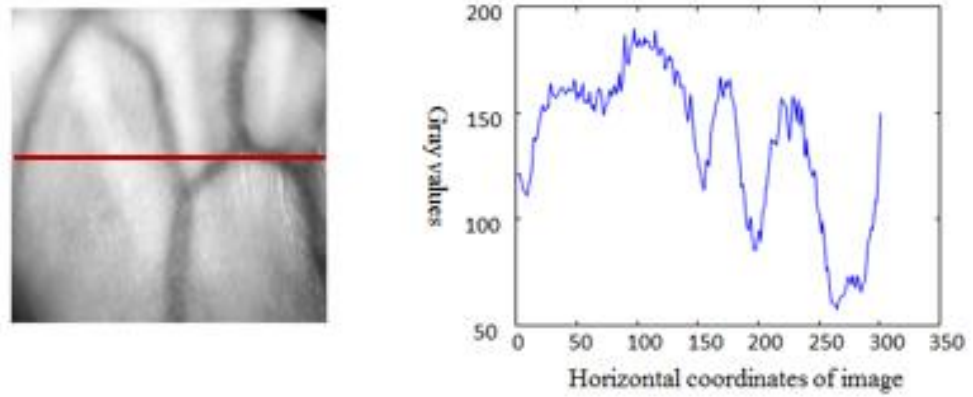


**Figure 3.9:** Profile of grey levels along the middle of an ROI image

Instead of a smooth grey level profile, there were significant local fluctuations throughout profiles due to noise effects. The low and high grey level values indicated vein and skin areas. To measure the extent of local fluctuations, a metric based on total variation (TV) was employed [Wang et al., 2010]:

$$TV(F) = \sum_i \sum_j [(f(i, j) - f(i-1, j))^2 + (f(i, j) - f(i+1, j))^2 + (f(i, j) - f(i, j-1))^2 + (f(i, j) - f(i, j+1))^2]^{1/2} \quad (3.4)$$

Where  $f(i, j)$  denotes the grey value of the pixel  $(i, j)$ .

$f(i-1, j-1)$	$f(i, j-1)$	$f(i+1, j-1)$
$f(i-1, j)$	$f(i, j)$	$f(i+1, j)$
$f(i-1, j+1)$	$f(i, j+1)$	$f(i+1, j+1)$

**Figure 3.10:** TV value pixels

### 3.5.2 Noise reduction

Different image filters were investigated and compared for noise reduction.

#### 1. Median filters

This method is nonlinear, and is used in image processing to reduce salt and pepper noise. The median filter works by moving through the image pixel by pixel, replacing each value with the median value of its neighbouring pixels. The pattern of neighbour is called the ‘window’. The median was calculated by first sorting all pixel values from the window into numerical order, and replacing the pixel with the middle (median) pixel value. In this work, a 2-D median filter [Lim, 1990] was applied for filtering (Figure 3.11b).

#### 2. Mean filter

Mean (or average) filtering is a method of ‘smoothing’ images by reducing the intensity variation between neighbouring pixels. The mean filter works by moving through the image pixel by pixel, replacing each value with the average value of its neighbour pixels, including itself. The filtering is processed by formula:

$$g(i, j) = \frac{1}{MN} \sum_{(i, j) \in S} f(i, j) \quad (3.5)$$

Where  $g(i, j)$  and  $f(i, j)$  denote the pixel values of the original and filtered image and  $S$  is the  $M \times N$  neighbourhoods. In this work, a square region was used with  $M \times M$  neighbourhood.

#### 3. Wiener filter

A Wiener filter is the most important approach for the removal of blur in images. The filter is designed based on the minimum mean-square error principle. In this work, a pixel-wise adaptive Wiener method was applied based on statistics estimated from the local neighbourhood of each pixel [Lim, 1990]. It estimates the local mean

and variance around each pixel:

$$\mu = \frac{1}{NM} \sum_{n_1, n_2 \in \eta} a(n_1, n_2) \quad (3.6)$$

$$\sigma^2 = \frac{1}{NM} \sum_{n_1, n_2 \in \eta} a^2(n_1, n_2) - \mu^2 \quad (3.7)$$

Where  $\eta$  is the  $N$ -by- $M$  local neighbourhood of each pixel in the image A. Then a pixel-wise Wiener filter is created using these estimates,

$$b(n_1, n_2) = \mu + \frac{\sigma^2 - v^2}{\sigma^2} (a(n_1, n_2) - \mu) \quad (3.8)$$

Where  $v^2$  is the noise variance. In this work, as the noise was not known, the average of all the local estimated variances were used.

#### 4. Gaussian filter

A Gaussian filter is similar to the mean filter, but it uses a different kernel shape, like a Gaussian hump. In image processing, the Gaussian filter is a 2-D convolution operator used to remove detail and noise in an image. The Gaussian function can be expressed as:

$$g(x, y) = \frac{1}{2\pi\sigma^2} e^{-\frac{x^2+y^2}{2\sigma^2}} \quad (3.9)$$

Where  $\sigma$  is the standard deviation of the Gaussian distribution. A Gaussian mask template is given by the formula (3.10) and (3.11) [Haddad and Akansu, 1991]. Different Gaussian kernel functions can be decided by choosing different standard deviations and template sizes  $M \times M$ ;

$$h(i, j) = \frac{h_g(i, j)}{\sum_i \sum_j h_g(i, j)} \quad (3.10)$$

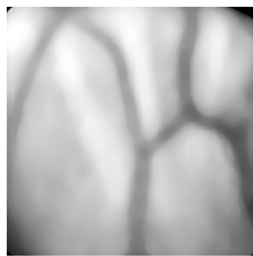
$$h_g(i, j) = e^{-\frac{i^2+j^2}{2\sigma^2}} \quad (3.11)$$

### 3.5.3 Filtering results

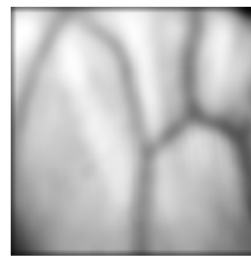
By observing vein pixels in DHV images, the width of the dorsal hand accounted for 10 to 15 pixels. Hence, all template windows used in filters were set to  $15 \times 15$  pixels. The setting of this template window size was to retain as much vein information as possible and reduce noise information. The filtered results of DHV images are shown in Figure 3.11.



(a) Original normalised ROI image



(b) Median filtered



(c) Mean filtered



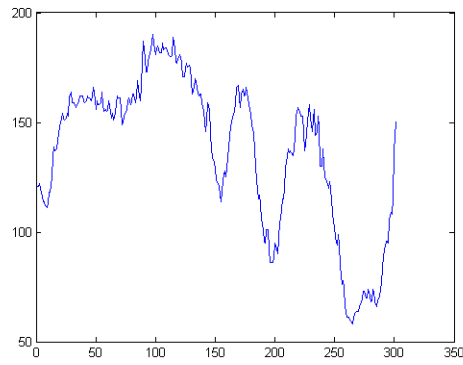
(d) Wiener filtered



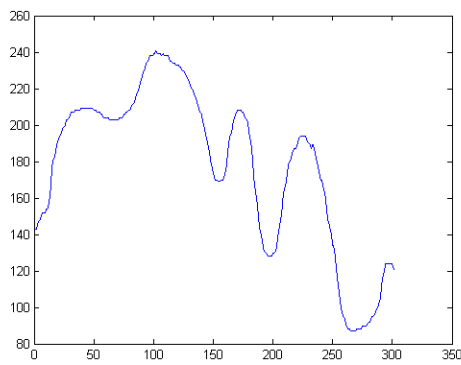
(e) Gaussian filtered

**Figure 3.11:** Results of filtering

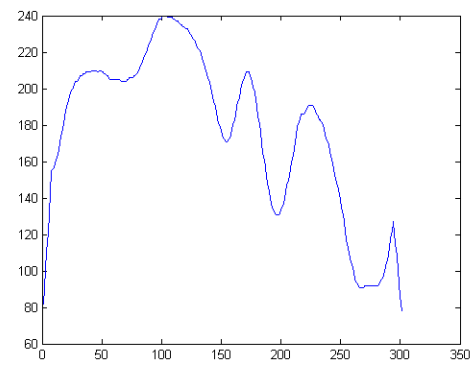
It can be seen from the filtering results (Figure 3.11), that images become smoother. To further compare these results (Figure 3.11), the grey value profiles of the middle row were plotted for each filtered image in terms of noise measurement (Figure 3.12).



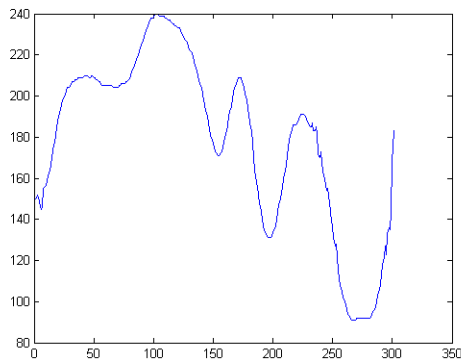
(a) Original profile



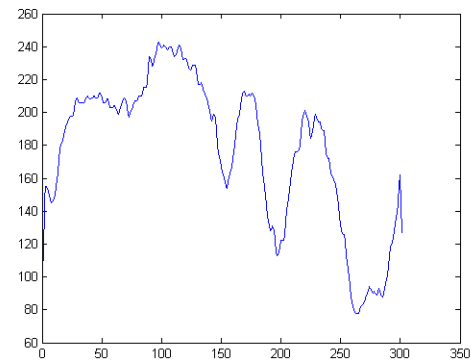
(b) Profile after Median filtering (M=15)



(c) Profile after Mean filtering (M=15)



(d) Profile after Wiener filtering (M=15)



(e) Profile after Gaussian filtering (M=15,  $\sigma=1$ )

**Figure 3.12:** Grey level profiles of middle row forms before and after filtering images. The X-axis represents the pixel position, and Y-axis represents the grey level.

**Table 3.1:** TV values comparison

	Before Filtering	After Filtering			
		Median	Mean	Wiener	Gaussian
<b>TV</b>	2403.0	1121.0	1315.2	1124.3	1607.3

For Gaussian filtering, the parameter  $\sigma$  was set to 1 based on the comparison between TV values obtained from Gaussian filtered images. All filtered results were further measured by calculating their TV (Table ). In this work, the Median filtering was used as it had the lowest TV value.

### 3.6 Image Enhancement

Image enhancement improves the interpretability or perception of information in images for viewers. It provides better inputs for further image processing. Therefore, it was optimal to apply image enhancement to enhance contrast and visibility of vein images before segmentation.

- *Histogram equalisation (HE)*

Histogram equalisation is a common technique for enhancing the appearance of images. Before histogram equalisation, the intensity levels are changed so that histogram peaks are stretched and valleys are compressed [Kadhum, 2012]. If an image has  $N$  pixels distributed in  $L$  discrete intensity levels and  $n_k$  is the number of pixels with intensity level  $i_k$ , then the probability density function (PDF) of the image is given by Equation (3.12). The cumulative density function (CDF) is defined in Equation (3.13).

$$f_i(i_k) = \frac{n_k}{N} \quad (3.12)$$

$$F_k(i_k) = \sum_{j=0}^k f_i(i_j) \quad (3.13)$$

For histogram equalisation techniques, the PDF is manipulated. It changes the PDF of a given image to generate a uniform PDF. The CDF is a self-contradictory phrase, resulting from confusion between probability functions and cumulative distribution functions. One drawback of this method is that it may increase the contrast of the background noise, while usable information is decreased (Figure 3.13).

- *Contrast Limited Adaptive Histogram Equalisation (CLAHE)*

For image enhancement, Pizer et al., proposed an improved HE algorithm called Contrast Limited Adaptive Histogram Equalisation (CLAHE) [Pizer et al., 1987]. The method operates on small regions in the image rather than the entire image. However, it not only applies the partial histogram equalisation inside windows, but also takes into consideration its mapping within the global histogram. The algorithm is expressed as:

$$h_L(a) = \alpha h_w(a) + (1 - \alpha)h_G(a) \quad 0 \leq \alpha \leq 1 \quad (3.14)$$

Where  $h_L(a)$  is the partial normalised histogram;  $h_w(a)$  is the normalised histogram inside window;  $h_G(a)$  is the normalised histogram outside window and  $\alpha$  is the local weight.

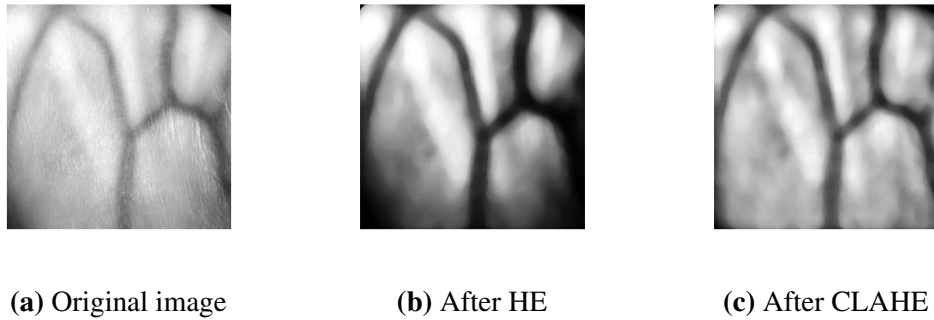


**Figure 3.13:** Image enhancements

The results of HE and CLAHE are shown (Figure 3.13). From the figure, it can be seen that all sharp edges are maintained after CLAHE, while after HE, parts of the skin areas are wrongly segmented as vein areas.

### 3.7 Concluding Remarks

In this chapter, DHV image pre-processing steps and methods were introduced. Regarding ROI extractions, thanks to the geometry correction of the original DHV images, the ROI was easily selected based on the centroid points of DHV images. Noise filters were investigated and discussed, with the median filter adopted as the ideal choice for noise reduction. Finally, the CLAHE image enhancement method was adopted to enhance contrast between vein and skin areas on dorsal hand images. This provided better ‘quality’ images for segmentation.

# Chapter 4

## DORSAL HAND VEIN SEGMENTATION

### 4.1 Introduction

Image segmentation divides images into a number of specific, unique areas. It is a key step spanning image processing and image analysis. Current image segmentation methods are divided into the following categories: threshold-based segmentation methods, region-based segmentation methods, edge-based segmentation methods and segmentation methods based on specific theory.

For those dorsal hand vein images captured under near infra-red light, the unique regions of interest are the veins and the skin areas. Considering the vast computing times, nearly all researchers have adopted threshold-based algorithms [Otsu, 1975; Wang and Leedham, 2006; Wang et al., 2010].

In this research, some threshold-based methods were studied and compared for improved segmentation of DHV images. To improve extraction of vein patterns and segment them with skin areas, a theory based on the curvature of vein image profiles was used [Miura et al., 2007]. Morphological filtering methods were adopted for further post-processing of segmented DHV images.

## 4.2 Segmentation Algorithms

### 4.2.1 Threshold methods

The threshold based algorithm is the simplest way of image segmentation. It uses a threshold to create binary images from grey-scale images. Whether fixed or local dynamic thresholds, the threshold methods are based on the following principles:

$$g(x,y) = \begin{cases} 255, & f(x,y) > T \\ 0, & f(x,y) \leq T \end{cases} \quad (4.1)$$

Where  $g(x,y)$ , denotes the image after threshold based segmentation,  $f(x,y)$  is the original image and  $T$  is the threshold value.

#### 1. Otsu's method

The premise of this method is to determine the threshold value, where the sum of foreground and background spreads is at a minimum, which means the intra-class (within-class) variance is minimal [Otsu, 1975]. This turns out to be the same as maximising the inter-class (between-class) variance.

Consider the pixels of a given image be represented in  $L$  grey levels, and the threshold is  $t$ . The pixels are divided into two classes: *class 1* and *class 2*, whose probabilities are estimated as:

$$q_1(t) = \sum_{i=1}^t P(i) \quad q_2(t) = \sum_{i=t+1}^L P(i) \quad q_1(t) + q_2(t) = 1 \quad (4.2)$$

And the class means are given by:

$$\mu_1(t) = \sum_{i=1}^t \frac{iP(i)}{q_1(t)} \quad \mu_2(t) = \sum_{i=t+1}^L \frac{iP(i)}{q_2(t)} \quad (4.3)$$

The mean grey level value over the whole image (grand mean) is

$$\mu = \sum_{i=1}^t iP(i) \quad (4.4)$$

The individual class variances are:

$$\sigma_1^2(t) = \sum_{i=1}^t [i - \mu_1(t)]^2 \frac{P(i)}{q_1(t)} \quad (4.5)$$

$$\sigma_2^2(t) = \sum_{i=t+1}^L [i - \mu_2(t)]^2 \frac{P(i)}{q_2(t)} \quad (4.6)$$

And variance of the whole image is:

$$\sigma^2 = \sum_{i=1}^L (i - \mu)^2 P(i) \quad (4.7)$$

The weighted intra-class variance is:

$$\sigma_w^2(t) = q_1(t)\sigma_1^2(t) + q_2(t)\sigma_2^2(t) \quad (4.8)$$

To pick the value that minimises  $\sigma_w^2(t)$ , the full range of  $t$  values would be run through. But the relationship between the intra-class and inter-class variances can be exploited to generate a recursion relation that permits a much faster calculation. For any given threshold, the total variance  $\sigma$  is the sum of the intra-class variances (weighted) and the inter-class variance:

$$\sigma^2 = \sigma_w^2(t) + \sigma_B^2(t) \quad (4.9)$$

Since the total is constant and independent of  $t$ , the effect of changing the threshold is merely to move the contributions of the two terms back and forth. Hence, minimising

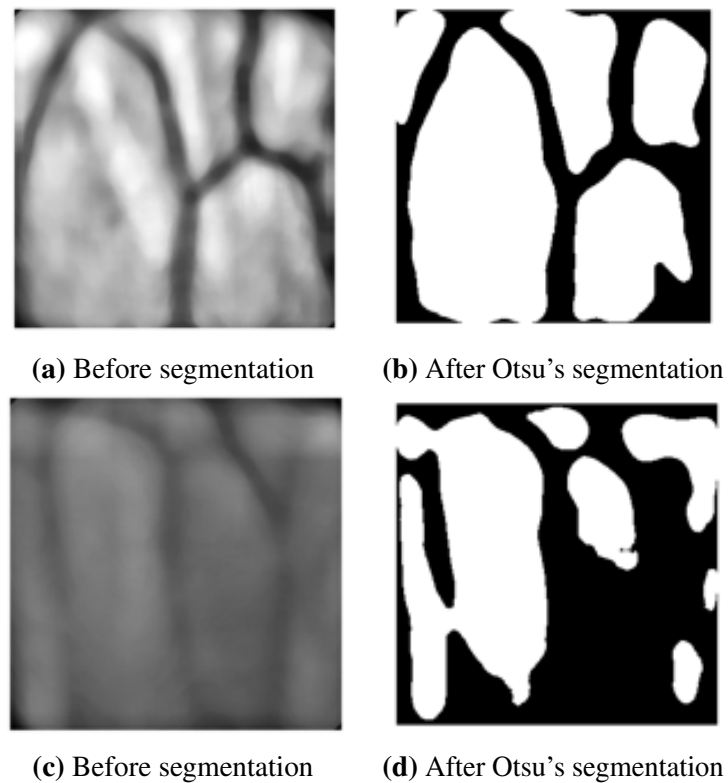


**Figure 4.1:** Otsu's segmentation

the intra-class variance is the same as maximising the inter-class variance.

$$\sigma_B^2(t) = q_1(t)[1 - q_1(t)][\mu_1(t) - \mu_2(t)]^2 \quad (4.10)$$

Now, the quantities in  $\sigma_B^2(t)$  could be computed recursively as we run through the range of  $t$  values to get the threshold that maximise  $\sigma_B^2(t)$ .

Since the threshold of this method is fixed, it often results in under-segmentation in some parts of the image and over-segmentation in others. In Figure 4.1d, the vein area is over-segmented as the threshold value is too low for that part of the image. In general, single fixed thresholds cannot meet the demands of good segmentation.

## 2. Niblack's method

As a local dynamic threshold method, Niblack's algorithm is effective in image segmentation [Niblack, 1985]. The main idea of the segmentation method is calculating the mean  $m(x,y)$  and variance  $s(x,y)$  of the points in  $r \times r$  neighbourhood

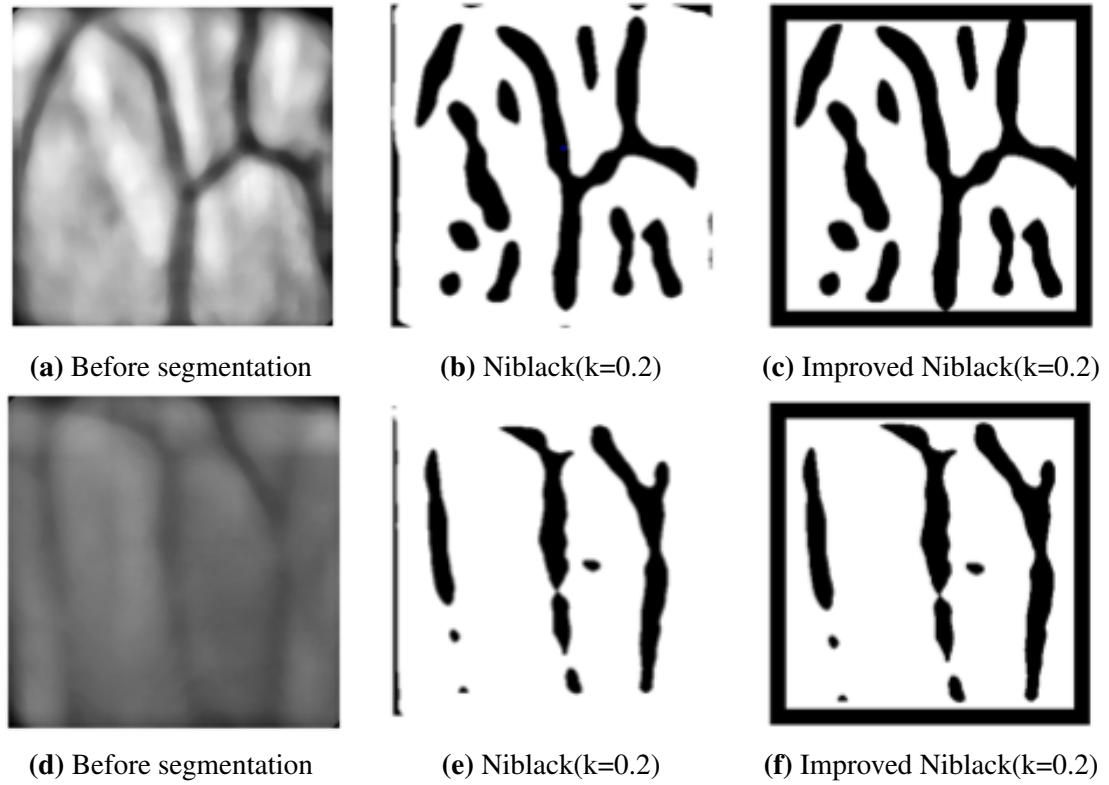


**Figure 4.2:** Niblack segmentation

of every pixel, then segmentation is carried out using *Equation (4.10)*,

$$\sigma_B^2(t) = q_1(t)[1 - q_1(t)][\mu_1(t) - \mu_2(t)]^2 \quad (4.11)$$

Where,  $T(x,y)$  is the threshold,  $k$  is the coefficient of correction. If a pixel value is lower than the threshold, it can be considered as a pixel from the vein area. An improved Niblack method was proposed by [Shi and Yi-Ding, 2008] who changed the calculation of the variance  $s(x,y)$  as:

$$s(x,y) = \sqrt{\frac{1}{r^2} \sum_{i=x-r/2}^{x+r/2} \sum_{j=y-r/2}^{y+r/2} ((f(i,j) - m(x,y))^2)} \quad (4.12)$$

In this work,  $r$  value is set to 15, reflecting the average vein width in DHV images was approximately 10 to 15 pixels. There will be missing vein information when  $r$  is too small, and the vein will be cut when  $r$  is too big. The correction coefficient  $k$  is determined by experiments. If  $k$  is too small, some skin area will be mistaken for vein area. If  $k$  is too

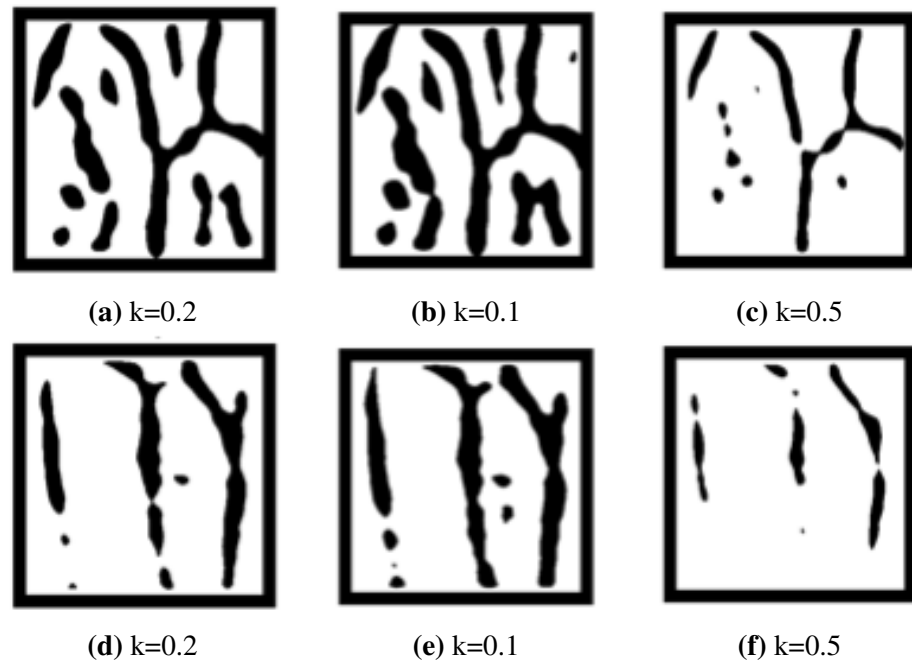


**Figure 4.3:** Comparative segmentation data using different  $k$  selections

big, some vein area will be missed. In this work,  $k$  was set to 0.2. Figure 4.2 shows the images after Niblack and improved Niblack methods. Figure 4.3 shows the influence of segmentation results using different  $k$  selections.

As can be seen (Figure 4.1 and Figure 4.2), the Otsu' method performed better than Niblack's method when analysing old hands with more complete hand patterns. However, using the improved Niblack's method was much better when processing samples from young hands.

It was concluded that these threshold based algorithms were not robust enough for the segmentation of DHV images. Therefore, a specific method using the maximum curvature of the vein image profiles was employed.

#### 4.2.2 Maximum curvature based segmentation

This section describes an algorithm used in the extraction of finger vein patterns [Miura et al., 2007]. The algorithm robustly extracted vein patterns when vein width and brightness fluctuated. The idea of the algorithm was to develop a method of calculating local maximum curvatures in cross-sectional profiles of vein images. In this research, the robust algorithm was adopted for dorsal hand vein pattern extraction and segmentation:

## 1. Find the vein centre

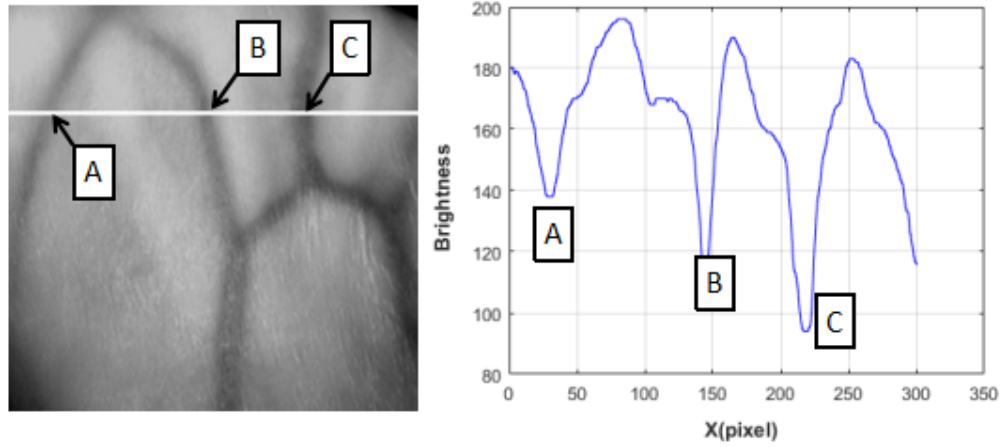


**Figure 4.4:** Cross-sectional profile of veins

As shown (Figure 4.4), the cross-sectional profile of a vein looks like a dent, since the vein is darker than the surrounding skin. These concave curves have large curvatures, thus the vein centres can be obtained by calculating local maximum curvatures in cross-sectional profiles.

Let  $F$  be an ROI image of DHV, and  $F(x,y)$  is the intensity of pixel  $(x,y)$ .  $P_f(z)$  is defined as a cross-sectional profile acquired from  $F(x,y)$  at any direction and position, where  $z$  is a position in a profile. Then the curvature  $c(z)$  can be represented as:

$$c(z) = \frac{d^2P_f(z)/dz^2}{\left[1 + (dP_f(z)/dz)^2\right]^{\frac{3}{2}}} \quad (4.13)$$

A profile is classified as concave or convex depending on whether  $c(z)$  is positive or negative. Thus the local maximums of  $c(z)$  in each concave area is calculated. These points indicate the centre positions of the veins. The positions of these points are defined as  $z'_i$ , where  $i=0,1,\dots,N-1$ , where  $N$  is the number of local maximum points in the profile. Scores are then assigned to the centre positions. A score  $S_{cr}(z)$ , is defined as follows:

$$S_{cr}(z'_i) = c(z'_i) \times W_r(i) \quad (4.14)$$

Where,  $W_r(i)$  is the width of the region where the curvature is positive and one of the  $z'_i$  is located. The width and the curvature of regions are considered in their scores, which are assigned to a plane,  $V$ , that is:

$$V(x'_i, y'_i) = V(x'_i, y'_i) + S_{cr}(z'_i) \quad (4.15)$$

All profiles are analysed in four directions: horizontal, vertical and vertical at  $45^\circ$ . Then, all centre positions of the veins are located.

## 2. Connecting vein centres

In this step, two neighbouring pixels on the right and left sides of pixel  $(x, y)$  are checked first. An operation is then applied to all pixels, represented as follows:

$$G_{d1}(x, y) = \min \{ \max(V(x+1, y), V(x+2, y)) + \max(V(x-1, y), V(x-2, y)) \} \quad (4.16)$$

Accordingly, calculation of the other directions are made with  $G_{d2}(x, y)$ ,  $G_{d3}(x, y)$ ,  $G_{d4}(x, y)$  obtained. Lastly, a final image  $G(x, y)$  is obtained by selecting the maximum  $G_{d1}$ ,  $G_{d2}$ ,  $G_{d3}$  and  $G_{d4}$  for each pixel. That is,  $G = \max(G_{d1}, G_{d2}, G_{d3}, G_{d4})$ .

The advantage of using the maximum curvature method is the robustness of selecting vein patterns. The centre points extracted ensure that pixels are within the vein areas, which retains key vein information (Figure 4.8c) and **Appendix B**.

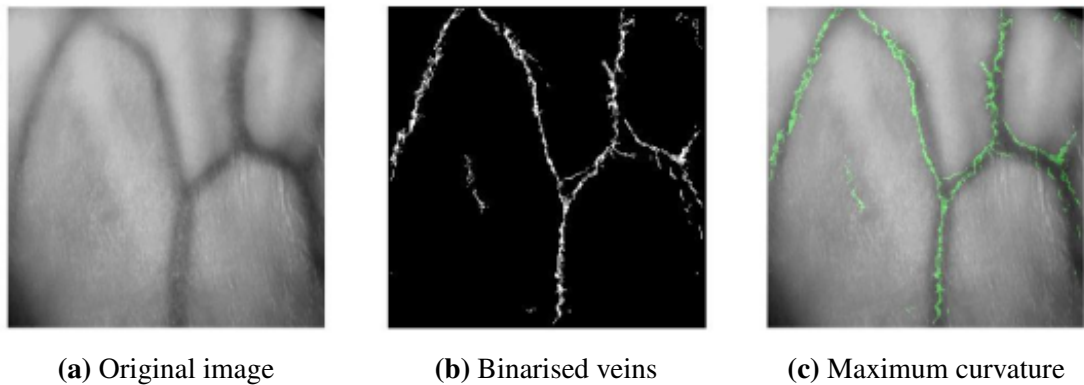


**Figure 4.5:** Dorsal hand vein segmentation using the maximum curvature method

### 4.3 Post-processing

As previously discussed, maximum curvature based segmentation algorithms can extract accurate vein pixels from the vein area. However, the segmentation process may cause new noise, such as spots, holes and burrs (Figure 4.6).

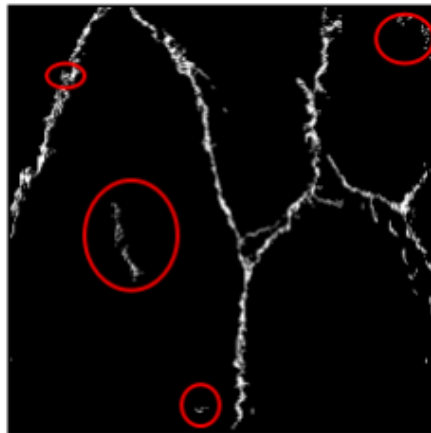


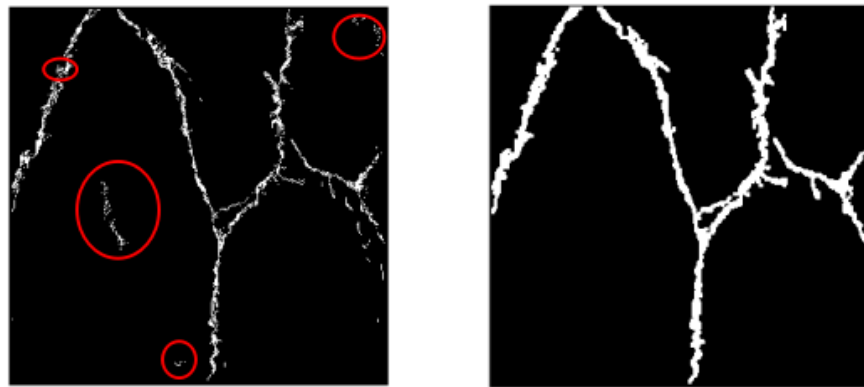
**Figure 4.6:** Wrongly segmented veins

To remove certain kinds of noise, which are caused by segmentation, morphological filtering methods are adopted for post-processing of vein images.

Opening and closing are the basic operations of morphological processing. Opening is operated with erosion followed by dilation. This process removes small objects in the foreground. On the other hand, closing is operated with dilation followed by erosion, which removes small holes [Serra, 1983].

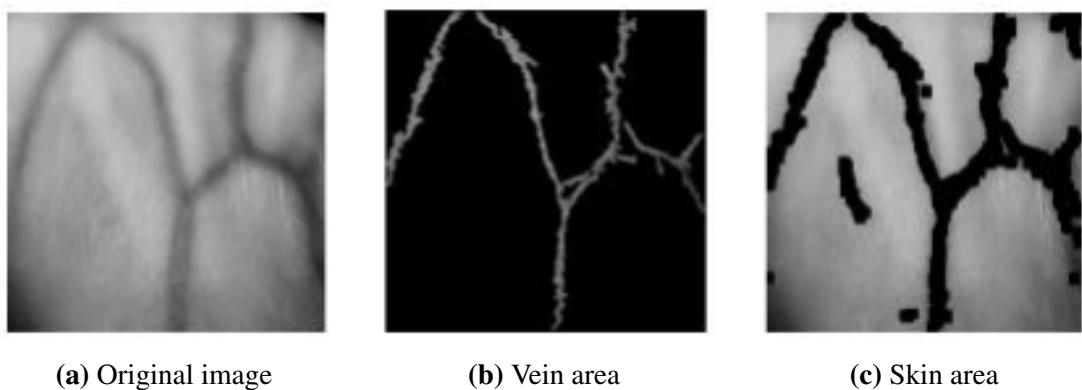
To remove small spots, segmented binary images are processed by closing followed by opening. Regarding some extra vein patterns, occupying only a small region (much smaller than the normal hand dorsal vein pattern) in most cases of the database, filters of removing small connected region are applied for cutting off the wrong pattern.

Figure 4.7 shows morphological filtering. Most spots are removed and holes filled, while the opening and closing operations lead to dilation of vein patterns. Since the vein pattern is extracted with the centre point of veins, the dilation process does not cause more noise when the filtering window size is small. Instead, the dilation process enriches vein pattern information.



**Figure 4.7:** Morphological processing

After post-processing, vein patterns are adjusted while skin areas are extracted by subtracting the whole image containing the dilated vein patterns. Figure 4.8 shows examples of veins and skin areas from one DHV image.



**Figure 4.8:** Segmented veins and skin areas from a DHV image

## 4.4 Concluding Remarks

In this chapter, some commonly used hand vein segmentation methods were investigated including Otsu, Niblack and improved Niblack. When using threshold methods, the segmentation results were satisfactory in high contrast areas, however, they bring noise to vein areas. This research adopted maximum curvature based algorithms for a more accurate vein pattern segmentation. The algorithm ensured the segmentation process retained key features of the veins, which extracts the centre points of all vein patterns. Similarly, the skin area was easily removed by subtracting the whole image from the dilated vein pattern. For better segmentation results, some morphological filters were discussed and used.

## **Chapter 5**

# **STATIC ANALYSIS OF DORSAL HAND VEIN IMAGES FOR BIOMETRIC APPLICATION**

### **5.1 Introduction**

In this research, the static dorsal hand vein image database can be divided into two groups: the old group (over 60 years old), and the young group, (under 30 years old). According to human dorsal hand attributes, age factors lead to differences between dorsal hands of young and the old. When viewed under near infra-red light, an old dorsal hand is different to a younger one. This quality makes it interesting to classify the two particular groups based on near infra-red hand vein biometrics.

The classification of old and young groups is conducive to the computing time of human identification using dorsal hand vein, which develops the vein biometric applications. On the other hand, the classification will be fundamental to research of age detection of people using dorsal hand vein biometrics, which explores further biometric applications.

This chapter focuses on features of the dorsal hand from two perspectives: consideration of dorsal hand images as a whole and consideration of segmented veins and skin areas separately. Regarding these features, intensity based statistics were investigated because

the skin and veins have different optical responses to infrared light. Both vein and skin features were investigated for classification of both groups. Additionally, other classifiers were introduced and studied.

## 5.2 Statistical Parameters Analysis

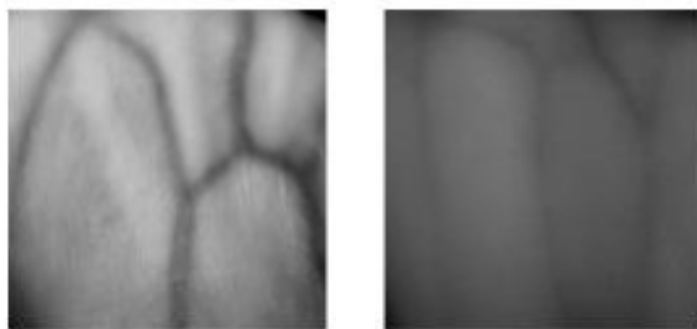
When one gets old, both haemoglobin and water levels change, indicating that intensity levels are different between old and young DHV images when viewed under near infrared light. This section therefore, introduces intensity based parameters of DHV images considering integral areas, vein and skin areas.

### 5.2.1 Histogram analysis

Histograms are statistical representations of features, they are the basis for numerous spatial domain processing techniques. Through analysis of DHV histogram images, the distribution of intensity can be calculated.

- *Histograms of ROI images*

DHV ROI images from aged groups were found to be brighter than those from young groups (Figure 5.1). Similarly, image contrasts were higher in old dorsal hands when compared to young dorsal hands (Figure 5.1). This suggests histogram distributions from both images would be different.



(a) ROI from the old group      (b) ROI from the young group

**Figure 5.1:** ROI images of old and young veins

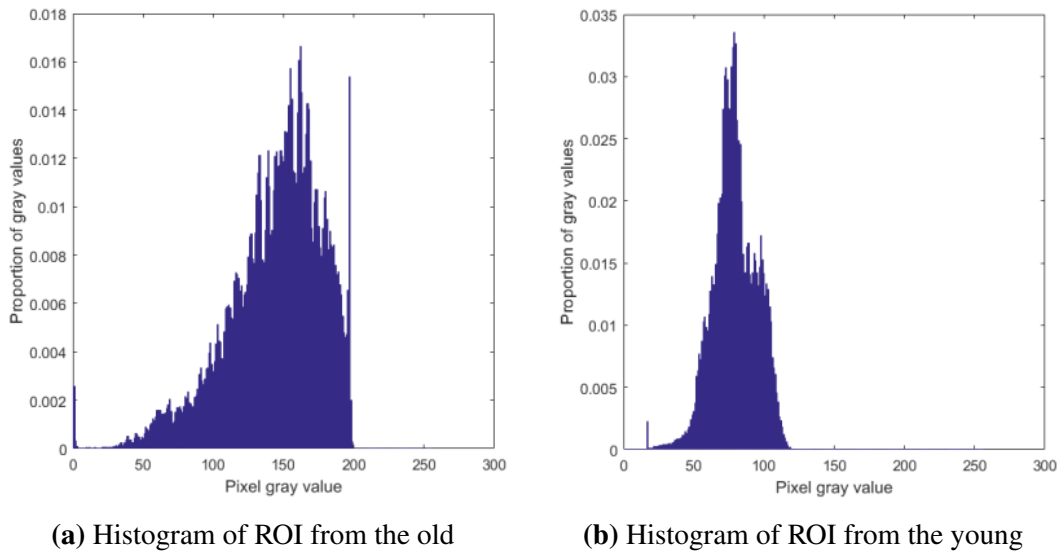
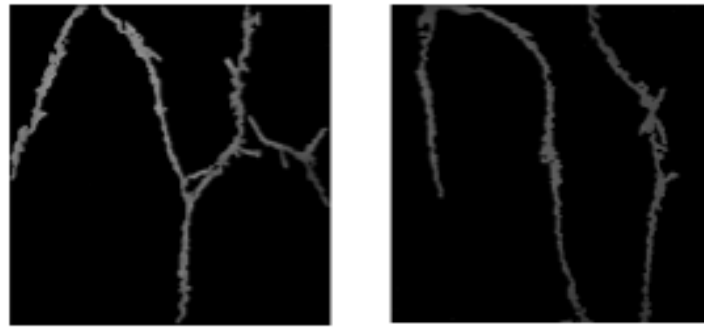


**Figure 5.2:** Histograms of ROI images from old and young veins

As can be seen (Figure 5.2), histogram distribution centres are different between old and young DHV images, suggesting dorsal hand vein images of the young appear darker than those from old groups. These ROI histograms are compatible with the fact that old dorsal hands appear brighter than young dorsal hands under NIR light, due to decreasing haemoglobin and water levels in veins and skin tissue, respectively. To further confirm these differences and investigate the impact of haemoglobin and water levels, vein and skin areas were analysed separately.

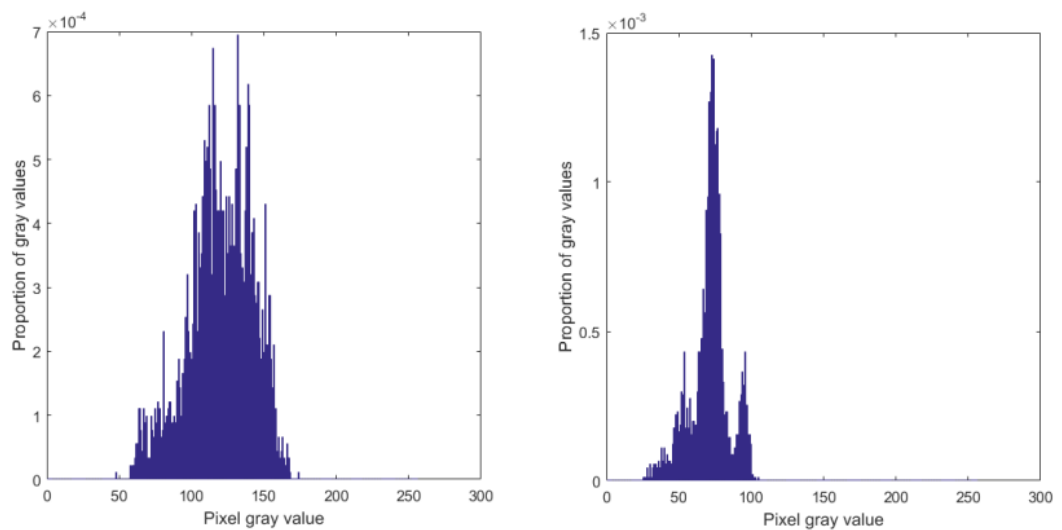
- *Histograms of vein areas*

For DHV images, vein areas are much smaller than those of the skin. Similarly, blood levels are lower than water levels in the skin area. However, vein areas do contain venous blood, of which haemoglobin levels decrease as a dorsal hand gets older. Thus, it was significant to analyse vein area histograms for classification.



(a) Vein image of old veins      (b) Vein image of young veins

**Figure 5.3:** Vein image of old and young veins



(a) Vein histogram from old hands

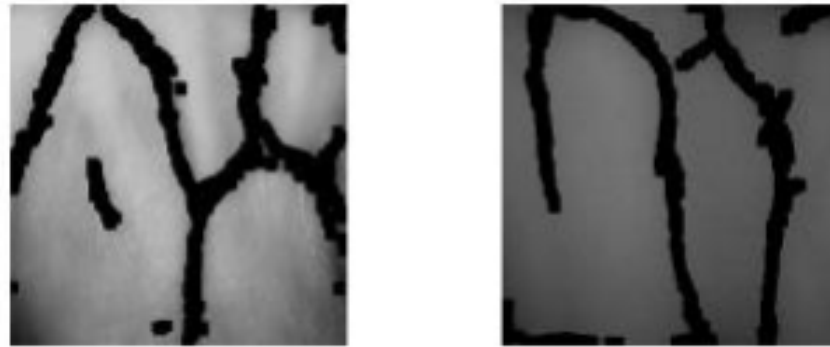
(b) Vein histogram from young hands

**Figure 5.4:** Histograms of vein areas from old and young hands

Figure 5.4 shows the different intensity distributions between old and young groups. For vein areas, intensities appeared brighter from aged groups when compared to young groups. These differences prove that haemoglobin levels decrease when individuals start to get old [Botonjic-Sehic et al., 2009].

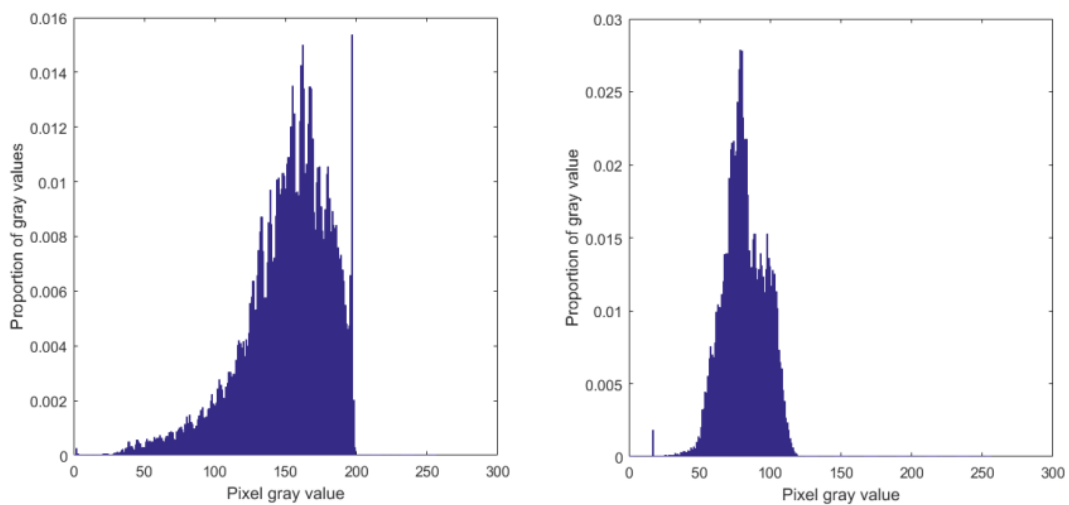
- *Histograms of skin areas*

As for most dorsal hands, the skin occupies most of the area. Hence, histograms of skin areas would be as similar as the whole ROT histogram. However, despite the vein area, it was significant to investigate histograms of skin areas to ascertain differences (if any) between old and young groups.



(a) Skin image of old participants

(b) Skin image of young participants

**Figure 5.5:** Vein image of old and young veins

(a) Skin histogram from old participants

(b) Skin histogram from young participants

**Figure 5.6:** Histograms of skin areas from old and young participants

As observed (Figure 5.6), distribution of skin areas from old and young participants were similar to that of ROI histograms. These data verified that with increasing age, skin becomes brighter under NIR light, due to decreasing water levels. In appearance, skin from the dorsal hand of the aged group appeared tight and loose.

### 5.2.2 Statistical parameters

As discussed previously, histograms reflect the intensity differences between old and young groups. These histogram distributions led to the analysis of all dorsal hands to confirm these results. Every pixel grey level in DHV images was directly related to the intensity, which indicated the absorption activity of NIR light. Considering computing time, it was necessary to examine basic statistical parameters of intensities from all dorsal hands. In this work, the statistical parameters were extracted as: maximum, minimum, mean, median, mode and standard deviation (Figure 5-7).

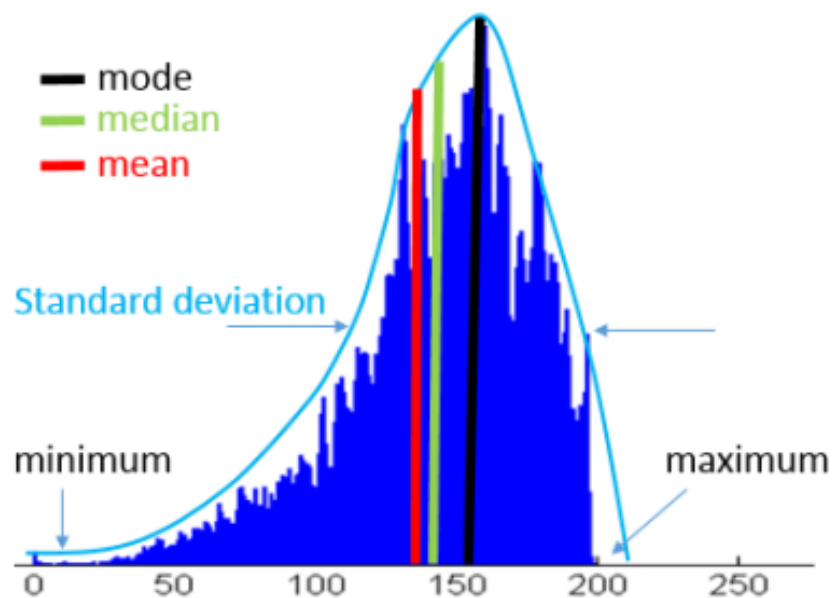


**Figure 5.7:** Sketch map of statistical parameters

In the static DHV database, images were derived from 40 old people and 10 young people. Since DHV images differ between the left and the right hand, the database contained a total of 100 hands. For 100 dorsal hands, 100 DHV images of ROI ( $300 \times 300$ ) were selected for statistical analysis. All basic statistical parameters were extracted from each hand. Boxplots examined the overall distribution of the 100 hands.

For all boxplots presented, the line at the centre of each boxplot reflected the median value of the data, and the top and bottom edges were 75% and 25% of the data. ‘Outliers’ were shown by (+) in red.

### 1. Minimum grey levels

Using minimum grey values of skin area was unreliable (Figure 5.8). This was

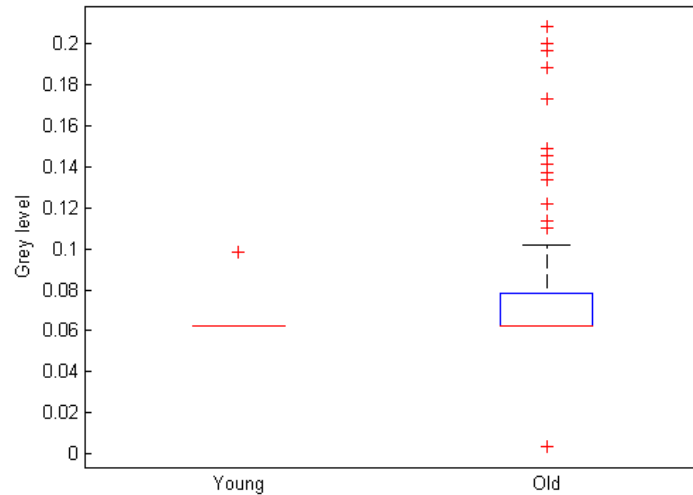


**Figure 5.8:** Comparison of hands from young and old groups based on minimum grey levels of skin areas

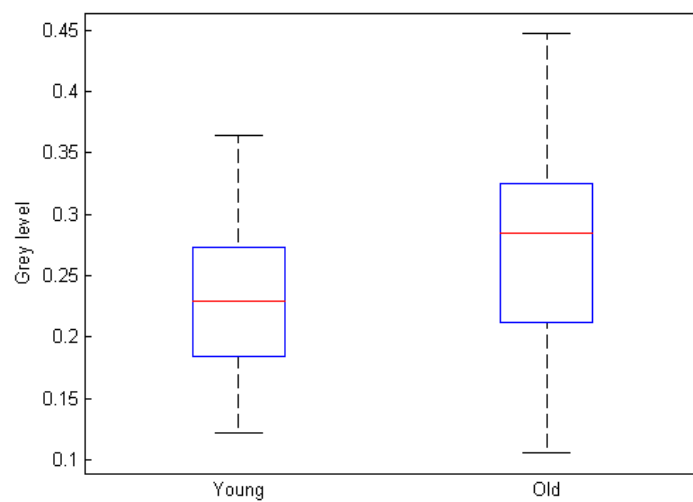


**Figure 5.9:** Comparison of hands from young and old groups based on minimum grey levels of vein areas

because, it was difficult to ascertain differences between the two groups from 100 dorsal hands, since the minimum grey value usually refers to 'noise'. Regarding vein areas, the differences exist, but are not obvious.

## 2. Maximum grey levels

When using maximum grey values of skin area from DHV images, differences

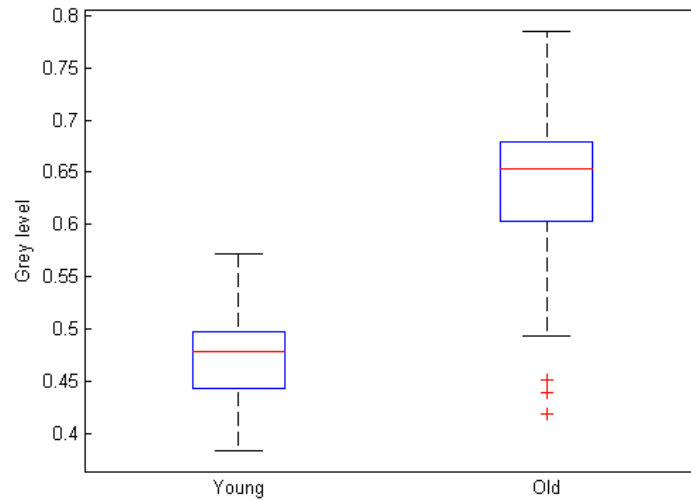


**Figure 5.10:** Comparison of hands from young and old groups based on maximum grey levels of skin areas

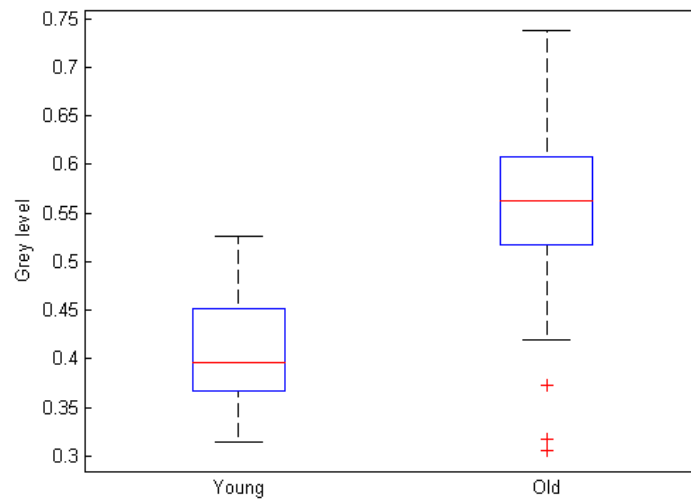


**Figure 5.11:** Comparison of hands from young and old groups based on maximum grey levels of vein areas

became obvious between the young and the old (Figure 5.10). Specifically in skin areas, the maximum grey value could guarantee the pixel from the skin when considering the segmentation errors. Likewise, the maximum grey values of vein areas similarly showed a difference.

### 3. Median grey levels

Using a median grey level approach performed better than maximum and minimum

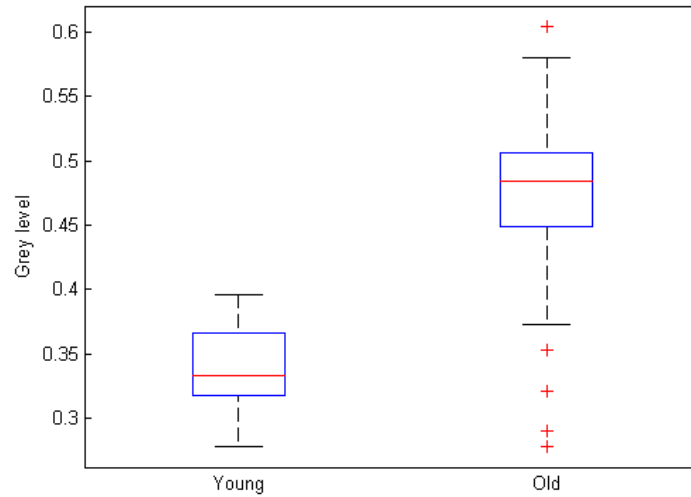


**Figure 5.12:** Comparison of hands from young and old groups based on median grey levels of skin areas

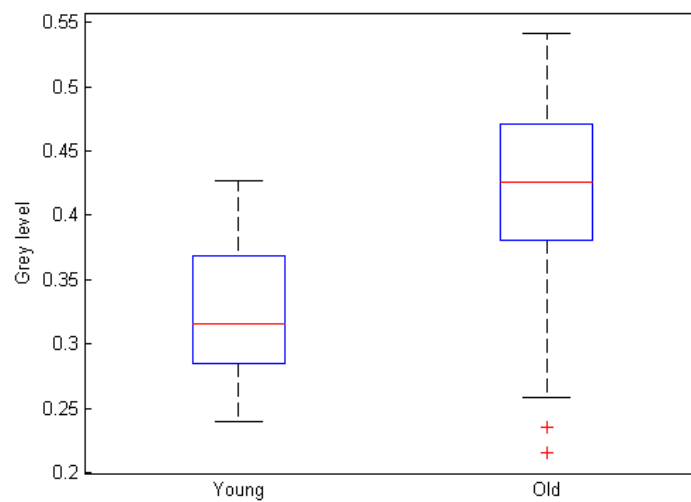


**Figure 5.13:** Comparison of hands from young and old groups based on median grey levels of vein areas

grey values when applied to both skin and vein areas (Figure 5.12 and Figure 5.13). The median value was effective as it usually represents the pixel from the exact vein and skin area.

#### 4. Mode grey levels

Mode grey levels denoted pixel grey values that appeared most often in skin areas

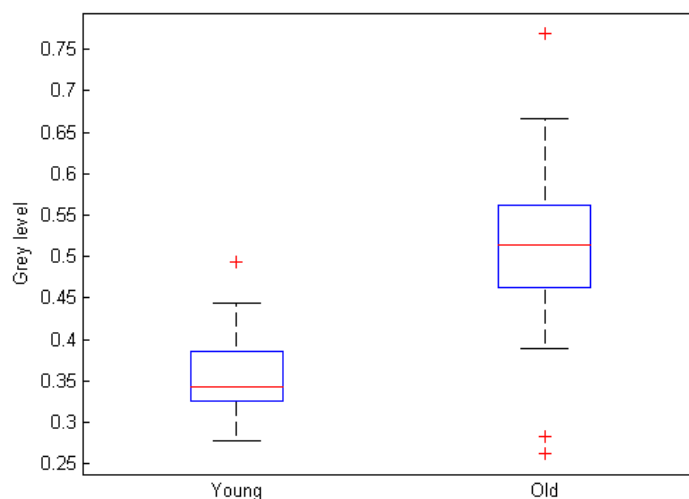


**Figure 5.14:** Comparison of hands from young and old groups based on mode grey levels of skin areas

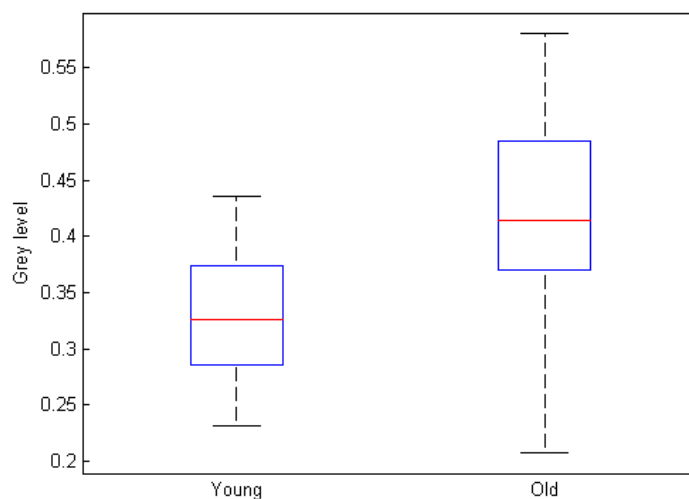


**Figure 5.15:** Comparison of hands from young and old groups based on mode grey levels of vein areas

or vein areas, ensuring that pixels were precisely selected from the vein or skin area. The mode parameter is and the contrast results were reliable (Figure 5.14 and Figure 5.15).

### 5. Mean grey levels

As shown (Figure 5.16 and Figure 5.17), young and old group distributions were

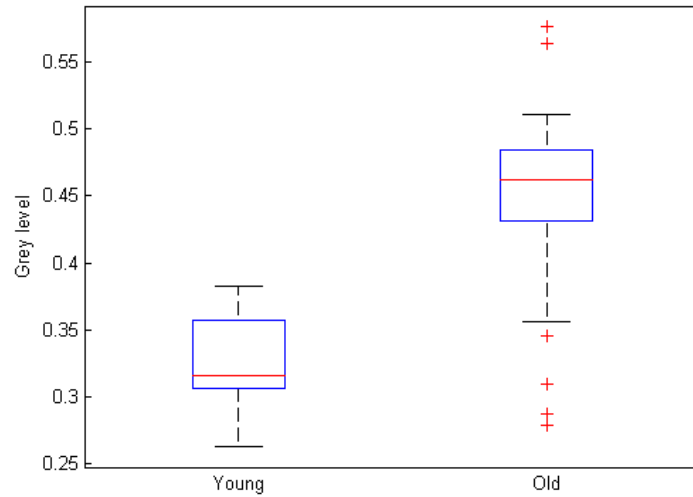


**Figure 5.16:** Comparison of hands from young and old groups based on mean grey levels of skin areas

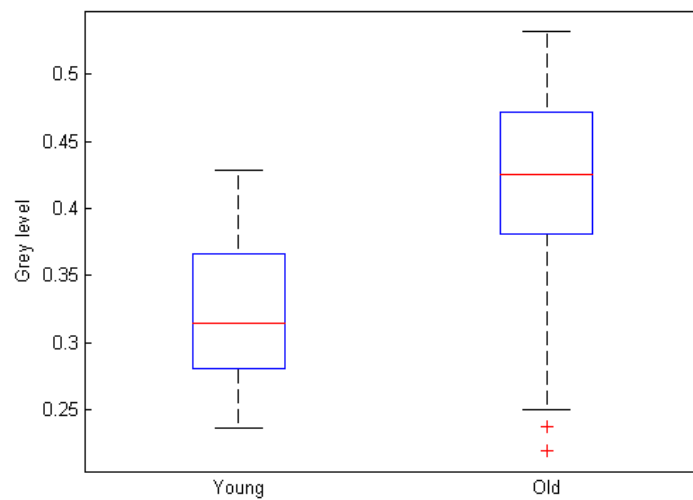


**Figure 5.17:** Comparison of hands from young and old groups based on mean grey levels of vein areas

completely separated. When using mean statistical parameters, all pixels (in veins or in skin areas) contributed to a representative value for contrasting old and young hands.

### 6. Standard Deviation (SD) of grey levels

The standard deviation is a measure quantifying the variance or dispersion of a set

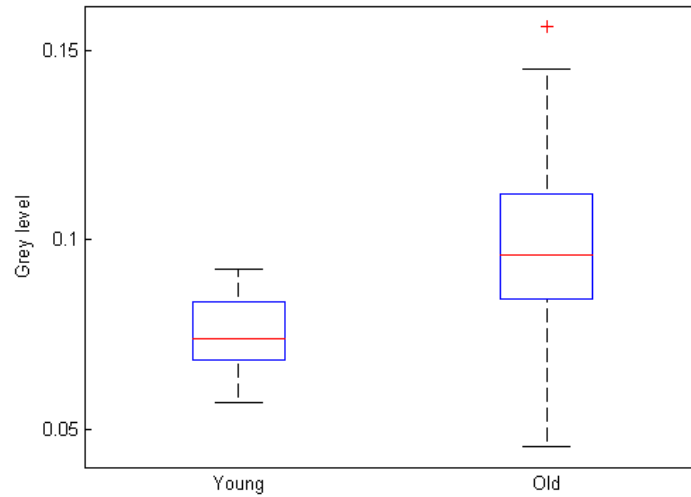


**Figure 5.18:** Comparison of hands from young and old groups based on SD grey levels of skin areas

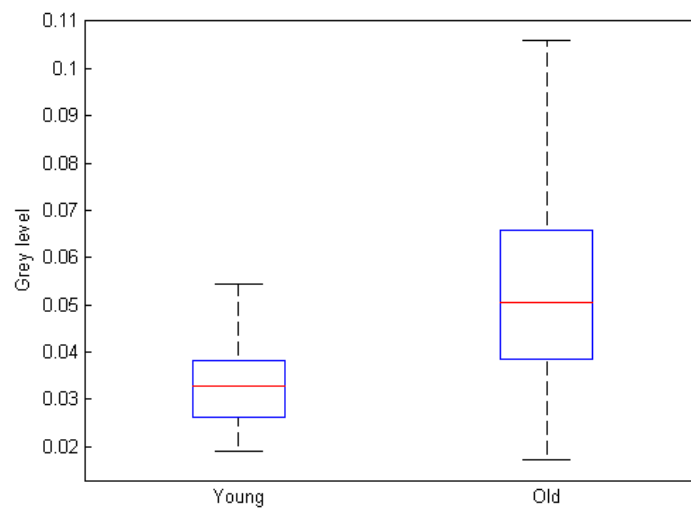


**Figure 5.19:** Comparison of hands from young and old groups based on SD grey levels of vein areas

of data values. As depicted (Figure 5.18 and Figure 5.19), the distribution of SD values of old participants was notable when compared to both skin or vein areas in young participants.

### 5.2.3 Selection of parameters for classification

Based on these analyses, statistical parameters were extracted as features for classification. As vein and skin areas represented different materials absorbing NIR light, it was important to separately analyse their features.

Six types of basic statistical parameter were discussed in this work: maximum, minimum, mean, median, mode and standard deviation values. As presented in former sections, minimum values were disappointing for classification purposes. Hence, the remaining 5 parameters were extracted from the skin and vein areas, as follows:

$$F_{skin} = [S_{max}, S_{mean}, S_{median}, S_{mode}, S_{std}]; \quad (5.1)$$

$$F_{vein} = [V_{max}, V_{mean}, V_{median}, V_{mode}, V_{std}]; \quad (5.2)$$

Where,  $F_{skin}$  and  $F_{vein}$  represent the features extracted from skin and vein areas using the maximum, mean, median, mode and standard deviation parameters.

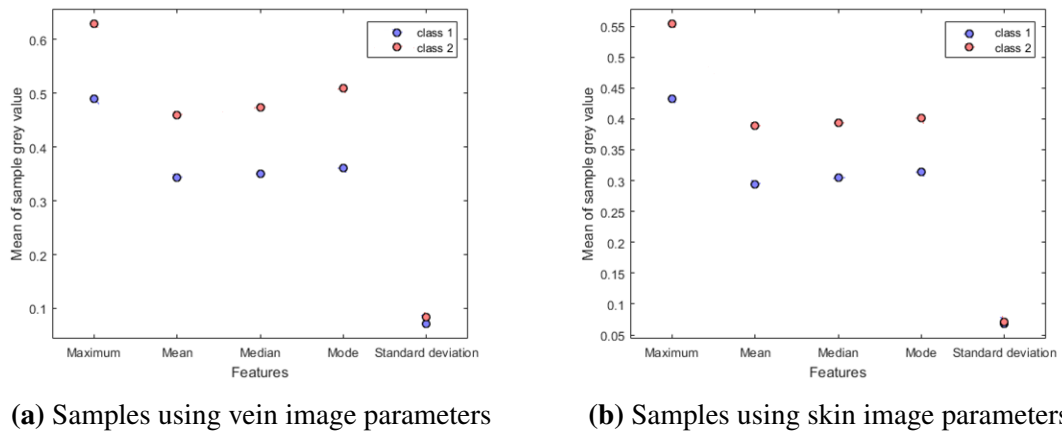


**Figure 5.20:** Plot profiles of sample averages from 500 DHV images of the right hand

As shown (Figure 5.20), class 1 and class 2 represents features extracted from young and old participant samples, respectively. The distribution of average variables of vein and skin areas indicates the discrimination between old and young participants. Thus, the five statistical parameters will be effective for classifying old and young groups of DHV images.

## 5.3 Classification Analysis and Experiments

### 5.3.1 Classifiers

For this work, the classification of old and young groups is a binary process. Binary classification classifies the elements of a given set into two groups based on a classification rule. The classifier refers to a mathematical function, implemented by a classification algorithm, which classifies input data to class (category). Since the database was not large and the features extracted were simple, *LDA* and *KNN* methods were used for binary classification.

- *Linear discriminant analysis (LDA)*

The linear discriminant analysis approach is a classification method originally developed in 1936 by R.A. Fisher [Fisher, 1936]. It is simple and mathematically robust. The algorithm is based on a concept of searching for a linear combination of variables that best separates two classes. In other words, *LDA* finds most discriminant projection by maximising between-class distance and minimising within-class distance. After projection of data onto the linear discriminant dimension, a classification threshold is placed at the midpoint between the two class means [Misaki et al., 2010].

In a two-class classification problem, the normal vector of the hyper-plane  $w$  is estimated as follows:

$$w \propto S_w^{-1}(m_1 - m_2) \quad (5.3)$$

$$y(x) = w^T(x - m) \quad (5.4)$$

Where,  $m_1$  and  $m_2$  are the mean of each class, and  $S_w^{-1}$  is a within-class covariance matrix. When the discriminant value  $y(x)$  for a sample  $x$  is positive, it is classified as *class 1*, otherwise as *class 2*. In *LDA*, each class covariance is assumed to be the same and estimated from the training  $x_n$  as the sample covariance:

$$S_w = \frac{1}{N_1} \sum_{n \in C_1} (x_n - m_1)(x_n - m_1)^T + \frac{1}{N_2} \sum_{n \in C_2} (x_n - m_2)(x_n - m_2)^T \quad (5.5)$$

The between-class covariance is:

$$S_B = (m_2 - m_1)(m_2 - m_1)^T \quad (5.6)$$

Then the objective is a Fisher linear discriminant:

$$J(w) = \frac{w^T S_B w}{w^T S_w w} \quad (5.7)$$

The *LDA* is to project on line in the direction  $w^T$  which maximizes  $J(w)$ .

- *K-Nearest Neighbourhoods (KNN)*

The KNN algorithm is among the simplest of all classification algorithms. The algorithm also has a relatively high convergence speed. It is a non-parametric technique, no a priori assumptions regarding the type of probability distribution are made [Cover and Hart, 1967].

Suppose each sample in one data set has  $n$  attributes (features) which is combined to form an *n-dimensional* vector:

$$x = (x_1, x_2, \dots, x_n) \quad (5.8)$$

Each sample is also denoted by  $C$ , which indicated the class the sample belongs to. Thus, there is a function  $f$ , which assigns a class  $C=f(x)$  to every vector. As the function is unknown, we assume it is smooth in some sense. Then a training set of  $T$  including the vectors together with their corresponding classes is given:

$$x^{(i)}, C^{(i)} \quad \text{for } i = 1, 2, \dots, T \quad (5.9)$$

Supposed a new sample  $u$  where  $x=u$ . The problem is to find the class that the new sample belongs to. Since the function  $f$  is unknown for computation of the class  $v=f(u)$ , how to classify the new sample become difficult. *KNN* methods aims to

identify  $k$  samples in the training set and to use these  $k$  samples to classify the new sample into a class  $v$ . The neighbours indicate a dissimilarity measure is needed for calculations between samples, based on independent variables. Normally, the Euclidean distance is used for the measure of distance. The Euclidean distance between points  $x$  and  $u$  is:

$$d(x, u) = \sqrt{\sum_{i=1}^n (x_i - u_i)^2} \quad (5.10)$$

When  $k=1$ ,  $KNN$  becomes the  $NN$  algorithm. In this case, we find the sample in the training set that is the nearest neighbour to  $u$  and set  $v=y$  where  $y$  is the class of the nearest neighbouring sample. For  $k>1$  the idea of  $1-NN$  is extended as follow: find the nearest  $k$  neighbours of  $u$  and then use a majority decision rule to classify the new sample.

When applying  $KNN$ , the optimal value of  $k$  must be searched for. One option for selecting  $k$  is by means of a Cross Validation (CV) procedure. There are many CV methods, the venetian blinds method was adopted for this work. With venetian blinds, each test set is determined by selecting every  $s^{th}$  object in the data set, starting at object numbered  $1$  through  $s$ , where  $s$  is the number of data splits specified for the cross validation procedure.

### 5.3.2 Classification Parameters

To evaluate the classifier and confirm classification results, several classification parameters should be considered [Friedman et al., 2001].

- *The confusion matrix*

The confusion matrix is a square matrix with  $G \times G + 1$ , where  $G$  is the number of classes. Each element  $n_{gk}$  represents the number of samples belonging to class  $g$  and assigned to class  $k$ . The last column collects the number of samples not assigned.

- *Sensitivity*

Sensitivity (also called the true positive rate) measures the proportion of positives

**Table 5.1:** Confusion matrix

		Assigned class				Not assigned
		1	2	...	G	G+1
True class	1	$n_{11}$	$n_{12}$	...	$n_{1G}$	$n_{1G+1}$
	2	$n_{21}$	$n_{22}$	...	$n_{2G}$	$n_{2G+1}$
	...	...	...	...	...	...
	G	$n_{G1}$	$n_{G2}$	...	$n_{GG}$	$n_{GG+1}$

that are correctly identified as positive,

$$S_{n_g} = \frac{n_{gg}}{n_g} \quad (5.11)$$

Where  $n_g$  is the total number samples belonging to the  $g$ -th class,  $n_{gg}$  is the number of samples belonging to class  $g$  and correctly assigned to class  $g$ .

- *Specificity*

Specificity (also called the true negative rate) measures the proportion of negatives that are correctly identified as negative,

$$S_{p_g} = \frac{\sum_{k=1}^G (n_k - n_{gk})}{n - n_g} \quad \text{for } k \neq g \quad (5.12)$$

Where  $n'_k$  is the total number of samples assigned to the class  $k$ -th,

$$n_k = \sum_{g=1}^G n_{gk} \quad (5.13)$$

Non assigned samples are not considered for the specificity calculation.

- *Accuracy (AC)*

The accuracy is the ratio of correctly assigned samples:

$$AC = \frac{\sum_{g=1}^G n_{gg}}{n} \quad (5.14)$$

- *Error rate (ER) and non-error rate (NER)*

The non-error rate is the average of class sensitivities:

$$NER = \frac{\sum_{g=1}^G S_{n_g}}{G} \quad (5.15)$$

The error rate is defined as:

$$ER = 1 - NER \quad (5.16)$$

### 5.3.3 Training experiments

For classification experiments, training and testing datasets were selected as follows: 500 ROI images from the left hands of all subjects were selected as the training set, 100 of which were from the young group and the rest from the old group. All right hand samples were selected as the testing set.

Selection was on the basis that left and right dorsal hands are normally different in terms of vein structures. This selection would make training and testing datasets both independent and representative. Thus the training set was organised as follows:

#### Training set

- Class young: 100 images from left hands of all young subjects
- Class old: 400 images from left hands of all old subjects

#### Testing set

- Class young: 100 images from right hands of all young subjects
- Class old: 400 images from right hands of all old subjects

Once the training datasets were set, the features representing DHV images were trained for classifier models and classified. Then, the relevant testing datasets were used for predictions of the aged groups from classification.

Regarding the *KNN* classifier, there was a disadvantage in selecting  $k$ . If  $k$  was too small, the results could be too sensitive to noise. If  $k$  was too big, then the result could be

incorrect, where neighbours included too many points from other classes (Cunningham and Delany 2007) (Zeidat, Wang et al. 2005). For this work, the optimal  $k$  was selected by cross validation using ‘venetian blinds’ for each sample.

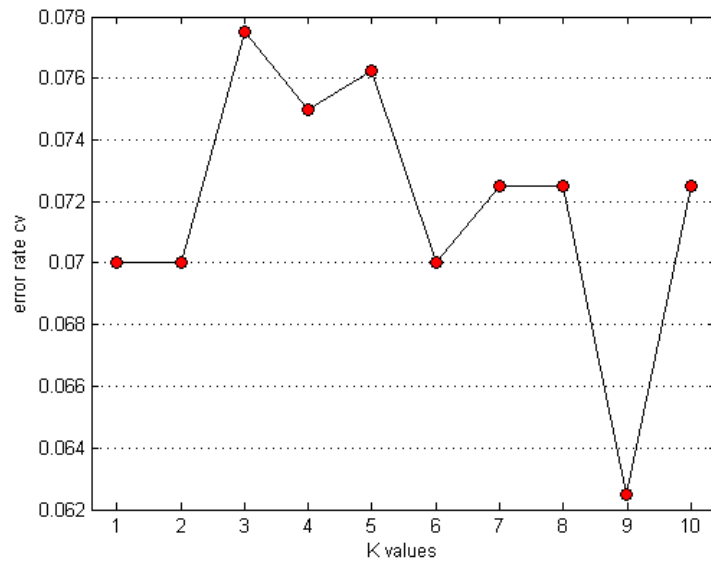


**Figure 5.21:** Parameter K plots for training skin features

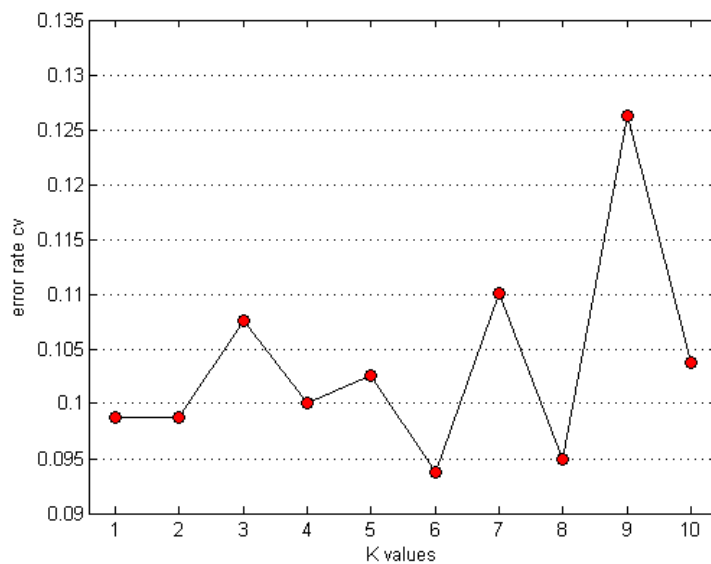


**Figure 5.22:** Parameter K plots for training vein features

As shown (Figure 5.21 and Figure 5.22), the optimal  $K$  for the KNN classifiers were selected using the cross validation method according to different features. As an evaluation, the error rate (ER) was adopted.

Regarding the vein features training using KNN, the optimal  $K$  was 6. For the skin features training, the optimal  $K$  was 9. The skin and vein features would then be trained using classifier KNN and LDA for comparison.

**Table 5.2:** Classification performances with KNN

Optimal K	Features	The confusion matrix			Classification Parameters			
		True class	Assigned O	Assigned Y	Sens	Spec	ACC	NER
K=6	$F_{vein}$	O	375	25	0.94	0.86	0.92	0.90
		Y	14	86	0.86	0.94		
K=9	$F_{skin}$	O	376	24	0.94	0.92	0.94	0.93
		Y	8	92	0.92	0.94		

**Table 5.3:** Classification performances with LDA

Features	The confusion matrix			Classification Parameters			
	True class	Assigned O	Assigned Y	Sens	Spec	ACC	NER
$F_{vein}$	O	370	30	0.93	0.80	0.90	0.86
	Y	20	80	0.80	0.93		
$F_{skin}$	O	379	21	0.95	0.79	0.92	0.87
	Y	21	79	0.79	0.95		

As shown (Table 5.2 and Table 5.3), classification results were satisfactory using KNN or LDA classifiers. In terms of the features used, the skin feature performed better than the vein feature: 93% compared to 90% using KNN and 87% compared to 86% using LDA. These data can be explained that the skin area is much bigger than that of the vein, and the water levels in the skin area are much higher than haemoglobin levels in the venous blood of veins. Regarding the classifiers used, KNN performed better than LDA.

Since both the skin and vein features worked well in classification, the features could be further tailored for classification. Of the five parameters of skin or vein features, the parameters 'Mean', 'Median' and 'Mode' were prominent and similar to each other. Here, the 'Mean' parameter was extracted for discussion. In consideration of both vein and skin areas, mean parameters were extracted respectively and connected as a new feature  $F$ , described as:

$$F = [S_{mean}, V_{mean}] \quad (5.17)$$

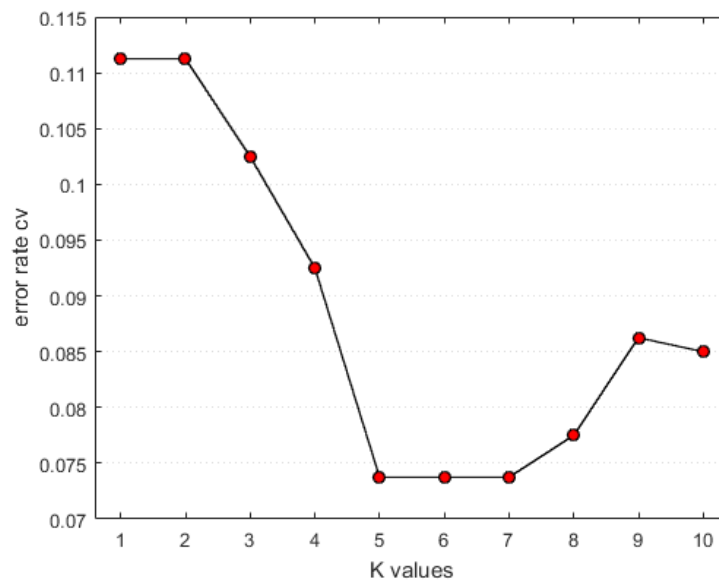


**Figure 5.23:** Parameter plots of K for training feature *F*

**Table 5.4:** Classification performances using feature *F* with KNN

Optimal K	Features	The confusion matrix			Classification Parameters			
		True class	Assigned O	Assigned Y	Sens	Spec	ACC	NER
K=5	F	O	378	22	0.94	0.83	0.92	0.89
		Y	17	83	0.83	0.94		

**Table 5.5:** Classification performances using feature *F* with LDA

Features	The confusion matrix			Classification Parameters			
	True class	Assigned O	Assigned Y	Sens	Spec	ACC	NER
F	O	376	24	0.94	0.79	0.91	0.86
	Y	21	79	0.79	0.94		

As depicted (Table 5.4 and 5.5), when parameters were reduced to feature *F*, the NER was reduced, whereas the classification result were reasonable.

### 5.3.4 Testing experiments

Once classifiers were trained, the testing dataset was used to predict the testing samples for classification of old and young DHV images. Specifically, testing samples were projected in the classifier models (but not used to calculate the model).

The prediction results were measured mainly by the classifier's performance parameter NER, since the prediction is about to identify whether the new dorsal hand image is old or not (young). However, calculation of the non-error rate was modified, considering the un-balanced samples between young and old, described as the correctly prediction rate (CPR):

$$CPR = Sens(Y) \times 0.2 + Sens(O) \times 0.8 \quad (5.18)$$

Where,  $Sens(Y)$  and  $Sens(O)$  denote the sensitivity of class young and class old, which means correctly classified as young and correctly classified as old.

**Table 5.6:** Results of correct prediction rates

	LDA			KNN		
	$F_{vein}$	$F_{skin}$	F	$F_{vein}$	$F_{skin}$	F
CPR	89.6%	91.8%	86.2%	90.4%	92.6%	89.4%

Overall, KNN performed better than LDA as a classifier. The skin area parameters performed the best, attaining 92.6% correction rate with KNN. The features extracted from vein areas could be used for classification as it reached over 90% CPR. The reduced  $F$  feature was reasonable due to the meaningful parameters connection from skin and vein areas. All in all, the intensity statistical parameter based features were satisfactory for classification of old and young DHV images.

Regarding the 2-dimensional feature  $F$ , the plotting of the predictions of the testing dataset and the classification boundaries are depicted (Figure 5.24). The coloured regions show the decision boundaries induced by the optimal  $KNN$  classifier and the training set. The testing data points, which are denoted by '+' (red represents the young group while blue represents the old group), are evaluated with the classified model. That red '+' falling in the red region and blue '+' falling in the green region are assigned as correctly predicted points. As depicted (Figure 5.24), most of the test data points fell into the correct regions, confirming the classification results.

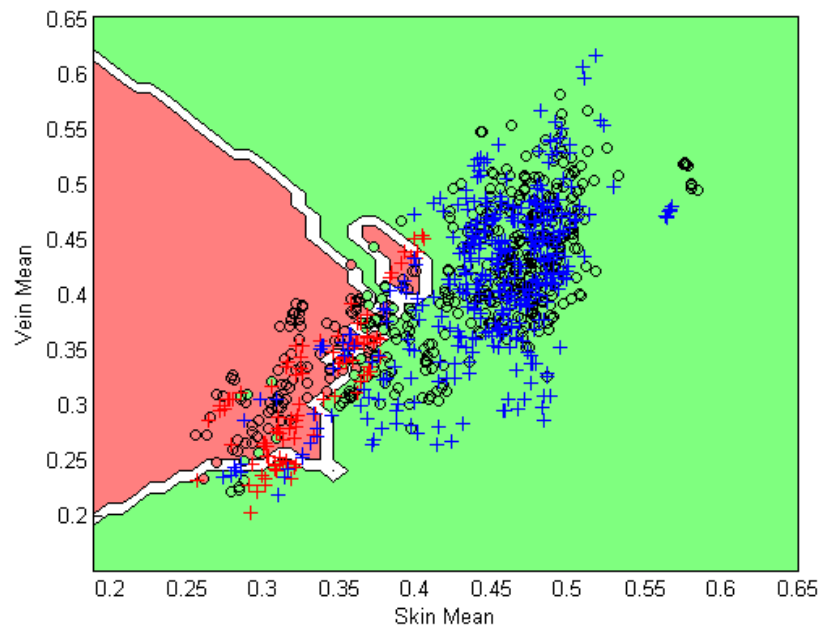


**Figure 5.24:** Plotting the testing set using  $F$  features by KNN

## 5.4 Concluding Remarks

In this chapter, static DHV images were analysed based on statistical parameters extracted from skin and vein areas. Five basic parameters were justified as features for vein and skin images. Two classifiers, KNN and LDA were adopted for the classification of old and young groups. The static DHV database was split into a training set and a testing set, considering the size and number of samples.

Experimental results showed that old and young groups were classified with a relatively high prediction rate, due to differences in intensity based features extracted from skin and vein areas of DHV images. There were no overlaps of dorsal hands between training and testing datasets, ensuring classification and prediction results. KNN performed better as a classifier tool when compared to LDA.

From this chapter, it was concluded that features interrelated with intensity grey levels can effectively distinguish between young and old groups. This distinction was based upon decreasing haemoglobin and water supplies to veins and skin areas. The distinction could be used for the recognition of old and young groups, via hand vein biometric applications.

## **Chapter 6**

# **DYNAMIC ANALYSIS OF DORSAL HAND VEIN IMAGES FOR BIOMETRIC APPLICATION**

### **6.1 Introduction**

Up to now, nearly all dorsal hand vein biometric applications have focussed on personal identification. Little research has concentrated on exploring the characteristics of certain biometrics. In terms of DHV images, and despite the age related features as discussed, some dynamic attributes could be investigated for biometric applications. Several groups are devoted to the dynamic analysis of biometrics [Ming-Zher et al., 2011; Takano and Ohta, 2007; Xu et al., 2014]. Inspired by this work, this chapter investigated the changing variations underlying dorsal hand vein images.

According to NIR imaging and the absorption attributes of veins and skin, intensity based values were selected to detect changing patterns, which were used as clues for dynamic analyses (Figure 6.1) of DHV images for vital sign (liveness) detection. In this work, changing patterns were decided by peak detection of the signal interested in the spectrum.



**Figure 6.1:** Dynamic DHV analysis

## 6.2 Signal Extraction and Filtering

As time progresses, variations occur inside the veins and skin [Field et al., 1924]. As previously discussed, the mean intensity is a fundamental parameter for vein and skin areas. Thus, mean grey ROI levels in dorsal hand vein image sequences could be extracted for dynamic analyses.

### 6.2.1 Signals extracted from regions of interest

Using centroid based ROI extraction, the centre part of the dorsal hand was extracted by representing each frame of the DHV image. In this case, the  $300 \times 300$  ROI was extracted for dynamic DHV analysis.

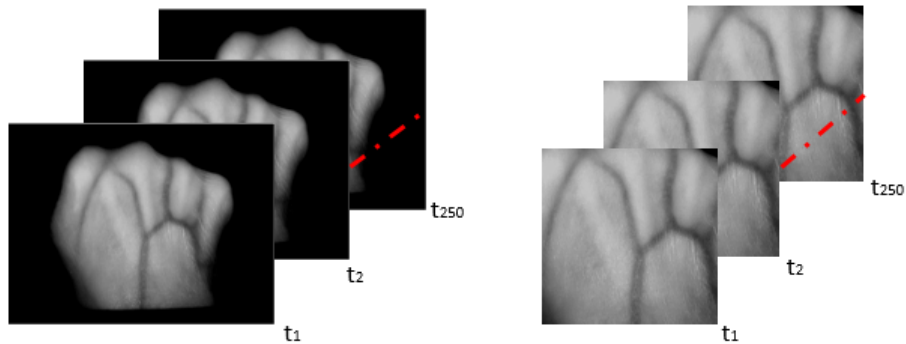


**Figure 6.2:** DHV video sequences and ROI extraction for each frame

After extraction, each ROI image was spatially averaged over all pixels to yield a measurement value for each frame and to form the ROI raw signal  $y(t)$ . To reduce the DC component, the raw signal was subtracted from its mean value.

$$y'(t) = y(t) - \mu \quad t = 1, 2, \dots, T \quad (6.1)$$

Where,  $\mu$  is the mean of  $y(t)$ , and  $T$  denotes the length of the video. In this work, all videos were 10 seconds long with a frame rate of 25. Thus, the signal length was 250 frames.

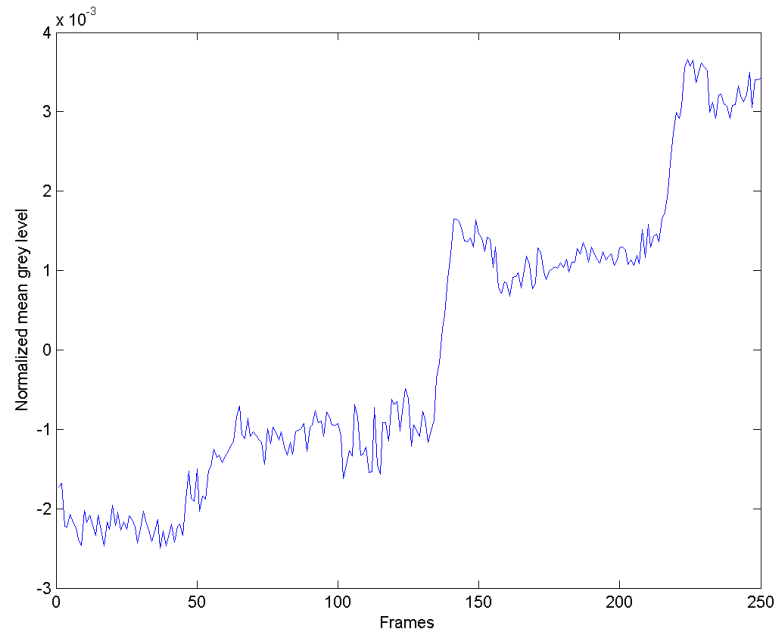


**Figure 6.3:** An example of a ROI based signal  $y'(t)$

As can be seen (Figure 6.3), it was obvious that certain changing patterns existed in the ROI raw signal. The signal tendency was moving upward, which meant the averaged value on the dorsal hand increased over time. In observing all dynamic videos, the upward tendency was explained as a changing illumination of DHV images due to moving dorsal hands.

On the other hand, with different ROI rectangular sizes, signals were plotted showing likely tendency and patterns (Figure 6.4(a)-(d)). In this work,  $300 \times 300$  areas were selected for discussion.

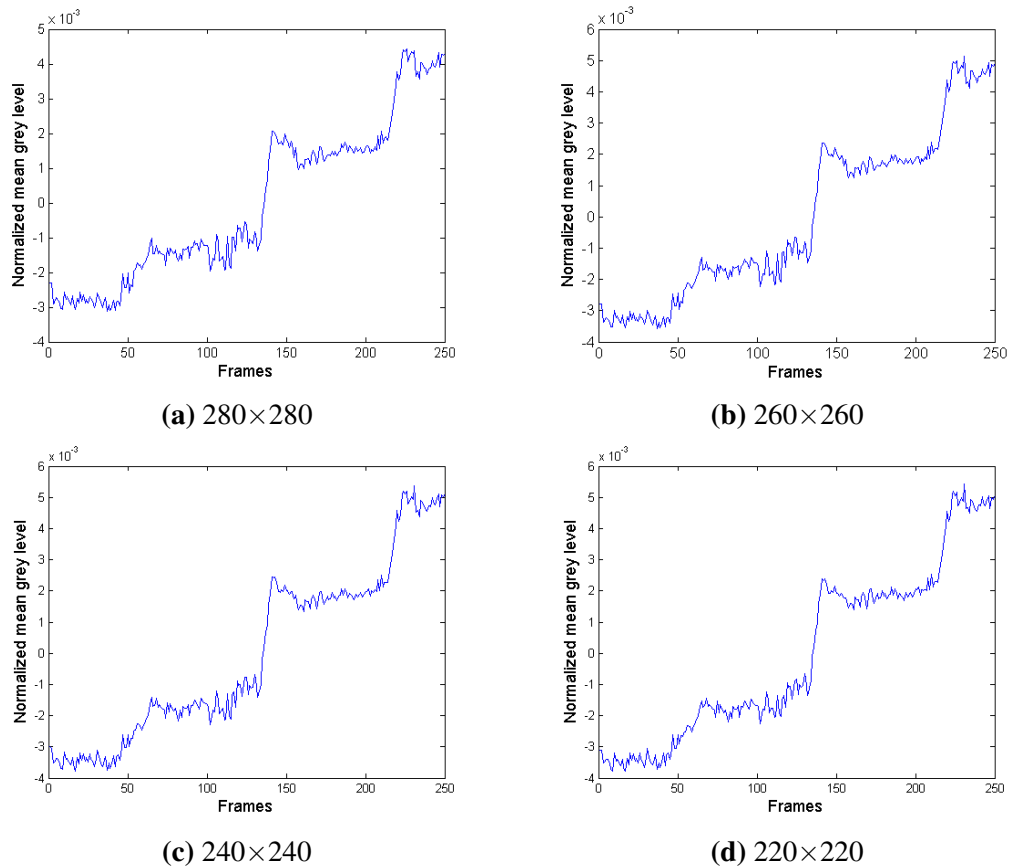


**Figure 6.4:** Signals from different ROI selections

## 6.2.2 Signal Filtering

Randomness appeared in videos, thereby generating noise. On one hand, noise occurred from light entering the camera during imaging processes. On the other hand, motion artefacts were bound to happen in DHV videos. This noise would have an extreme impact on changing patterns, thus it was important to apply filtering methods before the signal spectrum analysis.

A band-pass filter was used to reduce the noise. This device attenuates frequencies outside the band of interest. The band of interest was adopted according to the physiological activities of an individual. Here a second-order Butterworth filter was used. The cut off frequencies were set to contain the band of interest: 0.2-3 Hz (Figure 6.5).

A Butterworth filter was adopted because:

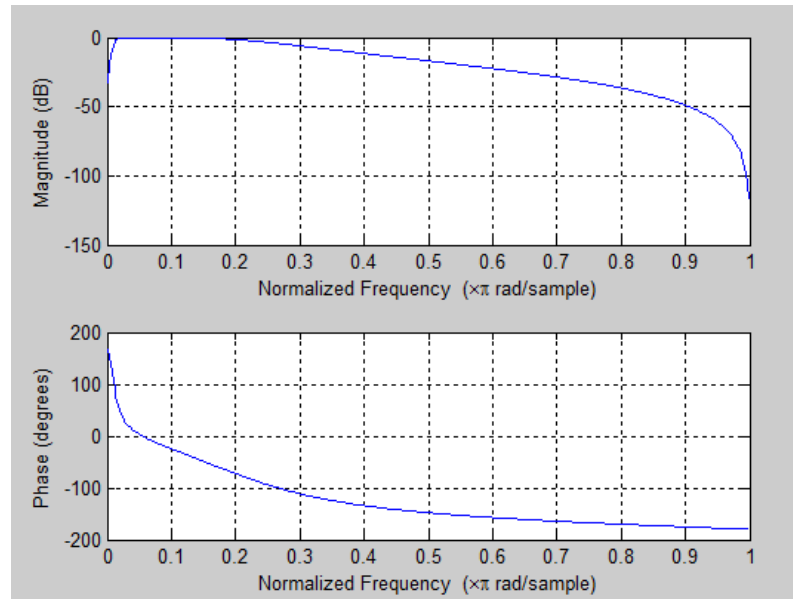


**Figure 6.5:** Frequency response to the Butterworth filter

1. It is an IIR filter and the order required for a given bandwidth is much lower than that of an FIR filter. Lower orders usually mean less computation and therefore faster operations.
2. It has flat pass-bands and stop-bands when compared to other IIR structures that show ripples. This avoids the favouring of certain frequencies over others in the valid range.

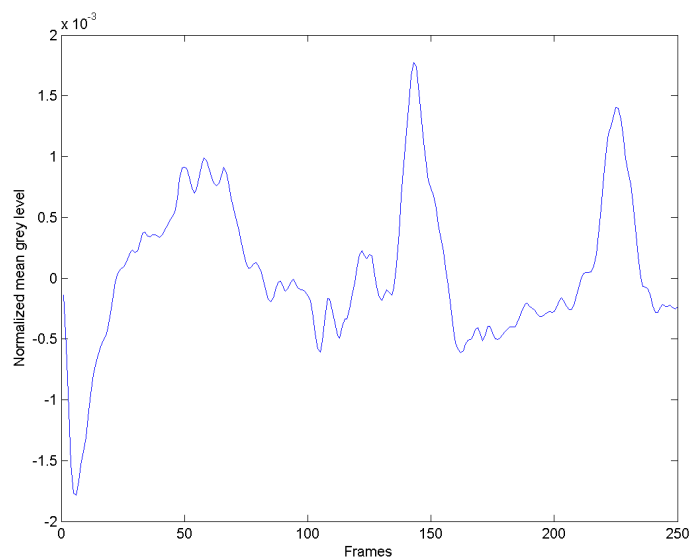


**Figure 6.6:** ROI signals after band pass filtering

As shown (Figure 6.6), the changing pattern became more obvious after band pass filtering, and the original upward tendency caused by hand motion was removed.

To reduce leakage, the input intensity based signal was multiplied by a function, forcing the resulting boundary values to zero. Here, the Hanning window filtering was used because it offered good resolution and good leakage rejection. As observed (Figure 6.7), the Hanning window length was the same size of the signal.

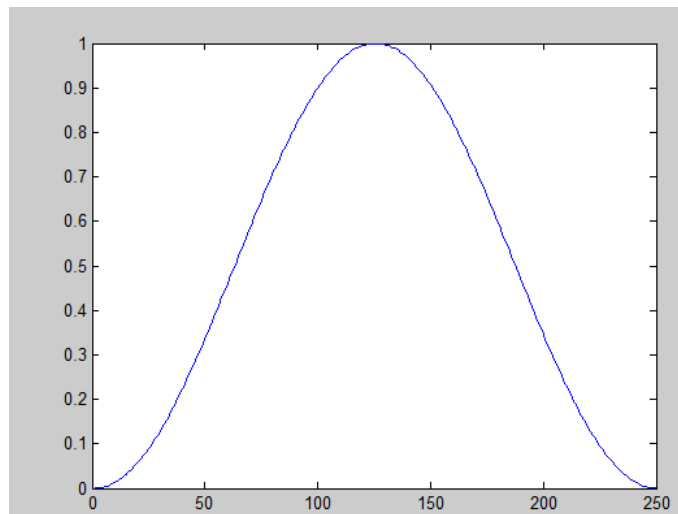


**Figure 6.7:** The Hanning window for the 250 frame signal

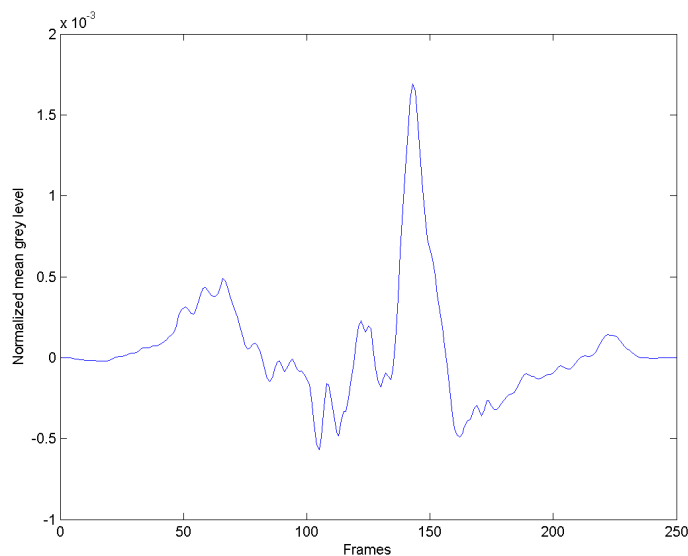


**Figure 6.8:** ROI signals after Hanning window

## 6.3 Spectrum Analysis of the Extracted Signals

To make clear the changing patterns underlying the DHV image sequences, it was ideal to analyse signals in the frequency domains, to assess its frequency components. The changing pattern in the time domain indicated there should be dominant frequency peaks representing cycles of variation.

For this research, a simple Discrete Fourier Transform (DFT) investigated the most prominent peaks in the spectrum. Inspired by (Takano and Ohta) some physiological parameters could be detected using low-cost and non-contact methods [Takano and Ohta, 2007]. Such parameters included the Respiration Rate (RR), normally 12-20 breaths per minute [Ganong and Barrett, 2005], and the heart rate (HR). Based on analysis of extracted signals in former sections, it was assumed that RR related patterns were present and that frequency interest band components could be set in [0.2Hz 3Hz] for discussion, which including the normal RR range of frequency and HR range of frequency.

### 6.3.1 Discrete Fourier Transform

Discrete Fourier Transform (DFT) is the computational basis of spectral analysis. It identifies component frequencies in data. For signals known as  $N$  instants separated by sample times  $T$ , the DFT can be expressed as:

$$F(j\omega) = \sum_{k=0}^{N-1} f[k]e^{-j\omega kT} \quad (6.2)$$

Where,  $f[k]$  denotes the sample points from a continuous signal,  $T$  is the sampling period and  $N$  is the length of the finite sequence of data. Since there are only a finite number of input data points, the DFT treats the data as if it were periodic, i.e.  $f(N)$  to  $f(2N-1)$  is the same as  $f(0)$  to  $f(N-1)$ .

In this work, the signals are computed with a fast Fourier transform (FFT) algorithm [Duhamel and Vetterli, 1990]. Since the frequency resolution is determined by the number of samples included in the FFT, it can be increased by including more samples. Specifically, the video sequences were recorded at a frame rate of 25 fps (e.g. sampling rate  $F_s = 25\text{Hz}$ ).

If the frequency resolution  $\delta f$  was 1/60 Hz, the length should be:

$$L = \frac{F_s}{\Delta f} = \frac{25}{\frac{1}{60}} = 1500 \text{ frames} \quad (6.3)$$

The frequency resolution was determined to meet the requirements of a normal human respiration rate. As the signal was 250 frames long, it was padded by zeros to 1500 points FFT.

### 6.3.2 Peak detection

According to the time domain analysis of extracted signals, a periodic signal existed. Thus, a prominent frequency or peak should be detected using FFT.

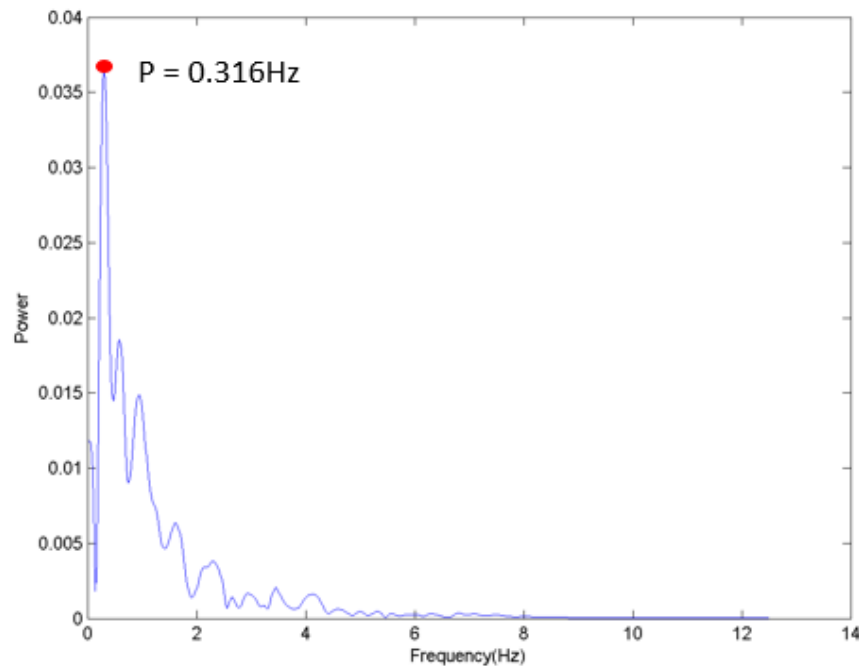


**Figure 6.9:** ROI main peak detection

As shown (Figure 6.9), a dominant peak appeared in the spectrum from ROI images. This indicated that there were RR like indices existing as cycles of variation. The peak conformed to former observations of signals from the ROI. Although there were no verification references for the ‘peak’, it was assumed the peak was representative of a live dorsal hand under NIR light, because it was so close to a normal human respiratory cycle (12 times/minute to 24 times/minute).

To further investigate the underlying cycle of activity from live dorsal hands and considering the computing time, the ROI ( $300 \times 300$ ) signals were extracted from all DHV images in the video database and analysed in spectrum to obtain their 'main peaks' (Figure 6.10).

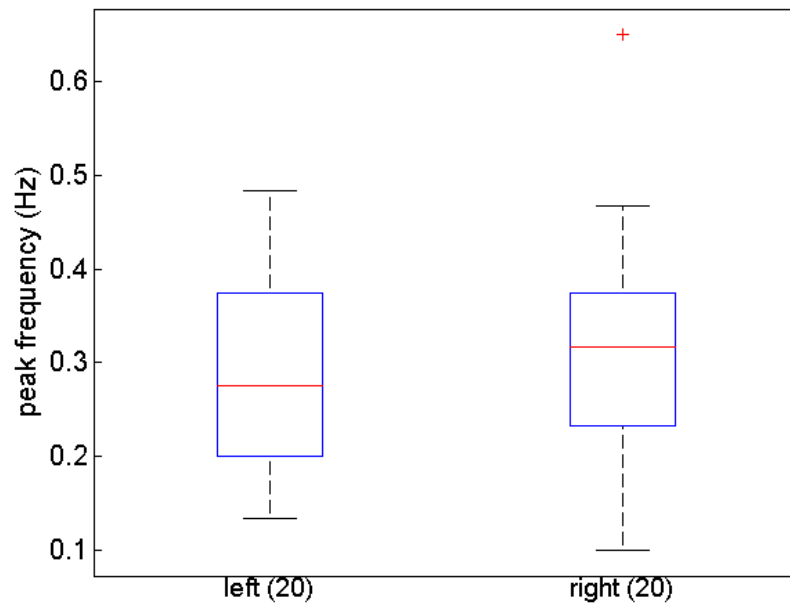


**Figure 6.10:** Peak frequency detection of all ROI signals in the video database

As depicted (Figure 6.10), the main peak frequency values from both left and right dorsal hands centred in the range 0.2-0.4Hz. This corresponded to respiratory like activity (12 times/minute to 24 times/minute).

## 6.4 Dynamic Analysis of live dorsal hands

As previously discussed, certain changing patterns occurred with regard to time scales. Although the underlying index of dorsal hands could not be verified as respiration activity, the cycle observed from ROI intensity based signals indicated that a dorsal hand under NIR light exhibited characteristics representing human vital signs, namely liveness.

### 6.4.1 Live and fake dorsal hand vein images contrast

For biometric applications, liveness detection is an effective way of anti-spoofing. Within spoofing circles, a common deceit is to print images of biometric features. Thus printed paper may sometimes cheat biometric identification systems. In this research, liveness detection was based on DHV videos, which focused on dynamic analyses of underlying patterns caused by human vital signs.

A fake dorsal hand plus veins was made of paper and recorded under NIR light for 10 seconds. Extraction of ROI signals from the fake hand was the same as that of the real hand (Figure 6.11).

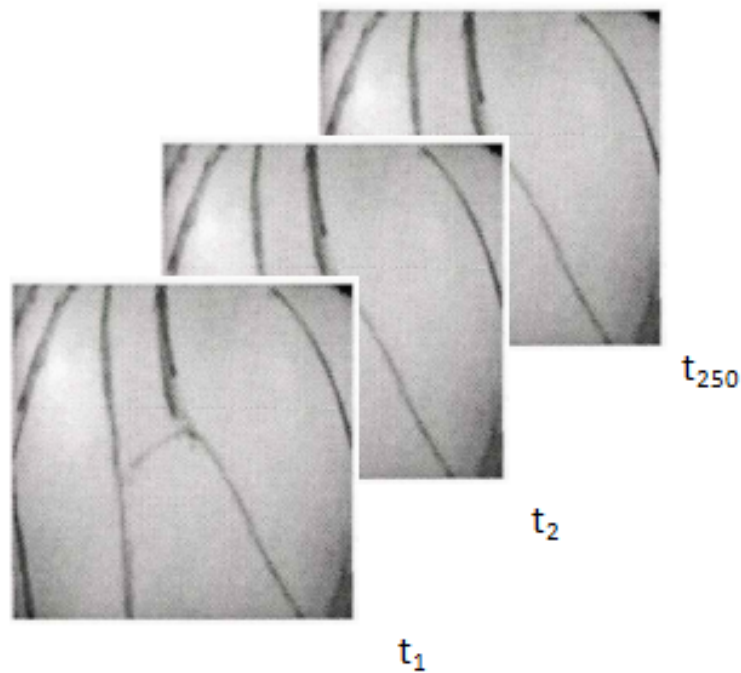


**Figure 6.11:** A fake dorsal hand ROI image sequences

Sharing the same extraction DHV signal procedure, the intensity based raw signal of the fake video was extracted as a red signal (Figure 6.12). The spectrum of the ROI signal from the fake video was illustrated as a red curve (Figure 6.13).

Signals from the fake hand video and the live hand video were plotted in the same figure (Figure 6.12). Signal amplitudes from the fake hand were much smaller than those of the live hand signals, suggesting the mean grey level variations of the fake hand were too low for detection, when compared with the live hand.

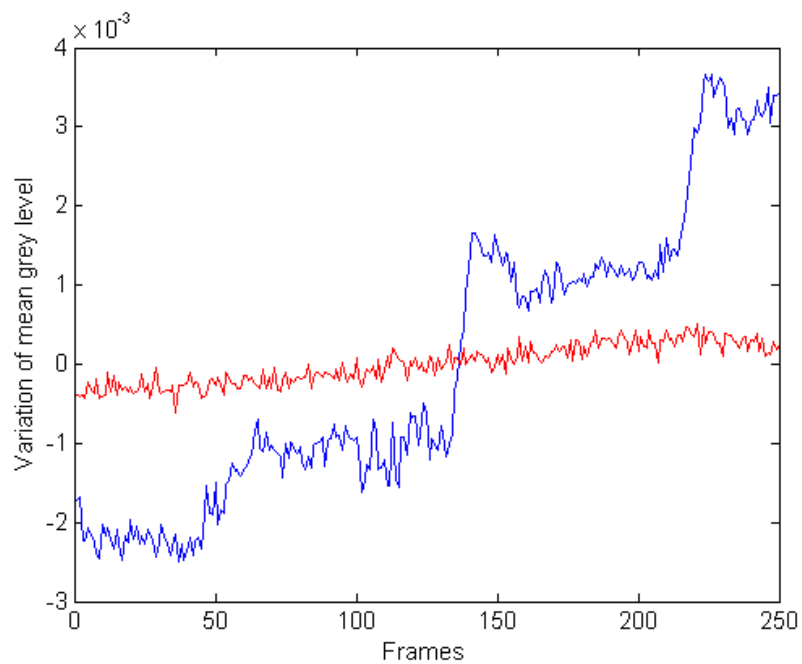


**Figure 6.12:** Comparison of a fake signal (red) with a real signal (blue)

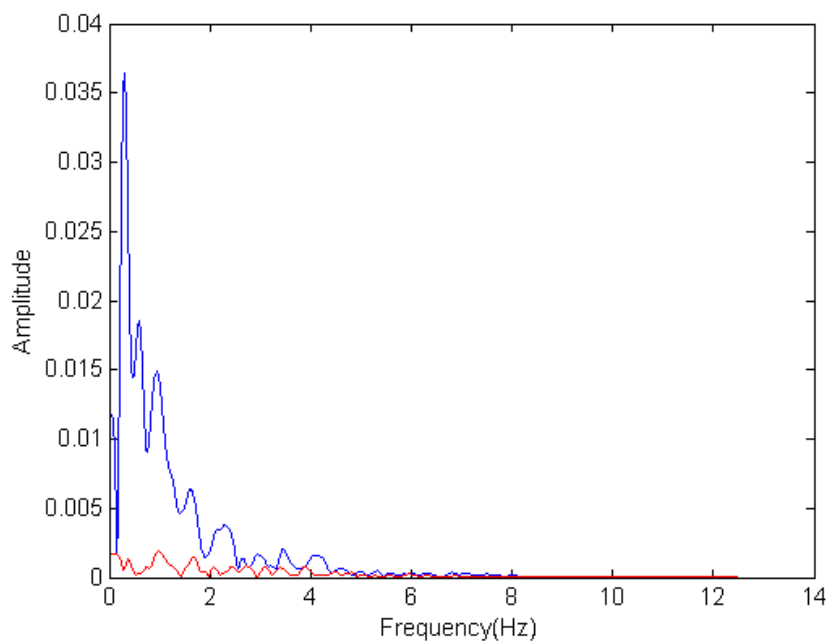


**Figure 6.13:** Spectrum comparison of a fake signal (red) with a real signal (blue)

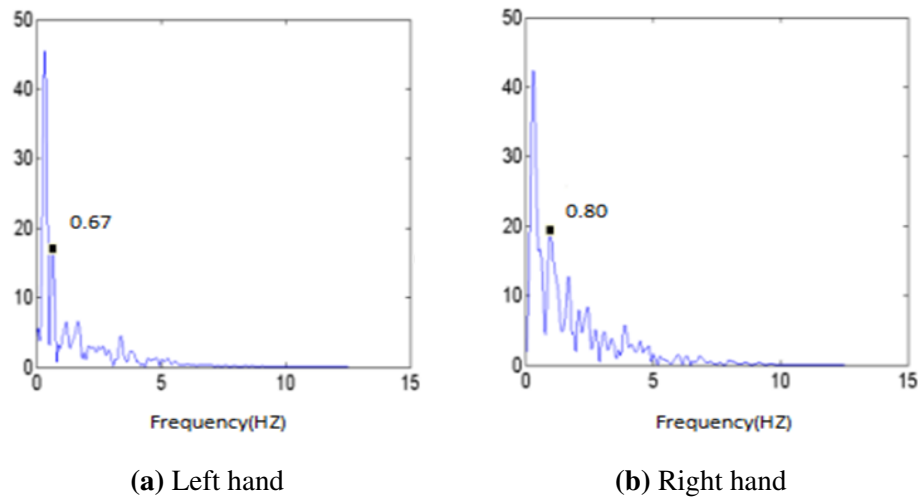


**Figure 6.14:** Peak detection in hands from the same person

When applied to spectrum analysis, no obvious peaks appeared in the band of interest (Figure 6.13). Therefore, the signal peak of a live dorsal hand represented liveness of the biometric. These observations could help develop anti-spoofing techniques for biometric applications.

#### 6.4.2 Possible vital signs analysis

As shown (Figure 6.9), except for the main peak, other peaks were present. Inspired by measurements of physiological parameters on webcam videos (Ming-Zher, McDuff et al. 2011), these indistinctive peaks were analysed for heart rate (HR).

Since there were no verification references for a human heart rate, a comparative analysis between left and right hands from the same individual was carried out. Based on observations that the heart rate is normally steady over a short period of time, the dynamic database was used to investigate left and right hands from the same person.

It was assumed that HR, like peak frequencies, was consistent in both hands from one person. Monitoring the Heart Rate would be regarded as another important soft biometric for liveness detection.

Figure 6.14 shows a comparison of the left dorsal hand with the right dorsal hand when extracting indistinctive peaks in the frequency domains. The peaks extracted were similar yet not the same. To further verify a putative consistency of ‘HR’ frequencies between

hands, all DHV video samples (from 20 people) were extracted and the peaks plotted (Figure 6.15).

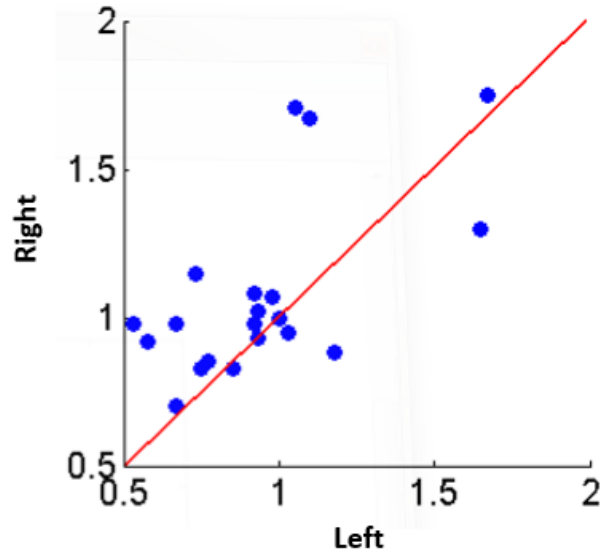


**Figure 6.15:** Right hand peak values versus left hand peak values from 20 samples

As shown (Figure 6.15), a point near the diagonal line indicates a symmetrical pair of indistinctive peak ROI signals from the left and right dorsal hand. The scattering data show that 12 out of 20 samples were consistent in terms of latent peaks. All points were within the band of interest (0.5 Hz - 2 Hz) which included normal heart rate frequencies.

## 6.5 Concluding Remarks

In this chapter, dynamic DHV images were used to extract time-related signals. With filtering and spectral analysis, dominant peaks were selected. Compared with a fake dorsal hand video, the dominant peak extracted from the live dorsal hand potentially reflected liveness detection in dorsal hand veins. Dynamic analysis of dorsal hand vein images had potential biometric applications and provided a preliminary clue to the detection of human respiration rates and heart beat rates.

# Chapter 7

## CONCLUSIONS AND FUTURE WORK

### 7.1 Conclusions

The research presented in this thesis investigated dorsal hand vein biometric characteristics. Analytical techniques incorporated static and dynamic analysis of dorsal hand vein images based on near infra-red imaging. Employing this technological approach enabled us to explore biometric applications beyond personal identification.

Through literature reviews and background research, dorsal hand vein biometrics were found to be effective and secure for personal identification, Using dorsal hand vein biometrics, based on low cost near infra-red for multiple biometric applications is a challenging, but valuable research strategy.

By understanding the acquisition systems of near infra-red dorsal hand vein images, it was ascertained that reflection modes of imaging were suitable for dorsal hand vein patterns. Dorsal hand veins and skin areas were different in their optical responses to NIR light, suggesting separate analyses of dorsal hand vein images.

A database of dorsal hand vein images was built and segregated into two categories: static DHV images and dynamic DHV images. The main subjects of the database were from old group of people, who were investigated for dorsal hand vein biometric applications.

With regards to static DHV images, two groups were defined: a young group (people under 30) and an old group (people over 60). The database contained 1000 images from 50 individuals (40 young people and 10 old people). Within the old group, 20 subjects recorded dynamic hand videos.

Dorsal hand vein images were pre-processed by geometry correction, ROI extraction, grey level normalisation, noise reduction and image enhancement. The centroid ROI extraction yielded good data. When mean filtering was applied, it provided the best performance with a smooth grey level profile and low local fluctuations. Regarding segmentation processes, some approaches were studied and evaluated. The threshold based methods worked well in high contrast areas. A specific method of segmentation, the maximum curvature based algorithm was finally adopted for this research. The algorithm ensured that the segmentation process retained key vein features, maintaining the centre points of all vein patterns.

Regarding static analysis of DHV images, intensity based features were extracted for classification of young and old groups. It was based on physiological knowledge that both vein and skin characteristics change as people aged. Haemoglobin levels in vein areas and water concentrations in skin areas decrease with age, reflecting a brighter NIR intensity in old hands when compared to the young. Based on this, and analysis of basic intensity statistics of vein and skin areas, a classification of young and old groups was attained. These observations lay the foundation for exploring dorsal hand vein biometric applications.

Regarding dynamic analysis of DHV images, time dimensions were included for the analysis of variations. Mean grey level values were extracted from the ROI of each frame and connected as biometric signals. These were used for spectrum analysis to find a prominent peak for liveness investigation. A fake dorsal hand video was introduced and compared to the live dorsal hand video. This approach validated the vital signs of the live dorsal hand.

The analysis of static and dynamic dorsal hand vein images carried out in this thesis, focused on new avenues in biometric technology. Experimental results confirmed differ-

ences between old and young groups based on dorsal hand vein images. The research also propose a new method of liveness detection for biometrics.

## 7.2 Original Contributions

The main original contributions from this study are:

- New attributes of dorsal hand vein biometrics, such as aging factors and vital signs underlying dynamic dorsal hand vein images, were discovered via quantitative static analysis. These approaches lay the foundation for further research on age recognition and respiration rate detection.
- Features based on intensity and basic statistical parameters were proposed and yielded satisfactory performances in the classification of young and old groups from biometrics perspectives. The means to predict groups of people, can reduce computing times of one-to-one recognition in dorsal hand vein biometric applications.
- Potentially, a new method of liveness detection was proposed based on dynamic analyses using near infra-red dorsal hand vein images.

## 7.3 Future Work

Based on these research findings and data collected, some potential future objectives are summarised;

- **Englarging the database**

Ideally, the database should be enlarged for further research. The classification results of old and young groups could be validated and expanded when more data are included. Regarding the video based DHV images, more detailed information should be recorded during acquisition processes. For example, respiratory rates and heart rates could be recorded using appropriate devices for further investigation and validation.

- **Exploring the classification of different age groups**

Further static analyses could focus on the classification of old group in the database. Since vein and skin alters with age, intensity based features could be used for the classification of different age groups. As shown in Figure 7.1, young and old groups were separate while sub-groups of old group could not be classified easily. Thus, more features should be taken into consideration and combined for classification of groups.

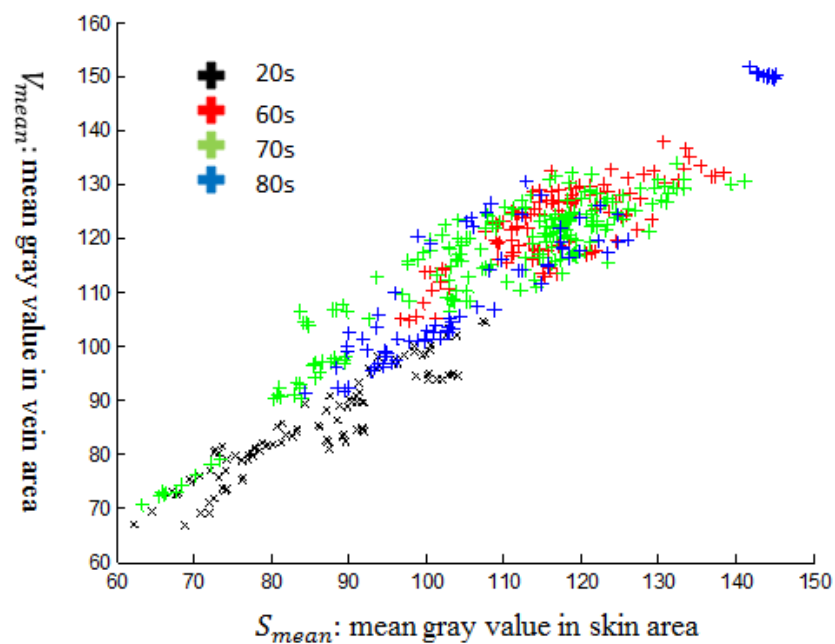


**Figure 7.1:** Age distribution using combined mean values

- **Combining dorsal hand vein images with other biometric modalities**

For this research, dorsal hand vein biometrics could be combined with other biometric features, like characteristics from the face or wrist. At the same time, dorsal hand vein images based on NIR could be combined with other imaging methods. Employing these combinations would be advantageous to research on dorsal hand vein biometrics.

# References

- Abhyankar, A. and Schuckers, S. (2006). Fingerprint liveness detection using local ridge frequencies and multiresolution texture analysis techniques. In *Image Processing, 2006 IEEE International Conference on*, pages 321–324. IEEE.
- Accute Optical Technology Co., L. (2012). Bandpass coating filter.
- Akhtar, Z. (2012). *Security of multimodal biometric systems against spoof attacks*. PhD thesis.
- Badawi, A., Mahfouz, M., Tadross, R., and Jantz, R. (2006). Fingerprint-based gender classification. In *IPCV*, pages 41–46.
- Barth, J., Klucken, J., Kugler, P., Kammerer, T., Steidl, R., Winkler, J., Hornegger, J., and Eskofier, B. (2011). Biometric and mobile gait analysis for early diagnosis and therapy monitoring in parkinson's disease. In *Engineering in Medicine and Biology Society, EMBC, 2011 Annual International Conference of the IEEE*, pages 868–871. IEEE.
- Bodade, R. and Talbar, S. (2009). Dynamic iris localisation: A novel approach suitable for fake iris detection. In *Ultra Modern Telecommunications & Workshops, 2009. ICUMT'09. International Conference on*, pages 1–5. IEEE.
- Bolle, R. and Pankanti, S. (1998). *Biometrics, Personal Identification in Networked Society: Personal Identification in Networked Society*. Kluwer Academic Publishers.
- Botonjic-Sehic, E., Brown, C. W., Lamontagne, M., and Tsaparikos, M. (2009). Forensic application of near-infrared spectroscopy: aging of bloodstains. *Spectroscopy*, 24(2):42–48.
- Boulgouris, N. V., Hatzinakos, D., and Plataniotis, K. N. (2005). Gait recognition: a challenging signal processing technology for biometric identification. *signal processing magazine, IEEE*, 22(6):78–90.
- Bowyer, K. W., Hollingsworth, K. P., and Flynn, P. J. (2013). *A survey of iris biometrics research: 2008–2010*, pages 15–54. Springer.
- Boyd, J. E. and Little, J. J. (2005). *Biometric gait recognition*, pages 19–42. Springer.
- Carlson, B. M. (2013). *Human embryology and developmental biology*. Elsevier Health Sciences.
- Carmeliet, P. and Jain, R. K. (2000). Angiogenesis in cancer and other diseases. *nature*, 407(6801):249–257.
- Carretero, O. A. (2005). Vascular remodeling and the kallikrein-kinin system. *J Clin Invest*, 115(3):588–591.
- Chen, W., L. P. and Lu, G. (2000). Study on near infra-red spectrum of ischemic cerebral infarction. *Journal of Hubei College of Traditional Chinese Medicine*.

- Chih-Lung, L. and Kuo-Chin, F. (2004). Biometric verification using thermal images of palm-dorsa vein patterns. *Circuits and Systems for Video Technology, IEEE Transactions on*, 14(2):199–213.
- Choi, H.-S. (2001). Apparatus and method for identifying individuals through their subcutaneous vein patterns and integrated system using said apparatus and method.
- Clarke, R. (1994). Human identification in information systems: Management challenges and public policy issues. *Information Technology & People*, 7(4):6–37.
- Conrad, M. C. and Green, H. D. (1964). Hemodynamics of large and small vessels in peripheral vascular disease. *Circulation*, 29(6):847–853.
- Cover, T. M. and Hart, P. E. (1967). Nearest neighbor pattern classification. *Information Theory, IEEE Transactions on*, 13(1):21–27.
- Cross, J. and Smith, C. (1995). Thermographic imaging of the subcutaneous vascular network of the back of the hand for biometric identification. In *Security Technology, 1995. Proceedings. Institute of Electrical and Electronics Engineers 29th Annual 1995 International Carnahan Conference on*, pages 20–35. IEEE.
- Dantcheva, A., Velardo, C., D'angelo, A., and Dugelay, J.-L. (2011). Bag of soft biometrics for person identification. *Multimedia Tools and Applications*, 51(2):739–777.
- Day, D. (2009). *Biometric Applications, Overview*, pages 76–80. Springer.
- Duhamel, P. and Vetterli, M. (1990). Fast fourier transforms: a tutorial review and a state of the art. *Signal processing*, 19(4):259–299.
- Field, H., Bock, A. V., Gildea, E. F., and Lathrop, F. L. (1924). The rate of the circulation of the blood in normal resting individuals. *Journal of Clinical Investigation*, 1(1):65–85.
- Fisher, R. A. (1936). The use of multiple measurements in taxonomic problems. *Annals of Eugenics*, 7(2):179–188.
- Friedman, J., Hastie, T., and Tibshirani, R. (2001). *The elements of statistical learning*, volume 1. Springer series in statistics Springer, Berlin.
- Fujitsu (2003). Fujitsu develops technology for world's first contactless palm vein pattern biometric authentication system.
- Gafurov, D. (2007). A survey of biometric gait recognition: Approaches, security and challenges. In *Annual Norwegian Computer Science Conference*, pages 19–21. Citeseer.
- Galbally, J., Alonso-Fernandez, F., Fierrez, J., and Ortega-Garcia, J. (2012). A high performance fingerprint liveness detection method based on quality related features. *Future Generation Computer Systems*, 28(1):311–321.
- Ganong, W. F. and Barrett, K. E. (2005). *Review of medical physiology*, volume 21. McGraw-Hill Medical eNew York New York.
- Gao, F. and Ai, H. (2009). *Face age classification on consumer images with gabor feature and fuzzy lda method*, pages 132–141. Springer.
- Gniadecka, M., Nielsen, O. F., Wessel, S., Heidenheim, M., Christensen, D. H., and Wulf, H. C. (1998). Water and protein structure in photoaged and chronically aged skin. *Journal of investigative dermatology*, 111(6):1129–1132.

- Gray, H. and Standring, S. (2008). Vascular supply and lymphatic drainage. gray's anatomy: the anatomical basis of clinical practice.
- Haddad, R. A. and Akansu, A. N. (1991). A class of fast gaussian binomial filters for speech and image processing. *Signal Processing, IEEE Transactions on*, 39(3):723–727.
- Jain, A., Hong, L., and Pankanti, S. (2000). Biometric identification. *Communications of the ACM*, 43(2):90–98.
- Jain, A. K. and Li, S. Z. (2005). *Handbook of face recognition*, volume 1. Springer.
- Jain, A. K., Ross, A. A., and Nandakumar, K. (2011). *Introduction to biometrics*. Springer Science & Business Media.
- Kadhum, Z. A. (2012). Equalize the histogram equalization for image enhancement. *Journal of Kufa for Mathematics and Computer*, 1(5).
- Kanade, T., Cohn, J. F., and Tian, Y. (2000). Comprehensive database for facial expression analysis. In *Automatic Face and Gesture Recognition, 2000. Proceedings. Fourth IEEE International Conference on*, pages 46–53. IEEE.
- Kang, H., Lee, B., Kim, H., Shin, D., and Kim, J. (2003). A study on performance evaluation of the liveness detection for various fingerprint sensor modules. In *Knowledge-Based Intelligent Information and Engineering Systems, International Conference, Kes 2003, Oxford, Uk, September 3-5, 2003, Proceedings*, pages 1245–1253.
- Kaur, R. and Mazumdar, S. G. (2012). Fingerprint based gender identification using frequency domain analysis. *International Journal of Advances in Engineering & Technology*, 3(1):295–299.
- Kumar, A. and Prathyusha, K. V. (2009). Personal authentication using hand vein triangulation and knuckle shape. *Image Processing, IEEE Transactions on*, 18(9):2127–2136.
- Kusuma, S., Vuthoori, R. K., Piliang, M., and Zins, J. E. (2010). *Skin anatomy and Physiology*, pages 161–171. Springer.
- Li, K. (2013). *Biometric Person Identification Using Near-infrared Hand-dorsa Vein Images*. PhD thesis.
- Lim, J. S. (1990). *Two-dimensional signal and image processing*. Prentice-Hall, Inc.
- Lingyu, W. and Leedham, G. (2006). Near- and far- infrared imaging for vein pattern biometrics. In *Video and Signal Based Surveillance, 2006. AVSS '06. IEEE International Conference on*, pages 52–52.
- Makihara, Y., Okumura, M., Iwama, H., and Yagi, Y. (2011). Gait-based age estimation using a whole-generation gait database. In *Biometrics (IJCB), 2011 International Joint Conference on*, pages 1–6. IEEE.
- Maltoni, D., Maio, D., Jain, A. K., and Prabhakar, S. (2009). *Handbook of fingerprint recognition*. Springer Science & Business Media.
- Ming-Zher, P., McDuff, D. J., and Picard, R. W. (2011). Advancements in noncontact, multiparameter physiological measurements using a webcam. *Biomedical Engineering, IEEE Transactions on*, 58(1):7–11.
- Misaki, M., Kim, Y., Bandettini, P. A., and Kriegeskorte, N. (2010). Comparison of multivariate classifiers and response normalizations for pattern-information fmri. *NeuroImage*, 53(1):103–118.

- Miura, N., Nagasaka, A., and Miyatake, T. (2007). Extraction of finger-vein patterns using maximum curvature points in image profiles. In *Iapr Conference on Machine Vision Applications*, pages 347–350.
- Moon, Y. S., Chen, J., Chan, K., So, K., and Woo, K. (2005). Wavelet based fingerprint liveness detection. *Electronics Letters*, 41(20):1112–1113.
- Nadort, A. (2007). The hand vein pattern used as a biometric feature. *Master Literature Thesis of Medical Natural Sciences at the Free University, Amsterdam*.
- Negin, M., Salganicoff, M., and Zhang, G. G. (2000). An iris biometric system for public and personal use. *Computer*, 33(2):70–75.
- Niblack, W. (1985). *An introduction to digital image processing*. Strandberg Publishing Company.
- Ntziachristos, V., Bremer, C., and Weissleder, R. (2003). Fluorescence imaging with near-infrared light: new technological advances that enable in vivo molecular imaging. *European radiology*, 13(1):195–208.
- O’Toole, A. J., Deffenbacher, K. A., Valentin, D., McKee, K., Huff, D., and Abdi, H. (1998). The perception of face gender: The role of stimulus structure in recognition and classification. *Memory & Cognition*, 26(1):146–160.
- Otsu, N. (1975). A threshold selection method from gray-level histograms. *Automatica*, 11(285-296):23–27.
- Pan, G., Sun, L., and Wu, Z. (2008). *Liveness detection for face recognition*. INTECH Open Access Publisher.
- Papakonstantinou, E., Roth, M., and Karakiulakis, G. (2012). Hyaluronic acid: a key molecule in skin aging. *Dermato-endocrinology*, 4(3):253–258.
- Pizer, S. M., Amburn, E. P., Austin, J. D., Cromartie, R., Geselowitz, A., Greer, T., ter Haar Romeny, B., Zimmerman, J. B., and Zuiderveld, K. (1987). Adaptive histogram equalization and its variations. *Computer vision, graphics, and image processing*, 39(3):355–368.
- Riggs, B. L., Khosla, S., and Melton III, L. J. (1999). The assembly of the adult skeleton during growth and maturation: implications for senile osteoporosis. *Journal of Clinical Investigation*, 104(6):671.
- Risler, N. R., Cruzado, M. C., and Miatello, R. M. (2005). Vascular remodeling in experimental hypertension. *The Scientific World Journal*, 5:959–971.
- Ross, A. and Jain, A. K. (2004). Multimodal biometrics: An overview. In *Signal Processing Conference, 2004 European*, pages 1221–1224.
- Rubin, H. (2003). Aging process: Part x-the skin, the skeleton and the brain.
- Ruiz-Albacete, V., Tome-Gonzalez, P., Alonso-Fernandez, F., Galbally, J., Fierrez, J., and Ortega-Garcia, J. (2008). *Direct Attacks Using Fake Images in Iris Verification*, pages 181–190. Springer Berlin Heidelberg, Berlin, Heidelberg.
- Schuckers, S. and Abhyankar, A. (2004). Detecting liveness in fingerprint scanners using wavelets: Results of the test dataset. In *Biometric Authentication, ECCV 2004 International Workshop, BioAW 2004, Prague, Czech Republic, May 15, 2004, Proceedings*, pages 100–110.

- Serra, J. (1983). Image analysis and mathematical morphology. 39(2):536.
- Shi, Z. and Yi-Ding, W. (2008). Biometric identification based on low-quality hand vein pattern images. In *Machine Learning and Cybernetics, 2008 International Conference on*, volume 2, pages 1172–1177.
- Smith, W. J. (2005). *Modern lens design*, volume 2. McGraw-Hill New York.
- Takano, C. and Ohta, Y. (2007). Heart rate measurement based on a time-lapse image. *Medical Engineering & Physics*, 29(8):853–857.
- Tan, X., Li, Y., Liu, J., and Jiang, L. (2010). *Face liveness detection from a single image with sparse low rank bilinear discriminative model*, pages 504–517. Springer.
- Thomas, V., Chawla, N. V., Bowyer, K. W., and Flynn, P. J. (2007). Learning to predict gender from iris images. In *Biometrics: Theory, Applications, and Systems, 2007. BTAS 2007. First IEEE International Conference on*, pages 1–5.
- Tom, R. J., Arulkumaran, T., and Scholar, M. (2013). Fingerprint based gender classification using 2d discrete wavelet transforms and principal component analysis. *International Journal of Engineering Trends and Technology*, 4(2):199–203.
- Waller, J. M. and Maibach, H. I. (2005). Age and skin structure and function, a quantitative approach (i): blood flow, ph, thickness, and ultrasound echogenicity. *Skin Research and Technology*, 11(4):221–235.
- Wang, L. and Leedham, G. (2006). Near-and far-infrared imaging for vein pattern biometrics. In *Video and Signal Based Surveillance, 2006. AVSS'06. IEEE International Conference on*, pages 52–52. IEEE.
- Wang, Y., Li, K., and Cui, J. (2010). Hand-dorsa vein recognition based on partition local binary pattern. In *Signal Processing (ICSP), 2010 IEEE 10th International Conference on*, pages 1671–1674. IEEE.
- Wilhelm, K.-P., Cua, A. B., and Maibach, H. I. (1991). Skin aging: effect on transepidermal water loss, stratum corneum hydration, skin surface ph, and casual sebum content. *Archives of dermatology*, 127(12):1806–1809.
- Wilson, C. (2010). *Vein pattern recognition: a privacy-enhancing biometric*. CRC press.
- Xu, S., Sun, L., and Rohde, G. K. (2014). Robust efficient estimation of heart rate pulse from video. *Biomedical Optics Express*, 5(4):1124–1135.
- Yoo, J.-H., Hwang, D., and Nixon, M. S. (2005). Gender classification in human gait using support vector machine. In *Advanced concepts for intelligent vision systems*, pages 138–145. Springer.
- Yu, S., Tan, T., Huang, K., Jia, K., and Wu, X. (2009). A study on gait-based gender classification. *Image Processing, IEEE Transactions on*, 18(8):1905–1910.

# Appendix A

## The AGE DISTRIBUTION OF THE DATABASE

This appendix gives the detailed age information of the subjects in the static DHV database, shown as follows:

**Table A.1:** Age distribution of the static DHV database

Group	Age	Number
Young	25	3
	26	4
	27	2
	28	1
Old	60-69	11
	70-79	21
	80-89	8

## Appendix B

# SEGMENTATION RESULTS OF OLD HANDS

This appendix gives the results of the segmentation of the DHV images from 40 different old individuals.

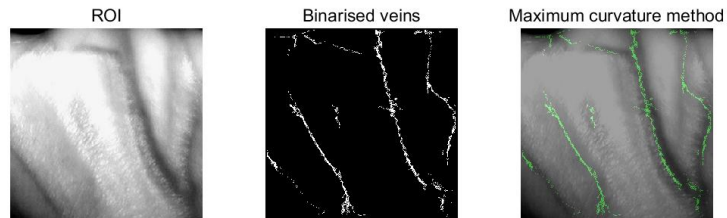


**Figure B.1:** Segmentation result of Old No.1

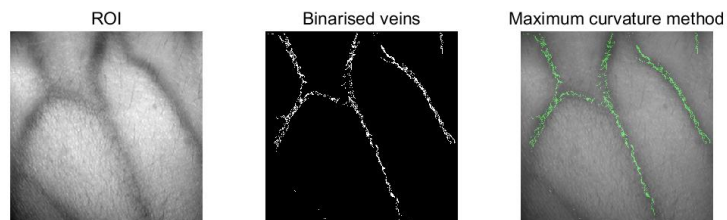


**Figure B.2:** Segmentation result of Old No.2

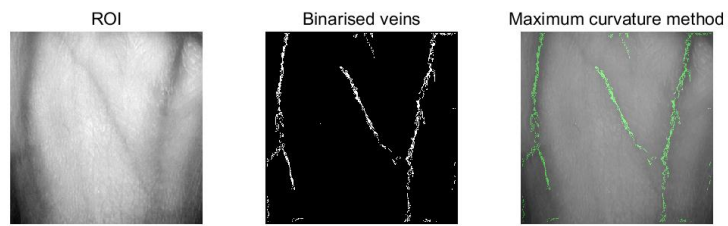


**Figure B.3:** Segmentation result of Old No.3

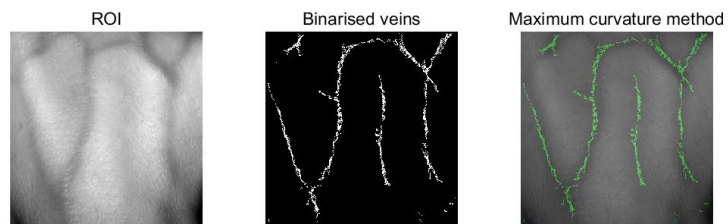


**Figure B.4:** Segmentation result of Old No.4

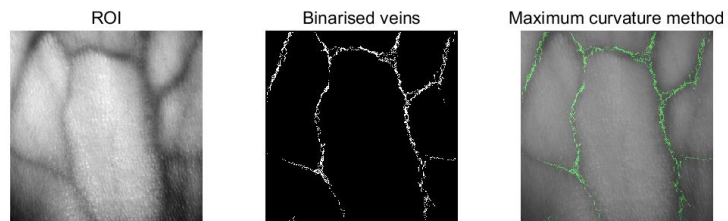


**Figure B.5:** Segmentation result of Old No.5

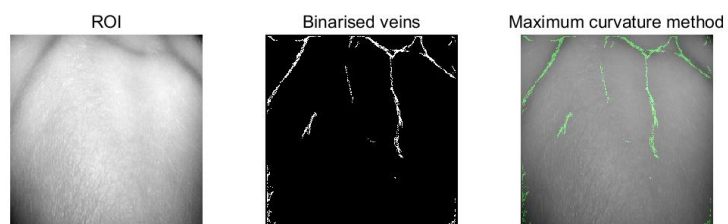


**Figure B.6:** Segmentation result of Old No.6

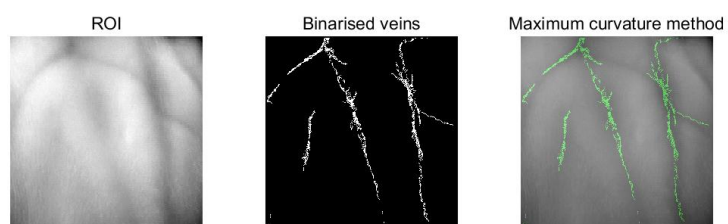


**Figure B.7:** Segmentation result of Old No.7

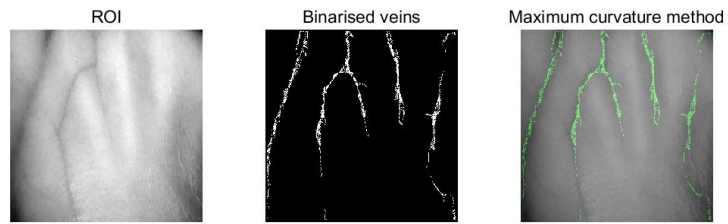


**Figure B.8:** Segmentation result of Old No.8

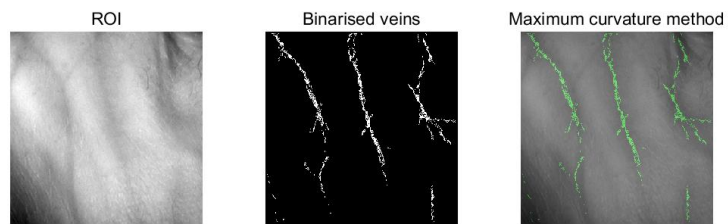


**Figure B.9:** Segmentation result of Old No.9

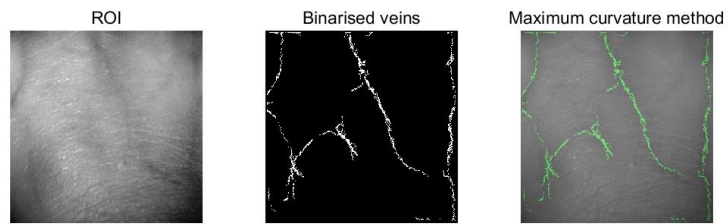


**Figure B.10:** Segmentation result of Old No.10

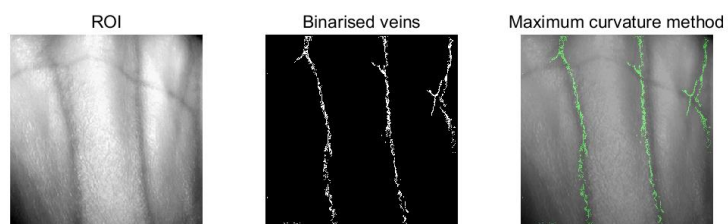


**Figure B.11:** Segmentation result of Old No.11

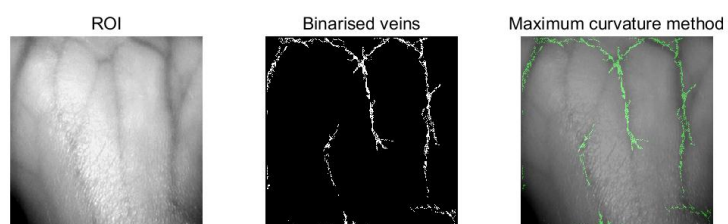


**Figure B.12:** Segmentation result of Old No.12

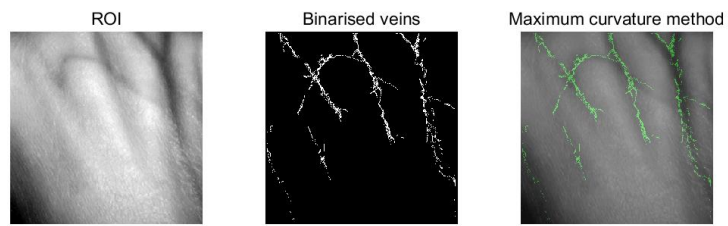


**Figure B.13:** Segmentation result of Old No.13

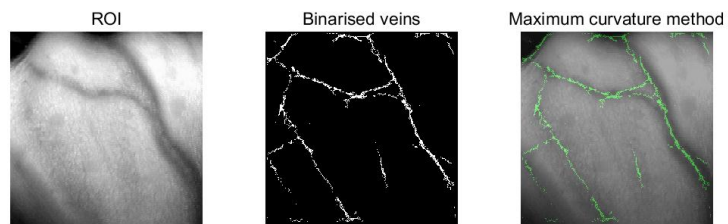


**Figure B.14:** Segmentation result of Old No.14

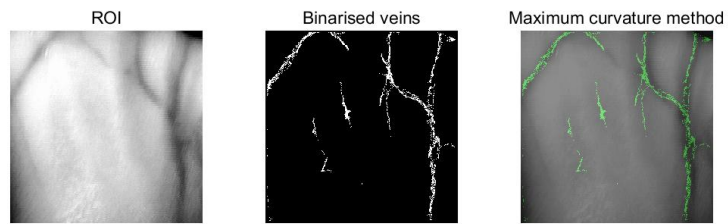


**Figure B.15:** Segmentation result of Old No.15

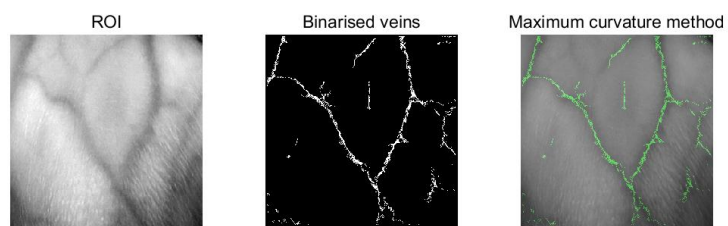


**Figure B.16:** Segmentation result of Old No.16

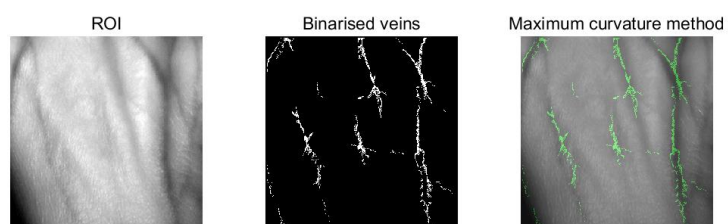


**Figure B.17:** Segmentation result of Old No.17

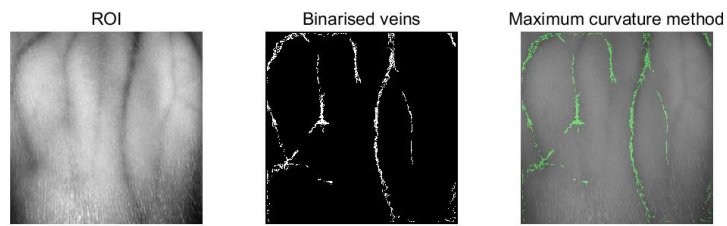


**Figure B.18:** Segmentation result of Old No.18

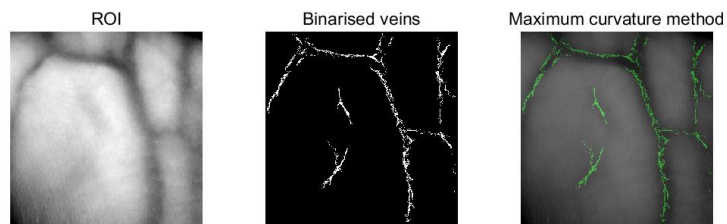


**Figure B.19:** Segmentation result of Old No.19

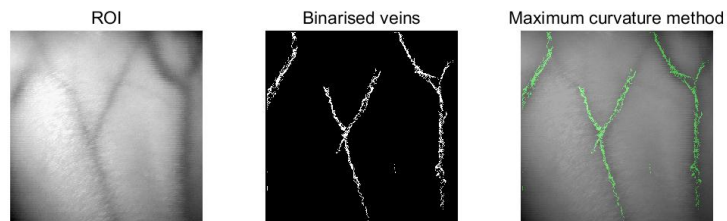


**Figure B.20:** Segmentation result of Old No.20

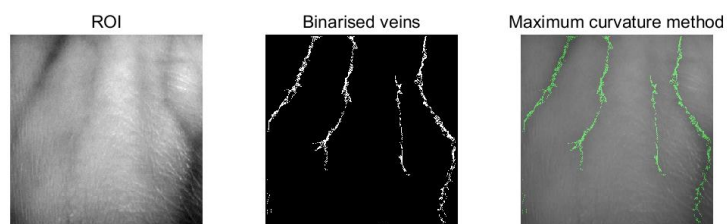


**Figure B.21:** Segmentation result of Old No.21

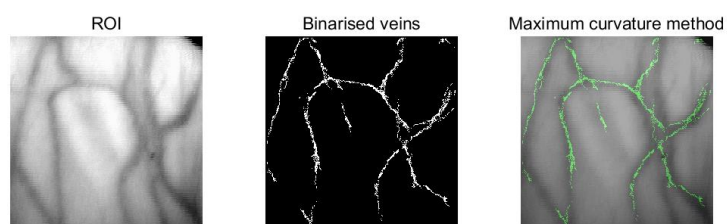


**Figure B.22:** Segmentation result of Old No.22

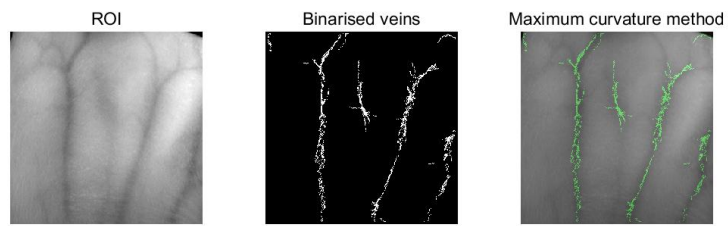


**Figure B.23:** Segmentation result of Old No.23

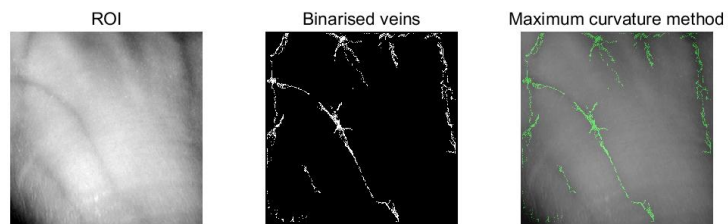


**Figure B.24:** Segmentation result of Old No.24

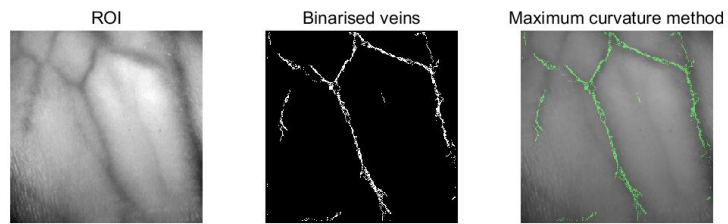


**Figure B.25:** Segmentation result of Old No.25

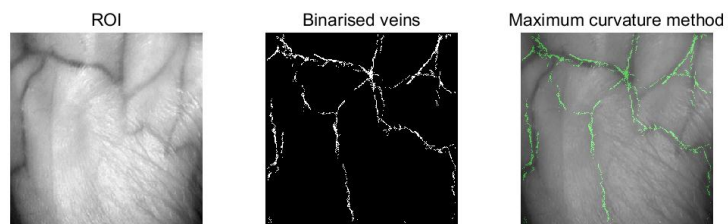


**Figure B.26:** Segmentation result of Old No.26

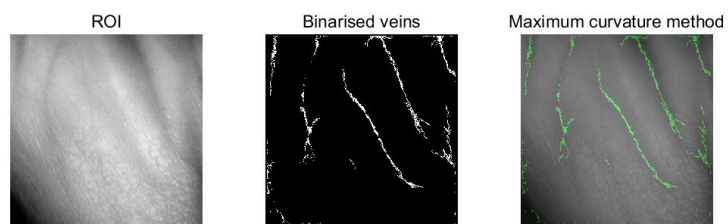


**Figure B.27:** Segmentation result of Old No.27

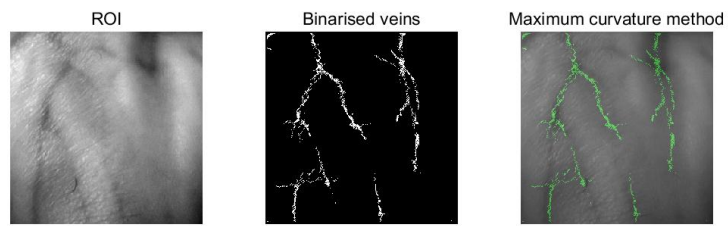


**Figure B.28:** Segmentation result of Old No.28

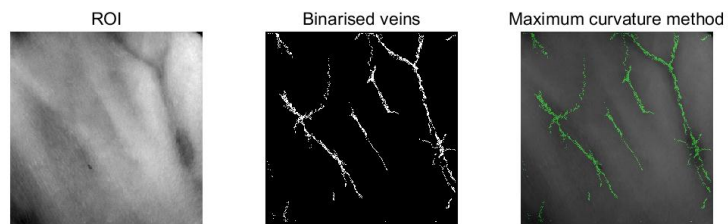


**Figure B.29:** Segmentation result of Old No.29

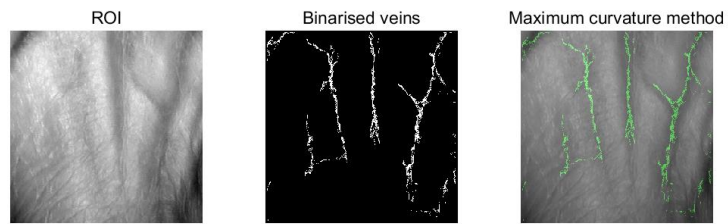


**Figure B.30:** Segmentation result of Old No.30

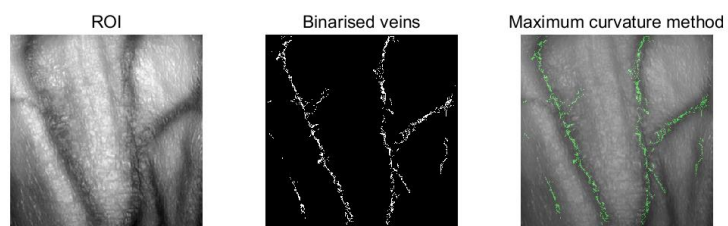


**Figure B.31:** Segmentation result of Old No.31

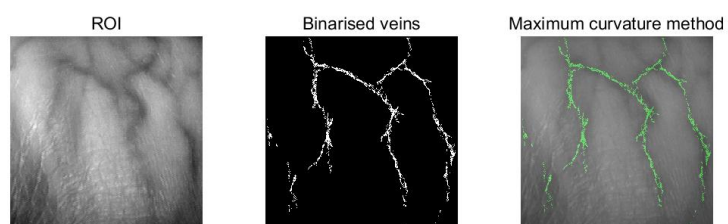


**Figure B.32:** Segmentation result of Old No.32

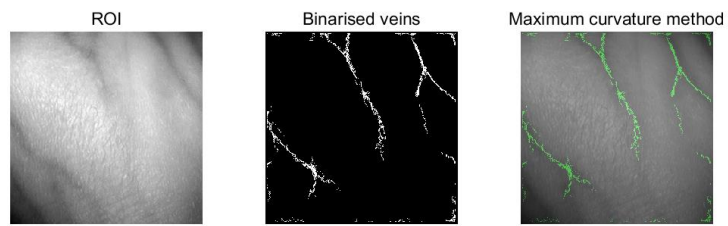


**Figure B.33:** Segmentation result of Old No.33

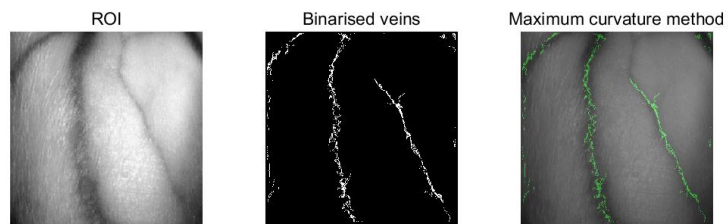


**Figure B.34:** Segmentation result of Old No.34

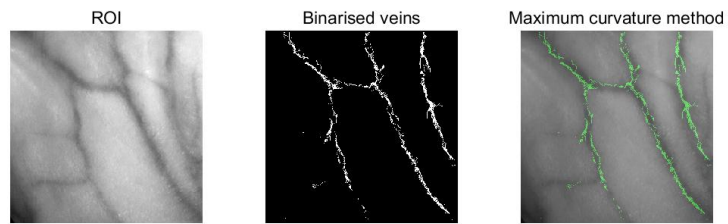


**Figure B.35:** Segmentation result of Old No.35

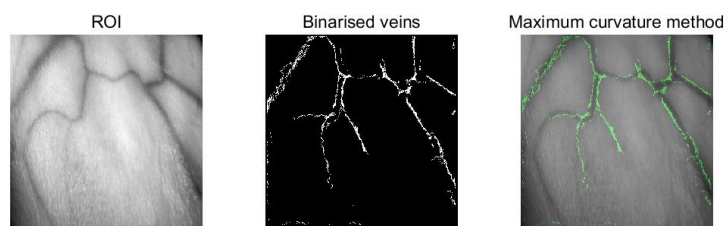


**Figure B.36:** Segmentation result of Old No.36

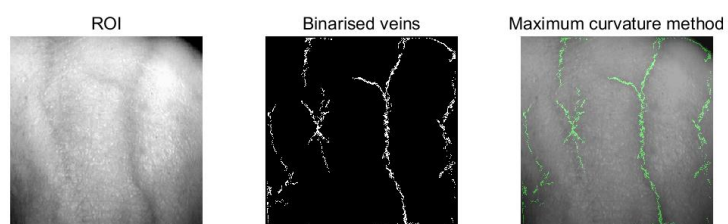


**Figure B.37:** Segmentation result of Old No.37

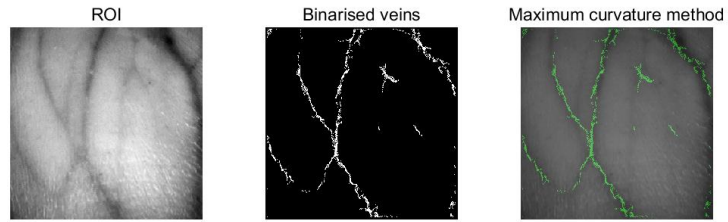


**Figure B.38:** Segmentation result of Old No.38

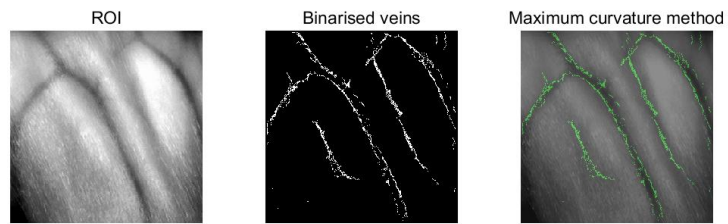


**Figure B.39:** Segmentation result of Old No.39

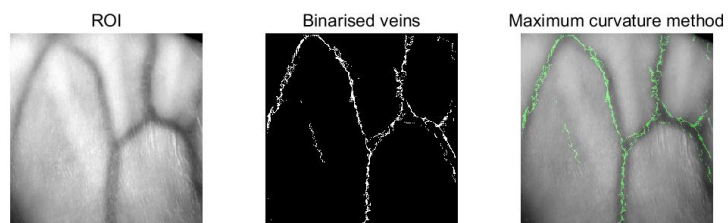


**Figure B.40:** Segmentation result of Old No.40

## Appendix C

# SEGMENTATION RESULTS OF YOUNG HANDS

This appendix gives the results of the segmentation of the DHV images from 10 different young individuals.

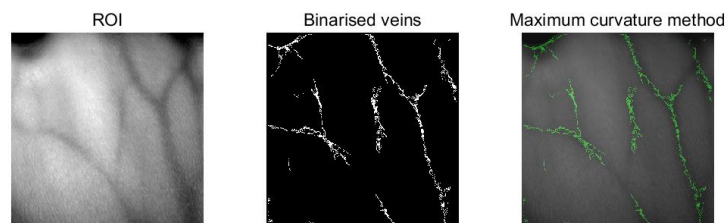


**Figure C.1:** Segmentation result of Young No.1

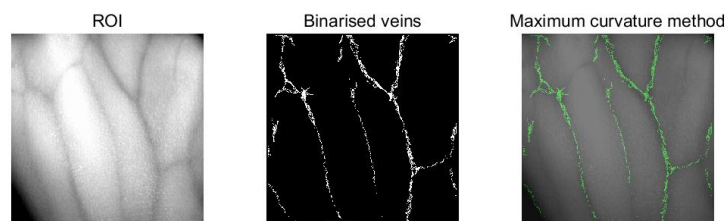


**Figure C.2:** Segmentation result of Young No.2

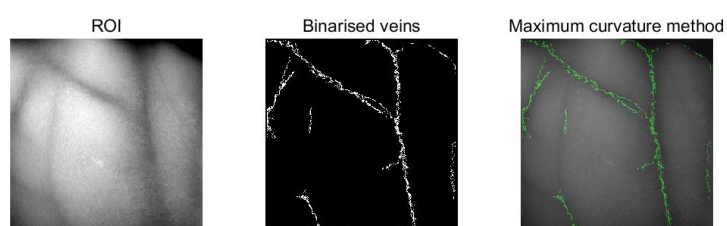


**Figure C.3:** Segmentation result of Young No.3

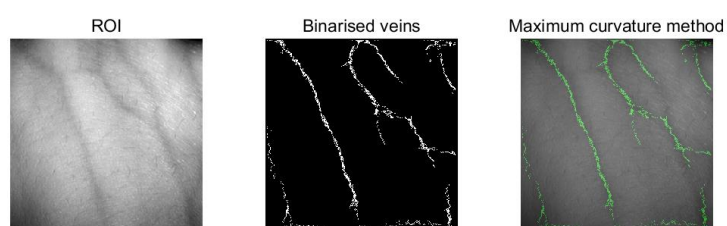


**Figure C.4:** Segmentation result of Young No.4

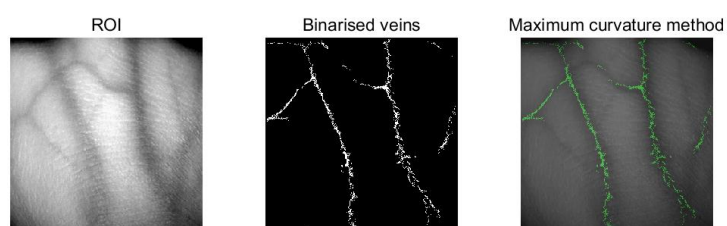


**Figure C.5:** Segmentation result of Young No.5

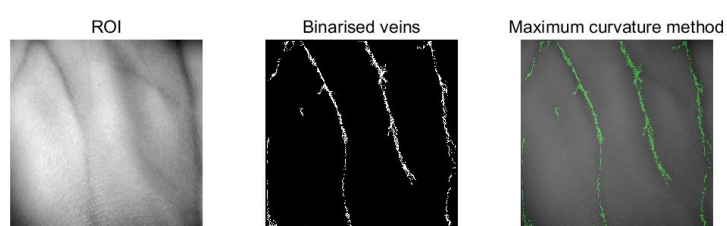


**Figure C.6:** Segmentation result of Young No.6

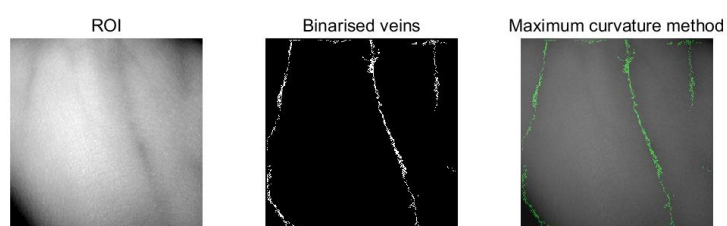


**Figure C.7:** Segmentation result of Young No.7

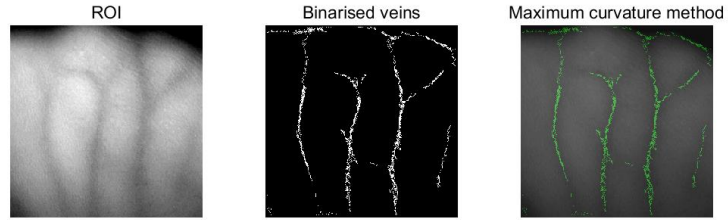


**Figure C.8:** Segmentation result of Young No.8

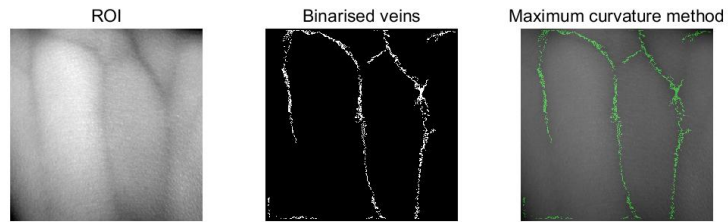


**Figure C.9:** Segmentation result of Young No.9

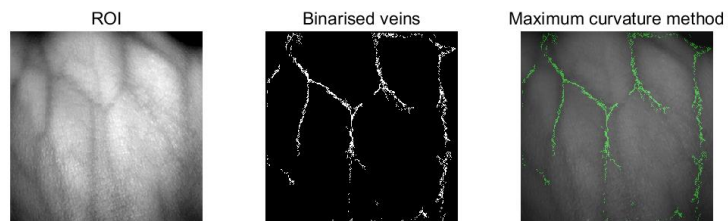


**Figure C.10:** Segmentation result of Young No.10